Deep Learning Approach for Water Management in Agriculture

A

Thesis submitted

for the award of the degree of

DOCTOR OF PHILOSOPHY

By

Gitika Sharma
(901803019)

Under the guidance of

Dr. Ashima Singh
(Associate Professor, CSED)

Dr. Sushma Jain
(Associate Professor, CSED)

THAPAR INSTITUTE
OF ENGINEERING & TECHNOLOGY
(Deemed to be University)

Computer Science and Engineering Department
Thapar Institute of Engineering and Technology
Patiala - 147004, India

June 2023

CERTIFICATE

This is to certify that the Thesis entitled"**Deep Learning Approach for Water Management in Agriculture**", submitted by **Gitika Sharma** (901803019), a research scholar in the *Computer Science and Engineering Department, Thapar Institute of Engineering & Technology, Patiala*, for the award of the degree of **Doctor of Philosophy**, is a record of an original research work carried out under the supervision of Dr. Ashima Singh, Dr. Sushma Jain and refers work of other researchers which are duly listed in reference section. The Thesis has fulfilled all requirements as per the regulations of the Institute and in our opinion has reached the standard needed for submission.

The results embodied in this Thesis have not been submitted to any other University or Institute for the award of any degree.

Gitika Sharma

Gitika Sharma
Registration No. 901803019

This is to certify that the above statement made by the candidate is correct and true to the best of my knowledge and belief.

Date: 23/06/2023
Place: Patiala

Dr. Ashima Singh
Associate Professor,
Computer Science and Engineering Department,
Thapar Institute of Engineering and Technology, Patiala,
India - 147004

Dr. Sushma Jain
Associate Professor,
Computer Science and Engineering Department,
Thapar Institute of Engineering and Technology, Patiala,
India - 147004

ACKNOWLEDGEMENTS

First and foremeost, thanks to almighty God for all his blessings without which nothing of my work would have been possible. The successful completion of any task would be incomplete without acknowledging the people who made it possible. I would like to take this opportunity to express my gratitude to all those who made this journey possible. Words are often too less to express one's deepest regards, but lets give it a go.

I would like to express my sincere gratitude to my supervisors, Dr. Ashima Singh (Associate Professor, CSED), and Dr. Sushma Jain (Associate Professor, CSED), who have supported me throughout my Ph.D. work with their patience, motivation, enthusiasm and immense knowledge. Apart from providing me with excellent supervision, strong cooperation and constant encouragement throughout this journey, they also shared their invaluable experiences with me to succeed in life. They have truly been the source of real inspiration for me and I will always remain indebted to them.

I also take the opportunity to thank head of deaprtment Dr. Shalini Batra, the former head Dr. Maninder Singh for providing me the necessary administrative assistance and infrastructure that helped me in the completion of my research work. I would also like to extend my sincere thanks to the doctoral committee members Dr. Maninder Kaur (Associate Professor, CESD), Dr. Karamjeet Singh (Assistant Professor, CSED), and Dr. Anoop Verma (Associate Professor, School of Energy and Environment) for their helpful suggestions and ensuring the progress of my research work regularly.

My deepest gratitude to my soul mate Mr. Himanshu Sharma for being a pillar of support and encouragement throughout my research work. His constructive criticism, involvement with my work, and critical reading of the text, helped me tremendously in improving upon the thesis. I would also like to pay my sincere regards to my in-laws family for their constant motivation and support.

The chain of my gratitude will definitely be incomplete if I forget to thank my mother Neelam Sharma and sister Sapna Sharma, for their unconditional love, support and encouragement in every phase of my life. It was their confidence in me that I started my Ph.D. Since then, the journey of Ph.D. has been a sweet and bitter ride at times which lead to a special mention for my mother who was with me through thick and thin, and gave me courage at the times when I felt really low. Her continuous motivation showed me the silver lining in the dark clouds. It would also

be unworthy of me if I forget to mention about the heavenly blessings constantly showered on me by my father *Lt.* Naresh Kumar.

I would also like to thank my friends and colleagues with whom I have traveled this journey of research. A special thanks to my Ph.D fellow Dr. Mandeep Kaur Saggi for her guidance and always being there as an elder sister. I would especially thank my friends Jaskaran, Manish and Aman for their much needed moral and emotional support. As one cannot mention the names of all well-wishers, friends and beloved ones, I would like to pay my regards to one and all who supported me during the journey of knowledge. I dedicate this research work to my deceased brother, Abhishek.

Gitika Sharma

ABSTRACT

Water is an indispensable natural commodity, a fundamental human need, and the most critical source for the existence of the human race and its development. Presently, the world is grappling with water scarcity issues which have risen to an alarming mark. Climate change projection shows that the situation will become grimmer and more prevalent in the near future. The agriculture sector is the primary consumer of water and uses almost 75-80% of the freshwater available worldwide. India, an agricultural country, requires a huge amount of water for irrigation. Still, it has only 4% of the world's freshwater to serve the food demands of about 18% of the global population. Thus, precise estimation of the irrigation requirements is a significant task to manage the available water resources efficiently and optimize water usage in agriculture.

Researchers are trying hard to develop efficient irrigation techniques. The water requirement problem requires more efficient, intelligent, and sustainable techniques to address the problem. Evapotranspiration (ET) is a significant factor in determining crop water requirements. The precise estimation of reference evapotranspiration (ET_0) and crop evapotranspiration (ET_c) is necessary to determine the irrigation requirements to maintain crop-water balance. Deep learning (DL) models are efficient in handling complex non-linear relationships with a massive amount of data. It shows the ability to handle time-series forecasting problems. Estimating evapotranspiration shows similar characteristics, such as complex non-linear relationships among meteorological parameters and the time-dependence nature of these parameters.

Therefore, the work reported in this thesis is carried out to develop deep learning-based models for the precise estimation of ET_0 and ET_c values. These proposed DL models are further investigated to handle the limited availability of meteorological data required for their reliable estimation. The main contributions of this thesis are as follows:

- Estimation of reference evapotranspiration using a hybrid deep neural network approach for limited meteorological data.

- Estimation of reference evapotranspiration using deep reinforcement learning-based ensemble approach to consider the effect of time-varying characteristics of the ET_0 process.

- Estimation of daily crop evapotranspiration using limited climate data and to forecast future changes in wheat and rice ET_c.

Two-hybrid deep neural network models, i.e., Convolution-Long Short Term Memory (Conv-LSTM) and Convolution Neural Network-LSTM (CNN-LSTM), are investigated for the estimation of reference evapotranspiration. Conv-LSTM performs the convolution operation in LSTM cells and CNN-LSTM uses the convolution layer for feature extraction of input data, and then the extracted features are fed to LSTM layers. The climate dataset of two stations in India: Ludhiana and Amritsar, is adopted to develop the proposed models. It includes daily maximum temperature (T_{max}), minimum temperature (T_{min}), wind speed (WSP) measured at the height of 2m, solar radiation (R_s), relative humidity (RH), vapor pressure (VP), and sunshine hours (SSH) data from the period 2003 to 2015 of Ludhiana station and 2000 to 2016 of Amritsar station. The study also focuses on climate data scarcity conditions, and thus, different input combinations of climate parameters have been used to investigate the minimum required parameters to model the ET_0 process. Several performance measures are used to assess the precision of the model and to perform sensitivity analysis. Temperature and radiation are observed as the prime data inputs required to estimate ET_0 values. The proposed hybrid models are then compared with existing temperature and radiation-based empirical models such as Hargreaves, Makkink, and Ritchie. The comparison reveals that CNN-LSTM and Conv-LSTM outperform these existing models. Moreover, Conv-LSTM performs better than CNN-LSTM.

To investigate the time-varying characteristics of the ET_0 process, a deep reinforcement learning (DRL) based ensemble approach, *DeepEvap*, is proposed for the estimation of ET_0 values by using three climate parameters as input variables i.e., T_{min}, T_{max}, and R_s. The modeling procedure of the proposed ensemble model consists of three phases. In phase I, the data preprocessing technique is performed on the meteorological data to clean the existing impurities(e.g., outliers, missing data) as it affects the performance of any machine learning (ML) based approach. In phase II, four different deep neural network-based models are used to build the estimation model of ET_0 and calculate the prediction results. In phase III, the DRL approach is used to ensemble the prediction results of these four models. The meteorological datasets of two stations of India: Ludhiana and Patiala, are selected to validate the proposed approach. Simulation results show that the proposed DeepEvap approach is competitive for ET_0 prediction by achieving a coefficient of determination (R^2) = 0.96, mean sqaure error (MSE) = 0.0018 mmd^{-1}, and explained variance score (EVS) = 0.96. It significantly outperforms four baseline models. Moreover, DeepEvap also integrates four deep neural network models and works better than existing stack based and weighted ensemble approaches.

Two-hybrid DL models, i.e., Convolution Neural Network-eXtreme Gradient Boosting (CNN-XGB) and Convolution Neural Network-Support Vector Regression (CNN-SVR) are proposed to estimate daily ET_c values of wheat and rice crops. Further, limited climate data (T_{min}, T_{max}, mean temperature (T_{mean}), and (R_s)) is used for the prediction of ET_c values to handle data-scarce situations. Also, the future climate data obtained using two emission scenarios: Representative Concentration Pathways (RCP) 4.5 and RCP 8.5 for the time period 2023-2033, is used to project changes in ET_c. The results demonstrate that the proposed hybrid models provide satisfactory performance with the Nash-Sutcliffe Efficiency (NSE) = 0.95 and 0.976 for rice and wheat ET_c values, respectively. The simulation of future data (IPSLCM5A-LR (Institute Pierre-Simon Laplace Circulation Model 5A - Low Resolution) and HadGEM2 (Hadley Centre Global Environmental Model version 2) obtained from MarkSim GCM) reveals the increase in T_{min} by 7.03%, 7.33%, and T_{max} by 10.5%, 11.5% for RCP 4.5 and RCP 8.5 respectively. Also, an increase in ET_c of rice crop has been reported by 20-22% while increment of wheat ET_c has been noticed by 3-4%. Thus, using limited climate data, the proposed approach efficiently estimates ET_c of wheat and rice crops and could assist water resource managers in achieving agricultural water sustainability.

Contents

List of Figures

List of Tables

List of Acronyms

ICTs	Information and Communication Technologies
IoT	Internet-of-Things
ML	Machine Learning
DL	Deep Learning
SDI	Subsurface Drip Irrigation
IS	Irrigation Scheduling
ET	Evapotranspiration
ET_0	Reference Evapotranspiration for grass surface
ET_r	Reference Evapotranspiration for alalfa surface
ASCE-PM	American Society of Civil Engineers Penman-Monteith
FAO	Food and Agriculture Organization
PM	Penman-Monteith
k_c	Crop Coefficient
ET_c	Crop Evapotranspiration
PWS	Plant Water Status
LWP	Leaf Water Potential
CWSI	Crop Water Stress Index
IRT	Infrared Thermography
SM	Soil Moisture
CWR	Crop Water Requirement
AI	Artificial Intelligence
CAGR	Compound Annual Growth Rate
CNN	Convolution neural network
RNN	Recurrent Neural Network
LSTM	Long short term memory
CNN-LSTM	Convolution neural network-Long short term memory
Conv-LSTM	Convolution-Long Short Term Memory
DRL	Deep Reinforcement Learning
CNN-XGB	Convolution neural network-eXtreme Gradient Boosting
CNN-SVR	Convolution neural network-Support Vector Regression
RCP	Representative Concentration Pathway

EC	Evolutionary Computation
ANFIS	Adaptive Neuro-Fuzzy Inference System
ANN	Artificial Neural Network
S-ANFIS	Subtractive Clustering-based Fuzzy Inference System
G-ANFIS	Grid Partition-based Fuzzy Inference System
F-ANFIS	Fuzzy C-means Clustering based Fuzzy Inference System
GEP	Gene Expression Programming
GP	Genetic Programming
GA	Genetic Algorithms
MLR	Multiple Linear Regression
ELM	Extreme Machine Learning
SVM	Support Vector Machine
MFP	Multivariate Fractional Polynomial
MARS	Multivariate Adaptive Regression Splines
LSSVR	Least Squares Support Vector Regression
RF	Random Forest
GRNN	Generalized Regression Neural Network
LR	Linear Regression
GBR	Gradient Boost Regression
GBDT	Gradient Boosting Decision Tree
LightGBM	Light Gradient Boosting Machine
SMC	Soil Moisture Content
RM5Tree	Radial Basis M5 Model Tree
RSM	Response Surface Method
MLPNN	Multi-layer Perceptron Neural Networks
RBFNN	Radial Basis Function Neural Network
RT	Random Tree
RS	Random Subspace
GBM	Gradient Boosting Machine
BP	Backpropagation Algorithm
Bi-LSTM	Bidirectional LSTM
GRU	Gated Recurrent Unit
GFF	Generalized Feedforward
LRN	Linear Regression network
MLP	Multilayer Perceptron
PNN	robabilistic Neural Network
WNN	Wavelet Neural Network
GWNN	Generalized wavelet neural networks
RBNN	Radial Basis Neural Network

DLNN	Deep Learning Neural Network
GANN	Genetic Algorithm Optimized by Backpropagation Neural Networks
GWNN	Generalized wavelet neural networks
RBNN	Radial Basis Neural Network
NARX	Nonlinear autoregressive exogenous
MOA	Met-heuristic Optimization Algorithm
FFA	Firefly Algorithm
WELM	wavelet-based ELM
OS-ELM	Online Sequential ELM
ALO	Ant Lion Optimizer
MVO	Multi-Verse Optimizer
GWO	Grey Wolf Optimizer
BBO	Biogeography-based Optimization
PSO	Particle Swarm Optimization
ACO	Ant Colony Optimization
CSA	Cuckoo Search Algorithm
FPA	Flower Pollination Algorithm
WOA	Whale Optimization Algorithm
RS	Remote Sensing
NDVI	Normalized Difference Vegetation Index
LST	Land Surface Temperature
LAI	Leaf Area Index
DNN	Deep Neural Networks
TCN	Temporal Convolution Networks
WRC	Swheat-rice crop system
IMD	India meteorological department
KNN	K-nearest neighbor
MAE	Mean Absolute Error
RMSE	Root Mean Square Error
Pbias	Percent Bias
MARE	Mean Absolute Relative Error
NSE	Nash-Scuttle Efficiency
IA	Index of Agreement
R^2	Coefficient of Determination
HG	Hargreaves model
MK	Makkink
RC	Ritchie

List of Symbols

Symbol	Description	Unit
T_{max}	maximum air temperature	(°C)
T_{min}	minimum air temperature	(°C)
T_{mean}	mean air temperature	(°C)
R_s	solar radiation	(MJ m^{-2} day^{-2})
SSH	sunshine hours	(h)
R_n	net radiation	(MJ $m^{-2}day^{-1}$)
P_e	effective rainfall	(mm)
P	rainfall	(mm)
RH	relative humidity	(%)
RH_{max}	maximum relative humidity	(%)
RH_{min}	minimum relative humidity	(%)
RH	mean relative humidity	(%)
WSP	wind speed	2 m height (ms^{-1})
R_a	extraterrestrial radiation	(MJ $m^{-2}day^{-1}$)
Δ	slope of saturation vapor pressure function	(kPa $°C^{-1}$)
γ	psychometric constant	(kPa $°C^{-1}$)
G	soil heat flux density	(MJ $m^{-2}day^{-1}$)
e_a	actual vapour pressure	(kPa)
e_s	saturation vapour pressure	(kPa)
$(e_s - e_a)$	vapour pressure deficit	(kPa)
ρ	mean daily percentage of annual daytime hours	hours
h_c	crop height	(cm)
T_{dew}	dew point temperature	(°C Td)
Pr	Precipitation	(mm)
LAI	leaf area index	
P	Pressure	
k_c	crop coefficient	
R^2	coefficient of determination	

Chapter 1

Introduction

Water policy is among the most critical worldwide concerns. It aims to regulate water consumption and determine the best strategies to avoid exploitation and squandering of existing freshwater resources [1]. India is a water-scarce country that is further exacerbated by the detrimental effects of climate change, inadequate water management, and flawed pricing policies.

Indian population represents 18% of the world's population with only 4% of global freshwater, out of which 75-80% is consumed for agricultural purposes [2]. However, despite growing water scarcity, India's irrigation practice is still very inefficient. Thus, water management in agriculture is always encouraged to meet the growing demand for food [3]. Therefore, it is necessary to design and implement efficient irrigation practices to reduce the amount of water required for irrigation water while sustaining or improving yield production.

Agriculturists need to know the crop-specific water requirement to obtain satisfactory crop yield and to avoid over or under irrigation [4]. This problem can be tackled with the adoption of smart farming and analytics, which can be a boon to Indian agriculture. Smart farming is the practice of using advanced Information and Communication Technologies (ICTs) to revolutionize the agricultural world. It promises to provide more sustainable and efficient agricultural output through its three main pillars: Internet-of-Things (IoT), cloud, and analytics. Analytics solutions make use of IoT, GPS technologies, Big Data, and Cloud Computing to generate pertinent data and provide actionable insights with the help of Artificial Intelligence (AI) algorithms. Figure 1.1 depicts the role of analytics in smart farming. Crop and seed selection, seed sowing, land preparation, crop growth monitoring, and irrigation requirements are a few applications of AI-assisted analytics in smart farming.

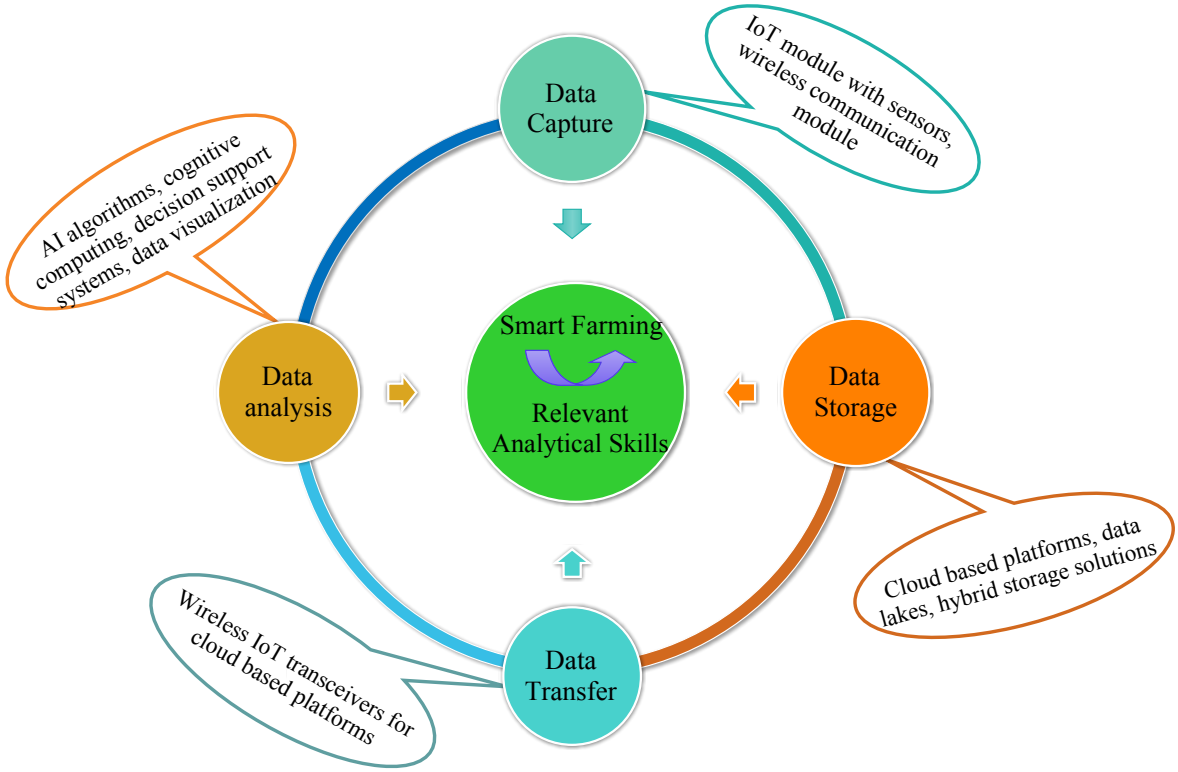

Figure 1.1: Role of analytics in smart farming (Modified from [1])

1.1 Background

The agricultural sector has a vital role in the economic development of a nation. The explosive growth in global population, climate change, and water scarcity have made it challenging to meet the ever-increasing food demand. Water scarcity has threatened sustainable development since food can not be grown without it. It is expected to affect approximately 1800 million people by 2050 [5]. Increasing population, industry, and agriculture demands put heavy pressure on water resources, contributing to water scarcity as shown in Figure 1.2. Despite this, climate change will further worsen the situation in the future.

The global population is expected to reach 9.7 billion by 2050, increasing the demand for healthy food and water [6]. Areas where food is grown, do not expand; therefore, agricultural cropping systems must make optimal use of limited available water and land resources to feed the world's growing population. Agriculture uses approximately 75-80% of available freshwater globally for irrigation purposes and is considered as a victim and reason for water scarcity.

Irrigation is the practice of applying water to the soil to increase agricultural growth, maintain landscapes, and revegetate damaged soils in arid regions during

periods of insufficient rainfall.

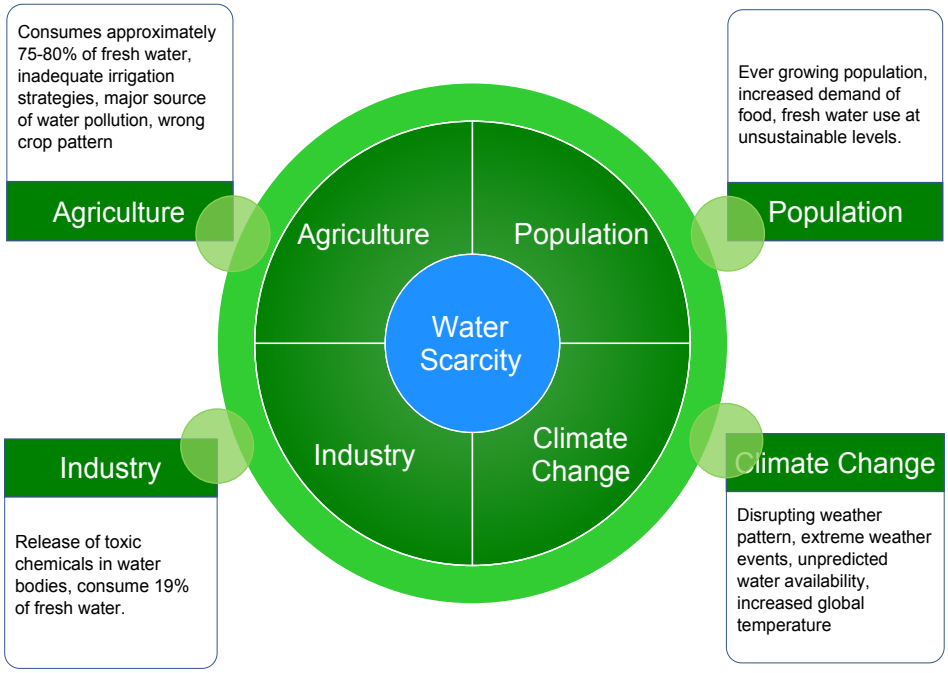

Figure 1.2: Major reasons of water scarcity

Approximately, 1.55×10^9 hectares of agricultural land cultivated globally accounts for around 11% of the Earth's entire land area and is expected to increase to 13% by 2050 [7]. Further, 17% of these agricultural areas are subject to irrigation management [8]. However, this relatively modest area equipped for irrigation may provide as much as 30–40% of global crop production [9]. It indicates that irrigated land is more likely to be the source of most of the increase in food production. However, 90% of agricultural water is consumed for irrigation purposes [10]. Therefore, due to the limited supply of water resources, rising demand for water from other sectors, and climate change, efficient use of available water resources for irrigation is becoming increasingly important.

In this context, efficient irrigation techniques are essential for maximizing water efficiency while maintaining crop yield and quality. Excessive water in the soil can impede root respiration, impact root growth, and cause soil degradation issues such as surface runoff, soil erosion, and nutrient leaching, in contrast, lack of water may result in a decrease in crop yield. In addition, improper irrigation techniques result in severe soil salinization, and climate change threatens to worsen this tendency in many regions. Over the past few years, the irrigation technologies have evolved

globally at a steady pace starting from manual irrigation to upcoming AI-assisted irrigation technology. This journey of evolution started from the first generation with the use of multi-client electronic hydrants. The variable frequency pump was a second-generation irrigation technology. The micro irrigation method was the third generation of irrigation technology but was only partially deployed due to the costly initial expenditure.

The fourth generation of irrigation technology was subsurface drip irrigation (SDI) which was developed to address the challenges of surface drip irrigation, particularly the issue of emitter clogging. Deficit irrigation was the fifth generation of irrigation technology which was developed to deliver less water without impacting crop yield [11] [12]. Intelligent irrigation systems based on AI are the current trend in providing cost-effective and efficient models for water management in agriculture.

1.2 Motivation

Evapotranspiration is a crucial part of the hydrological cycle and plays a vital role in sustainable water resource management. The accurate estimation of evapotranspiration is a prerequisite for irrigation scheduling and also for hydrological, climatological, and ecological research studies. Past studies have also concluded that evapotranspiration-based irrigation scheduling is the optimum choice among other irrigation scheduling methods [13]. This irrigation scheduling method is easy to deploy, economical, and fairly accurate. Moreover, it can be used without considering field conditions and require only meteorological and crop coefficient values.

Precise estimation of evapotranspiration is essential for designing, planning, and effectively implementing irrigation scheduling particulars in water-scarce areas to increase agricultural productivity. It can be measured directly using a lysimeter or eddy covariance. However, due to technical complexities and high cost, it is calculated using some empirical equations such as FAO-56 Penman–Monteith (FAO56-PM) or American Society of Civil Engineers Penman–Monteith (ASCE) equations. These equations require meteorological data (solar radiation, temperature, vapor pressure, humidity, and wind speed) as inputs and are widely accepted and used in various applications and research worldwide. However, the availability of these meteorological data is a challenging issue in developing countries. So, there is a need to develop a model that uses limited available climate data as input to predict ET_o with no compromise on estimation accuracy.

Recently, deep learning models have shown show high potential for time series

forecasting problems because of the ability to handle temporal structures such as trends and seasonality and learn temporal dependency. Deep learning models effectively address problems with massive amounts of data, multi- variate with complex relationships, and multi-step time series forecasting tasks. The problem of prediction of evapotranspiation values also exhibits the same characteristics, such as there exist complex non-linear relationships between multiple variables, and these variables follow time series behavior. Nevertheless, these methods are less widely applied to the evapotranspiration process. The above mentioned reasons motivate the proposal of novel deep learning-based approaches for predicting evapotranspiration to design intelligent irrigation scheduling.

1.3 Objectives

The following objectives were outlined:-

- To develop an approach for reference evapotranspiration estimation using deep learning techniques.
- To develop an approach for crop evapotranspiration of different crops using deep learning techniques.
- To evaluate the performance of the selected deep learning techniques.

1.4 Thesis Organization

Chapter 1: Introduction
The chapter 1 provides an overview of the current status of water scarcity and the requirement to design efficient irrigation strategies. Different irrigation scheduling techniques based on evapotranspiration, soil moisture, and crop water stress are discussed in detail. It also presents the role of AI in smart irrigation strategies. The chapter clearly elaborates the motivation behind development of deep learning-based water management techniques in agriculture and enlists the objectives of the present research work. The chapter ends with a discussion on the outline of the thesis.

Chapter 2: Literature Survey
The chapter 2 presents a detailed literature survey to outline the research efforts concerning the prediction of reference evapotranspiration and crop evapotranspiration using AI-based approaches. The chapter finally concludes with research gaps identified from the survey.

Chapter 3: Study Areas and Dataset

The chapter 3 describes the study areas and dataset used to conduct the research studies in the present research work. The geographical conditions of the three stations of Punjab: Ludhiana, Amritsar, and Patiala, are discussed. It also describes these stations' meteorological parameters using various statistical measures. The chapter also presents the wheat and rice crop dataset description.

Chapter 4: Hybrid Deep Learning Models for Reference Evapotranspiration (ET_0)

The chapter 4 presents two deep learning-based hybrid models, i.e., CNN-LSTM and Conv-LSTM to predict daily ET_o values of Ludhiana and Amritsar stations. It also addresses the data-scarcity issue by investigating different input combinations of meteorological parameters to predict ET_o. The chapter elaborates the methodology used and the performance evaluation parameters for the assessment of proposed hybrid DL models. Further, the results of the proposed hybrid models are evaluated and compared with existing temperature and radiation-based models.

Chapter 5: Deep Reinforcement Learning based Ensemble Approach for ET_o

The chapter 5 investigates a deep reinforcement learning-based ensembling approach to predict ET_o using limited meteorological parameters. It presents the background and preliminary information required to understand the proposed ensemble models. The ET_o process is represented as a mixed integer non-linear programming problem with the objective to minimize the mean square error. Further, the chapter discusses the four baseline models, i.e., CNN-LSTM, Conv-LSTM, CNN-XGB, and CNN-SVR, and the proposed methodology adopted to conduct the study. The experimental results and their comparison to existing ensemble approaches are thoroughly explained at the end of the chapter.

Chapter 6: Hybrid Models for Estimation of Crop Evapotranspiration (ET_c)

The chapter 6 introduces two hybrid models, i.e., CNN-SVR and CNN-XGB, for the prediction of daily ET_c values of wheat and rice crops. The study is conducted at Ludhiana station, and general circulation models (GCMs) are used to generate future climate data of the station to observe the future water requirements of both crops. It also elaborates the development of the proposed models to predict daily ET_c values and the model evaluation parameters to examine the performance of proposed hybrid models. The chapter demonstrates the results obtained from the conducted research study and concludes the chapter.

Chapter 7: Conclusions and Scope for Further Work

The chapter 7 summarizes the contribution of the research work and highlights the key findings. Moreover, the chapter also discusses the issues that are yet to be addressed along with the potential future directions.

Chapter 2

Literature Review

This chapter provides an exhaustive review of the literature related to Artificial Intelligence approaches used for the prediction of reference and crop evapotranspiration.

2.1 Overview

Efficient irrigation scheduling is considered as one of the key components governing smart agricultufre. Under or over-irrigation causes yield loss, crop stress, nutrient leaching, and water loss. Therefore, the need for intelligent irrigation scheduling techniques is critical to deal with the aforementioned issues. Artificial Intelligence acts as a game-changer in designing and optimizing intelligent irrigation scheduling techniques for smart agriculture. The AI-centred approach carries enormous potential in estimating water requirements and the right time and place of irrigation.

Evapotranspiration is a crucial part of the hydrological cycle and plays a vital role in the sustainable water resource management [14] [15] [16] [17]. The accurate estimation of evapotranspiration is a prerequisite for irrigation scheduling as well as for hydrological, climatological, and ecological research studies [18]. The past few decades have experienced the development of various artificial intelligence-based techniques to model, predict and optimize the evapotranspiration prediction process. The following section presents an in-depth analysis of the role of AI in predicting evapotranspiration and design AI-enabled intelligent irrigation scheduling techniques.

2.2 AI/ML enabled ET_o Prediction Models

This section provides different AI models such as evolutionary and neuro-fuzzy, machine learning, neural network, and deep learning, and hybrid models used in past studies to predict ET_o values.

2.2.1 Evolutionary and Neuro-Fuzzy Models for ET_o Prediction

Evolutionary Computation (EC) methodologies are inspired by nature and address optimization problems in a randomized manner. These methodologies can provide a reliable and effective solution to solve complex issues in real-world applications. Also, Neuro-fuzzy systems are fuzzy systems created using a learning method based on a neural network. This section provides an overview of the recent literature regarding the applications of evolutionary computing and neuro-fuzzy approaches in modeling the evapotranspiration process. Table 2.1 summarizes the state-of-art evolutionary and neuro-fuzzy models for ET_o prediction.

Baba *et al.* [19] evaluated both Artificial Neural Network (ANN) and ANFIS model for ET_o prediction. The findings of their study revealed that both models could provide reliable accuracy using available climate data, and further the performance of both the models decreased by using the estimated R_s value. Kisi *et al.* [20] examined the potential of Subtractive Clustering-based Fuzzy Inference System (S-ANFIS) and Grid Partition-based Fuzzy Inference System (G-ANFIS) for modeling daily ET_o in the Mediterranean climate region of Turkey. Authors found that both ANFIS models achieved reliable results compared to empirical models using three to four input parameters. However, empirical models with two climate parameters performed better than two input ANFIS models.

ANFIS model have been used to identify most influential climate parameters for the estimation of ET_o in the study conducted by Petkovic´ *et al.* [21]. Authors identified SSH, vapory pressure (VP), and T_{min} as the most important parameter and further found that T_{max} and RH are the optimal input combination for two input parameters combination. Further, Keshtegar *et al.* [22] evaluated the ANFIS model by dividing data points to k-subset using uniform selection for daily ET_o prediction and comparison to ANN and M5Tree models revealed the superiority of subset-ANFIS model. Zakhrouf *et al.* [23] also investigated two types of neuro-fuzzy models, i.e., subtractive clustering model (S-ANFIS) and fuzzy C-means clustering model (F-ANFIS) to estimate daily ET_o under semi-arid climate region. The statistical measure shows that S-ANFIS outperformed F-ANFIS.

Genetic expression programming (GEP) is a logical progression of genetic programming (GP) and genetic algorithms (GA), and it uses symbolic regression to generate mathematical models. GEP generates non-linear entities (computer programs) represented in relatively basic linear string structures. The contribution of

GEP in developing an expression for ET_o estimation is widely explored [24]. Traore *et al.* [25] used public weather forecast data to forecast one week ET_o values using the GEP model. Authors suggested that by using general weather data (temperature data), reliable estimation of ET_o values is possible to plan irrigation scheduling.

Shiri [26] also conducted study using GEP for ET_o prediction. The performance of GEP model was compared to empirical models (Hargreaves, Turc, Priestley-Taylor, and Kimberly-Penman) for the similar input combination of temperature, radiation, and humidity. The obtained results demonstrated the superiority of the GEP model over empirical models. A similar study was also conducted to examine the suitability of GEP models for predicting ET_o using limited input data by Matter [27]. The author further compared the performance of GEP to empirical models, and it was observed that GEP yielded better results. Mattar and Alazba [28], extended this study by comparing GEP with multiple linear regression (MLR) models and other empirical models. According to this study, GEP turned out to be a powerful tool compared to all other models in case of an incomplete dataset.

Valipour *et al.* [29] examined the potential of GA and GEP on four different climate regions (arid, semiarid, very humid, and Mediterranean) for estimating ET_o. They concluded that GEP provides reliable accuracy using a minimal dataset for all climate regions. The right training/testing data selection is a crucial challenge in applying AI models. Kazemi *et al.* [30] compared various hold-out and k-fold validation temporal data partitioning strategies to estimate daily ET_o in arid region using GEP approach. They found that k-fold validation provides the lowest overestimation and underestimation of ET_o values.

Finally, it can be concluded that GEP models were proven capable of expressing physical phenomena of ET_o process into the mathematical form using less meteorological data. These models also show superiority over empirical models and claim to be alternatives to empirical models. ANFIS models combined with clustering and partitioning algorithm could deliver reliable performance and also show better results as compared to the ANN model using the same dataset in [22]. The real benefit of fuzzy logic-based models over ANN is that they allow for a more linguistic description of the data. Moreover, the studies mentioned above focused on providing a solution to the non-linear complex ET_o modeling process using a limited meteorological parameter to handle data-scarce situations. These studies identified different input combinations of meteorological parameters in other climate regions, confirming that factors affecting ET_o process depends on the type of climate or environment.

Table 2.1: Summary of evolutionary and neuro-Fuzzy models for ET_o prediction

Author (s)	**Climate region**	**Time stamp**	**Input parameters**	**Models**	**Input combination**
Pour-Ali Baba *et al.* [19]	Temperate	Daily	T, RH, SSH, WSP, R_s	ANFIS, ANN	T, RH, SSH, WSP; T, SSH
kisi *et al.* [20]	Mediterranean	Daily	T, R_s, WSP, RH	ANFIS-GP, ANFIS-SC	T, R_s; T, R_s, RH
Petkovic *et al.* [21]	Moderate-continental	Monthly	T_{min}, T_{max}, SSH, VP, RH_{max}, RH_{min}, WSP	ANFIS	SSH, VP, T_{min}; T_{max}, RH
Keshtegar *et al.* [22]	Semi-arid	Daily	T_{min}, T_{max},RH, WSP, R_s	ANN, M5Tree, subset ANFIS	T_{min}, T_{max}, RH, WSP, R_s
Zakhrouf *et al.* [23]	Semi-arid	Daily	T, RH, SSH, WSP	S-ANFIS, F-ANFIS , MLR	T, RH, SSH, WSP
Traore *et al.* [25]	Humid subtropical	Daily	T_{min}, T_{max}, SSH, RH, WSP	GEP	T_{min}, T_{max}
Shiri *et al.* [26]	Hyper-arid	Daily	T_{min}, T_{max}, R_s, RH ,WSP	GEP	T_{min}, T_{max}, WSP
Mattar [27]	Subtroical zone	Monthly	T_{min}, T_{max}, RH, WSP, R_s	GEP	T_{min}, T_{max}, RH, WSP

Author (s)	**Climate region**	**Time stamp**	**Input parameters**	**Models**	**Input combination**
Mattar and Alazba [28]	Subtroical zone	Monthly	T_{min}, T_{max}, R_s, WSP, RH	GEP, MLR	T_{min}, T_{max}, RH, WSP
Valipour *et al.* [29]	Arid, Mediterranean, Semi-arid, Humid	Monthly	R_s, RH, T_{min}, T_{max}, WSP, R_a	GA, GEP	Arid- T_{meann}, WSP; Mediterranean, Semi-arid - T_{min}, T_{max}; Humid - T_{meann}
Kazemi *et al.* [30]	Arid	Monthly	T_{min}, T_{max}, RH, R_s, WSP, P	GEP	T_{min}, T_{max}, R_s

2.2.2 Conventional Machine Learning Models for ET_o Predictions

ET_o can be expressed as a complicated multivariate non-linear regression process that is dependent on a large number of meteorological parameters. A significant number of environmental factors interact with ET_o in a complex way, implying the need for high-dimensional feature space to define the non-linear changes in ET_o with regard to changes in diverse environmental parameters. Therefore, it is difficult to create comprehensive empirical models that accurately describe all of the complicated processes. Machine learning techniques can overcome this problem, which can represent complex and non-linear interactions between inputs and output.

As a result, researchers have proposed machine learning techniques for ET_o estimation since these models do not require knowledge of internal variables and provide easy solutions for non-linear and multi-variable functions. This subsection provides insights into the contribution of ML techniques for ET_o modeling process in literature. Four types of ML models have been widely used in past studies: non-linear regression models, tree-based regression models, kernel-based regression models, and machine learning-based ensemble models. The contribution of neural networks has not been covered in this subsection and will be discussed separately in the following subsection. Table 2.2 summarizes the contribution of ML models for ET_o prediction.

Non-linear regression models are preferable to other AI approaches such as ANFIS, ANN, and Support Vector Machine (SVM) since they have less complexity. Furthermore, these models provide us with formulas or relationships to work with an acceptable level of accuracy. Khoshravesh *et al.* [31] attempted to use multivariate fractional polynomial (MFP), robust regression and Bayesian regression to predict ET_o in three semi-arid climate regions of Iran. The findings of this study stated that the accuracy of the MFP model was higher than the other two regression approaches, and also with the use of only T_{mean} and R_s, acceptable accuracy could be achieved.

Reis *et al.* [32] recommended multiple linear regression model over ANN and Extreme Learning Machine (ELM) model. The authors attempted to model ET_o using AI models (ANN, MLR, and ELM) by considering only temperature data as input in five semi-arid regions of Brazil. Further, the performance of these models was evaluated using local data of each station and pooled data of all five stations. They found out that all models provided more accurate results than the Hargreaves model in both scenarios, but MLR was recommended as it was easier to use than

the other two models.

The tree-based regression models have also gained popularity due to their high computational speed and satisfactory performance. These models are also explored in ET_o prediction. Kisi [33] introduced the M5 Model Tree (M5tree), Multivariate Adaptive Regression Splines (MARS), and Least Square Support Vector Regression (LSSVR) for modeling monthly ET_o. They further evaluated the proposed models to provide reliable results using cross-station data. It was reported that M5Tree could act as the best alternative approach for ET_o modeling over other proposed models and empirical models (Valiantzas and HS model) in the absence of local input and output data.

Feng *et al.* [34] evaluated the applicability of the Random Forest (RF) and Generalized Regression Neural Network (GRNN) model for predicting ET_o values using two input scenarios: only temperature data and complete data. It was observed that using temperature data, both RF and GRNN could provide reliable accuracy. However, the RF model provided slightly better performance than the GRNN model. RF model also performed better in study conducted by Niaghi *et al.* [35]. Authors applied GEP, SVM, Linear Regression (LR) and RF using three combinations of input data: T_{max}, T_{min}; T_{max}, T_{min}, WSP; and R_s, T_{max}, T_{min}. Results showed the superiority of RF model using input combination of R_s, T_{max}, T_{min} parameters.

Ponraj *et al.* [36] further analyzed three ML models, i.e., RF, Gradient Boost Regression (GBR) and MLR for ET_o modeling with or without using preprocessing techniques. They found out that preprocessed GBR model provided better results than the other two models. Moreover, they reported that the influence of soil temperature data was negligible for the estimation of ET_o. Fan *et al.* [37] evaluated four regression trees (RF, M5Tree, Gradient Boosting Decision Tree (GBDT) and XGBoost) against SVM and ELM model for modeling daily ET_o values using different combinations of meteorological data in different climate zone of China. Their findings indicated that R_s was the most important parameter than WSP and RH, and reliable accuracy could be achieved using tree-based models: GBDT and XGBoost in different climate zone of China.

This study was further extended by Fan *et al.* [38]. The authors introduced Light Gradient Boosting Machine (LightGBM) for predicting daily ET_o in the humid subtropical region. They compared the results to empirical and traditional tree-based ML models such as M5Tree and RF. The LightGBM is an enhanced gradient learning framework that uses decision trees and the concept of 'weak 'learners. Further,

the potential of LightGBM for ET_o prediction using cross-station meteorological data was also assessed. LightGBM was observed to be effective and generalizable using both local and cross-station data.

Huang [39] compared a newly introduced gradient boosting model called CatBoost to well-known ML models (SVM and RF) for estimating ET_o in the subtropical humid climate region of China. Statistical measures proved the superiority of CatBoost over SVM and RF models. It was also reported that two input combinations of climate data (T_{min}, T_{max}, R_s or T_{min}, T_{max}, WSP, RH) could be used for data scarcity situation to obtain reliable results. In addition to it, Catboost also showed less computational cost as compared to SVM and RF models.

Granata [40] performed a comparative study of four ML models, such as the M5P Regression Tree, Bagging, RF, and Support Vector Regression (SVR), to evaluate their capability for modeling ET_o in humid subtropical climate zone. Four different combinations of input climate data were used, and results indicated that except SVR, all other three models provided accurate results using R_s, sensible heat flux, soil moisture content (SMC), WSP, RH, and air temperature (T). Kisi *et al.* [41] proposed a novel regression model called Radial Basis M5 Model Tree (RM5Tree) and compared it with traditional M5Tree and Response Surface Method (RSM), Multi-Layer Perceptron Neural Networks (MLPNN) and Radial Basis Function Neural Network (RBFNN) models. They take three different input data combinations, and the results revealed the superiority of RM5Tree over other models using T_{mean}, R_s, WSP, and RH as the input parameter.

Mehdizadeh *et al.* [42] compared sixteen empirical models with four AI models (GEP, MARS, SVM-poly, SVM-RBF) for the estimation of monthly ET_o values. They found that MARS and SVM-RBF outperform other AI and empirical models. It is also concluded that R_s showed a higher impact on the accuracy of ET_o than R_n, and combining WSP with other input combinations enhanced the performance than using WSP as a sole input parameter. Pour *et al.* [43] showed the superiority of the SVM model over ANFIS and GEP for simulating monthly ET_o values in an arid region of Iran. Moreover, they suggested using the proposed approach in case of the unavailability of sunshine hours and relative humidity.

This study was further supported by Chia *et al.* [44]. They recommended SVM over other existing empirical models using the same input dataset. Seifi *et al.* [45] proposed hybrid model using Least Square Support Vector Machine with Gamma Test (LSSVM-GT) for the estimation of ET_o. Gamma test revealed that T_{min}, T_{max}

and WSP are main influential parameters. Comparison with other models such as ANN, ANFIS, and empirical models proved that LSSVM performed better using the gamma test in the arid region of Iran.

Ensemble learning-based approaches have also gained researchers' interest in modeling evapotranspiration process since these approaches are typically more stable, perform better, and have reduced computing costs. Manikumari *et al.* [46] proposed ensemble learning approach to combine ANN models for daily ET_o estimation. They reported that ensemble models achieved better performance than individual ANN models. Salam *et al.* [47] proposed two new ensemble learning-based models: Random Tree (RT), Bagging, and Random Subspace (RS) for ET_o prediction in the subtropical humid climate region of Bangladesh and compared the performance of these models to RF and SVM model. Statistical measures indicated that RT and RF provided better performance. Further, it was observed that R_s and WSP were most influenced parameters and combination of R_s, T_{min} and T_{max} provided satisfactory results and R_a, T_{min} and T_{max} were found as least input combination for ET_o estimation. Nourani *et al.* [48] employed linear ensemble (simple and weighted average) and non linear ensemble (neural ensemble) approaches. They reported that neural-based ensemble performed better than SVR, ANFIS, ANN, and MLR models for estimating single and multi ahead ET_o.

Martín *et al.* [49] further proposed a stacked-based learning approach to predict evapotranspiration using meteorological data of twenty stations of Spain. They used SVM, RF, GBM, and XGBoost as first-level predictors and XGBoost as second-level predictors. Further, the performance of the newly developed ensemble model was compared to state-of-art models (SVM, RF, XGBoost, GBM, ELM, MARS, and LASSO) and empirical models (temperature-based, radiation-based, and mass-energy transfer based). They reported that the stack-based ensemble approach could address the problem of variation in performance with the change in environment conditions (using different datasets) as it shows less variation in performance than other compared models.

The review of publications in this subsection revealed that traditional ML models had been effectively employed to predict ET_o values. Moreover, these models proved less costly in terms of computational cost. Also, ensembled learning approaches were used to address the issue of variation in the performance of ML models for different types of datasets. However, a continuous effort was made to develop AI models using the limited meteorological dataset to provide better performance than empirical models.

Table 2.2: Summary of conventional machine learning models for ET_o prediction

Author (s)	**Climate region**	**Time stamp**	**Input parameters**	**Models**	**Input combination**
Khoshravesh *et al.* [31]	Arid	Monthly	T_{mean}, R_s, RH, WSP, precipitation (Pr)	MFP, Robust regression and Bayesian regression	T_{mean}, R_s
Reis *et al.* [32]	Semi-arid	Daily	T_{min}, T_{max}, RH, SSH, WSP	ELM, ANN, MLR	T_{min}, T_{max}
kisi *et al.* [33]	Mediterranean	Monthly	T_{mean}, R_s, RH, WSP	LSSVR, MARS, M5 Tree	T_{mean}, R_s, RH, WSP
Feng *et al.* [34]	Humid	Daily	T_{min}, T_{max}, R_s, RH, WSP	RF, GRNN	T_{min}, T_{max}, R_a
Niaghi *et al.* [35]	Continental climate	Daily	T_{min}, T_{max}, R_s, WSP	GEP, SVM, LR, RF	T_{min}, T_{max},R_s
Ponraj *et al.* [36]	Arid sub-tropical	Daily	T_{min}, T_{max}, R_s, RH, WSP	MLR, RF, GBR	T_{min}, T_{max}, R_s, RH, WSP
Fan *et al.* [37]	Temperate continental; Temperate monsoon; Mountain plateau; Subtropical monsoon; and Tropical monsoon	Daily	R_s, RH, T_{min}, T_{max}, WSP, R_a	RF, M5Tree, GBDT, XGBoost	T_{min},T_{max},R_s-Tropical and Subtropical zones; T_{min}, T_{max}, R_a, WSP, RH- Temperate continental; Mountain plateau, Temperate monsoon zones

Author (s)	Climate region	Time stamp	Input parameters	Models	Input combination
Fan *et al.* [38]	Humid subtropical	Daily	T_{min}, T_{max}, SSH, R_a, RH, WSP , R_s	LightGBM, RF, M5Tree	T_{min}, T_{max}, R_s
Huang [39]	humid	Daily	R_s, T_{min},T_{max} WSP, RH	CatBoost, RF, SVM	T_{min}, T_{max}, R_s ; T_{min},T_{max} WSP, RH
Granata [40]	Humid subtropical	Daily	R_s, sensible heat flux (H), SMC, WSP, RH, T_{mean}	M5P Regression Tree, Bagging, RF, SVR	T, RH, R_n
kisi *et al.* [41]	Mediterranean	Daily	T, RH, R_s, WSP	RM5Tree, M5Tree, RSM, MLPNN, RBFNN	T, RH, R_s, WSP
Mehdizadeh *et al.* [42]	Arid, Semi-arid	Monthly	T, RH, R_s, WSP, VP, R_a	MARS, SVM-RBF, SVM-poly GEP	T, RH, R_s, WSP
Pour *et al.* [43]	Arid	Monthly	T, RH, SSH, WSP	SVM, ANFIS and GEP	T, RH, SSH, WSP
Chia *et al.* [44]	Tropical	Daily	T_{min}, T_{max}, RH, R_s	SVM	T_{mean},R_s

Author (s)	**Climate region**	**Time stamp**	**Input parameters**	**Models**	**Input combination**
Seifi *et al.* [45]	Arid	Daily	T_{min}, T_{max}, RH, SSH, WSP, Pr, T_{dew}, R_s	LSSVM-GT, ANN-GT, ANFIS-GT, ANFIS and ANN	T_{min}, T_{max}, WSP
Manikumari *et al.* [46]	Arid, Semi-arid	Monthly	T_{min}, T_{max}, RH, R_s, WSP, SSH	bagged-NN, boosted-NN and ANN	T_{min}, T_{max}, RH, R_s, WSP, SSH
Salam *et al.* [47]	Subtropical humid	Daily	T_{min}, T_{max}, RH, WSP, SSH, R_a	SVM, RF, RT, Bagging and Random Subspace (RS)	T_{min},T_{max},R_s
Nourani *et al.* [48]	Semi-arid, Humid, Subtropical, Mediterranean	Monthly	T_{min}, T_{max}, T_{dew}, P, WSP, Pan Evaporation(Ep) RH, Surface Pressure (Sp)	ANFIS, ANN, SVR, MLR	T_{min}, T_{max}, T_{dew}, P, WSP, RH, Ep and Sp
Martín*et al.* [49]	Arid, continental, Mediterranean	Daily	T_{min}, T_{max}, WSP, RH, R_s	Stacked Ensemble, SVM, RF, GBM, XGBoost, ELM, MARS, LASSO	T_{min}, T_{max}, WSP, RH, R_s

2.2.3 Neural Network and Deep Learning Models for ET_o Predictions

ANNs have been widely used in hydrological modeling over the last two decades due to their capacity to map the input and output connection without comprehending the physical process. An artificial neural network model is a mathematical model with highly interconnected processing units structured in layers that is substantially equivalent to the learning potential of the human brain. The most fundamental technique for creating an artificial neural network-based model of system behavior is to train the network using system samples. Recently, many publications employed ANN to simulate the reference evapotranspiration process. Some of the recent articles with significant contributions in this field are discussed in this subsection. Table 2.3 summarizes these research studies in brief.

Laaboudi *et al.* [50] investigated the effectiveness of ANN to estimate ET_o using incomplete dataset and compared the results to MLR model. It was reported that the MLR model could also predict ET_o at desirable accuracy. However, ANN has overcome the issue of multi-colinearity problem present in MLR. Kim *et al.* [51] investigated the performance of neural networks in predicting monthly ET_o using the bootstrap resampling technique on the GRNN (GRNN-backpropagation algorithm (GRNN-BP), Bootstrap GRNN-GA (BGRNN-GA)). The analysis revealed that increasing the quantity of the training data via bootstrapping could not enhance the GRNN models significantly. Further, the generalization ability of ANN and M5 tree model for modeling ET_o was investigated by Kisi and Kilic [52]. The authors concluded that the M5 tree model and the ANN could give excellent ET_o estimation when trained and tested locally. However, reliable accuracy could not be achieved without training and testing these models at different stations. The performance comparison of ANN with GEP was also performed by Yassin *et al.* [16] in their study. They evaluated the performance of ANN and GEP model to predict ET_o in the arid region of Saudi Arabia. The result demonstrated that the ANN model performs slightly better using an incomplete data set.

An attempt to use easily available public weather forecast data to estimate ET_o was made by Traore *et al.* [53]. They employed neural network-based four models named Generalized Feedforward (GFF), Linear Regression Network (LRN), Multilayer Perceptron (MLP), and Probabilistic Neural Network (PNN) using limited data (T_{max}, T_{min}, R_s, and R_a) retrieved from public weather forecast data. They concluded that more reliable results were obtained when R_s was used with temperature data instead of R_a. However, the authors concerned about the reliability of the

public weather data for the acceptability of the proposed approach. The best architecture of the ANN model in the sub-humid environment was identified by Nema *et al.* [54]. They compared ET_o values generated with FAO-56 PM to different ANN models, which included a variety of training functions and neuron numbers. They reported that the ANN trained using the Levenberg–Marquardt algorithm with nine neurons in a single hidden layer produced the best estimation results.

Researchers were constantly exploring ANN models for ET_o prediction from different perspectives. For instance, a study conducted by Antonopoulos *et al.* [55] showed that the ability of ANN to predict ET_o was dependent on the training and testing dataset samples. They trained ANN using different combinations of meteorological data and compared the results with existing empirical models. Results revealed that there was a significant effect on ANN accuracy by changing the training year; therefore, it was evident that training data affected the ANN simulation. Further, the superiority of ANN to ANFIS and GEP was also examined by Gavili *et al.* [56] for estimating ET_o in the continental climate region, Iran. They employed three artificial intelligence models (ANN, ANFIS, and GEP) and five empirical models, in which ANN produced the best predictions. In another study, Kaya *et al.* [57] compared MLP to other AI models such as SVM and MLR for predicting ET_o. Findings concluded that MLP performs better using a double combination of T-R_s and T-RH.

The most recent advancement in artificial intelligence models contributed to the introduction of the Extreme Learning Machine as an ANN option. Extreme Learning Machine is a quick learning technology that employs single-hidden layer feedforward neural networks to achieve excellent generalization performance. This variant of ANN was initially used to predict ET_o in Iraq by Abdullah *et al.* [58], where the authors claimed that this geographical area mirrored general atmospheric and geographical circumstances. The study reported that ELM provides accurate results using complete and incomplete datasets.

The success achieved by Abdullah *et al.* [58] gained the attention of other researchers to investigate further ELM for predicting ET_o in other climate regions. Feng *et al.* [59] attempted to evaluate the performance of ELM over other hybrid neural network models. They estimated ET_o using ELM, Genetic Algorithm Optimized by Backpropagation Neural Networks (GANN), and Wavelet Neural Networks (WNN) models. They found that ELM and GANN models provided equivalent performance using limited data and could be highly recommended in this scenario than other temperature-based empirical models. This study was further extended by

Gocic *et al.* [60]. They compared the performance of ELM in modeling monthly ET_o to empirical models such as adjusted Hargreaves, Priestley–Taylor, and Turc methods. They concluded that ELM could be a better alternative with limited data availability.

Patil and Deka [61] also proved the superiority of ELM over other AI models such as ANN and LS-SVM for predicting ET_o values. They used different input combinations of another station's temperature data and ET_o values. It was reported that using local temperature data and ET_o values of another station, ELM outperformed the Hargreaves model and could be recommended for weekly ET_o prediction. A comparable study conducted by Kumar *et al.* [62] demonstrated the advantages of ELM in terms of accuracy and computational speed over SVM, ANN, and genetic programming (GP) for modeling the ET_o process in the humid subtropical region of India.

The introduction of the multi-linear perceptron and extreme learning machines in the field of hydrology has also encouraged to explore another variation of the ANN model. The Generalized Wavelet Neural Networks (GWNN), Radial Basis Neural Network (RBNN) and GRNN are examples of it. Feng *et al.* [63] introduced a new approach to generalize the ability of ELM and GRNN in modeling the ET_o process using cross-station meteorological data (temperature data only). They trained both models in two scenarios: pooled and local data from six stations in China. Results revealed that both the models performed better in the case of pooled data training than training these models on regional data of stations. However, ELM was slightly more efficient in the local scenario, while the GRNN model performed well in the pooled system.

Banda *et al.* [64] performed comparative analysis of neuro-computing models (ANFIS, RBNN, GRNN and MLP) for predicting ET_o values. WSP and R_s were found as dominating parameters that affect the accuracy of ET_o. GRNN model was further compared to other AI models by Sanikhani *et al.* [65]. They used different AI models (GRNN, MLP, ANFIS-GP, ANFIS-SC, and GEP) to perform temperature-based modeling of ET_o for the Mediterranean region of Turkey. They compared these models to Hargreaves–Samani and its calibrated version and found that GRNN and GEP models provided better accuracy. Bellido-Jim'enez *et al.* [66] introduced new climate parameters called $Energy_T$ and Hourmin, based on temperature data only and also compared six AI models (MLP, GRNN, ELM, SVM, RF, and XGBoost) for modeling ET_o using these climate parameters in five different semi-arid regions of Andalusia. Results revealed that the newly introduced parameters could provide

reliable accuracy in regions where data is not easily available. Adamala *et al.* [67] investigated the GWNN for modeling ET_o process in four different climate zones (semi-arid, arid, humid and sub-humid). Further, the generalization ability of the GWNN model was compared to GANN, GWR, and GLR models, and the results showed that GWNN and GANN models provided accurate results in all climate zones.

Deep learning has received much attention in the past few years and has been used in various fields, outperforming conventional machine learning models and attaining state-of-art results. DL models also efficiently handle multivariate time series problems with massive data. Therefore, they have been explored to estimate ET in many recent studies. Recently, many research studies have focused on the potential of deep neural network models to predict ET. These research studies are briefly summarised in Table 2.4. Saggi *et al.* [68] used H_2O framework to develop Gradient Boosting Machine (GBM), Generalized Linear Model (GLM) and RF and deep learning model for estimation of ET_o and observed that DL model outperform all models using T_{min},T_{max}, R_s, RH, WSP, and SSH in semi-arid region of India. Chen *et al.* [69] examined DNN, CNN, and LSTM in predicting daily ET_o with limited meteorological data and proposed different combinations of meteorological parameters with reasonable accuracy.

Yin *et al.* [70] has reported the use of Bidirectional-LSTM (Bi-LSTM) for predicting daily ET_o in a arid region of China. Ferreira and da Cunha [71] examined the potential of LSTM, one-dimensional CNN, and a combination of LSTM-CNN, as well as ML models (ANN and RF) for predicting daily ET_o in the arid region of Brazil. They concluded that the proposed DL models outperformed ML models. Lucas *et al.* [72] employed ensemble CNN models to solve the ET_o time series problem in the subtropical region of Brazil. They conclude that CNN models outperform seasonal autoregressive integrated moving average (SARIMA) and seasonal Naive time series models. The study conducted by Nagappan *et al.* [73] shows the superiority of the Deep Learning Neural Network (DLNN) model to the RBFNN model with a reduced feature set of climate data to estimate ET_o. Granata *et al.* [74] explored LSTM and Nonlinear autoregressive exogenous (NARX) for modeling ET_o in different climatic conditions. It was observed that the NARX model performs well in the semi-arid region while LSTM outperforms NARX in humid subtropical climate conditions. Roy *et al.* [75] utilized decision theory based on Shannon's entropy to select best DL model among LSTM, Bi-LSTM, sequence-to-sequence regression (SSR-LSTM) and ANFIS for ET_o prediction and observe that Bi-LSTM outperformed all other DL models.

Table 2.3: Summary of neural network models for ET_o prediction

Author (s)	**Climate region**	**Time stamp**	**Input parameters**	**Models**	**Input combination**
Laaboudi *et al.* [50]	Subtropical desert	Daily	T_{mean}, RH, WSP, Insolation	ANN, MLR	T_{mean}, RH, WSP
Kim *et al.* [51]	Humid subtropical	Monthly	T, R_s, WSP, RH, T_{dew}, VP, soil temperature (ST)	GRNN-GA, GRNN-BP, BGRNN-GA	T_{min}, T_{max}, R_s
Kisi and Kilic [52]	Mediterranean	Daily	T, R_s, WSP, RH	ANN, M5Tree	T_{min}, T_{max}, R_s
Yassin *et al.* [16]	Arid	Daily	T_{min}, T_{max}, T_{mean}, RH_{min}, RH_{max}, WSP, SSH, R_s, h_c	ANN, GEP	T_{min}, T_{max}, T_{mean}, RH_{min}, RH_{max}, WSP, SSH, R_s, h_c
Traore *et al.* [53]	Humid subtropical	Daily	T_{min}, T_{max}, R_a, R_s	GFF, LR, MLP, PNN	T_{min}, T_{max}, R_s
Nema *et al.* [54]	sub-humid	monthly	T_{min}, T_{max}, RH, SSH, Rainfall	ANN	T_{min}, T_{max}, RH, SSH, Rainfall

Author (s)	**Climate region**	**Time stamp**	**Input parameters**	**Models**	**Input combination**
Antonopoulos *et al.* [55]	Mediterranean	Daily	T_{mean}, RH, R_s, WSP	ANN	T_{min}, T_{max}, R_s
Gavil *et al.* [56]	Continental	Monthly/ Daily	T_{min}, T_{max}, RH, SSH, WSP	ANN, ANFIS and GEP	T_{min}, T_{max}, RH, SSH, WSP
kaya *et al.* [57]	Humid continental	Daily, Monthly	T_{mean}, RH, WSP , R_s	SVR, MLP*, MLR	T_{mean}, R_s; T_{mean}, RH
Abdullah *et al.* [58]	Mediterranean, Semi-arid	Monthly	T_{min}, T_{max}, WSP, RH, R_s	ELM	T_{min}, T_{max}, R_s
Feng *et al.* [59]	Humid	Daily	T_{min}, T_{max}, R_s, WSP, RH	ELM, GANN, WNN	T_{min}, T_{max}, R_s
Gocic´ *et al.* [60]	Humid continental	Monthly	T_{min}, T_{max}, WSP, VP, SSH, R_a	ELM	T_{min}, T_{max}, R_a
Patil and Deka [61]	Arid	Weekly	T_{min}, T_{max}, WSP, R_a, RH, R_s	ELM , ANN, LS-SVM	T_{max}, T_{min}, R_a and ET_o values of another station

Author (s)	Climate region	Time stamp	Input parameters	Models	Input combination
Kumar *et al.* [62]	Humid sub-tropical	Daily	T_{min}, T_{max}, SSH, RH, P	SVM, ELM, ANN, GP	T_{min}, T_{max}, SSH, RH, P
Feng *et al.* [63]	Warm and humid	Daily	T_{min}, T_{max}, WSP, SSH, RH, R_s	GRNN and ELM	T_{min}, T_{max}
Banda *et al.* [64]	Arid, Semi-arid	Daily	T_{min}, T_{max}, R_s, WSP, RH	MLP, RBNN, GRNN, ANFIS	T_{min}, T_{max}, R_s
Sanikhani *et al.* [65]	Mediterranean	Monthly	R_s, RH, T_{min}, T_{max}, WSP, R_a	GRNN*, MLP, ANFIS-GP ANFIS-SC, GEP	T_{min}, T_{max}, R_a
Bellido-Jim´enez *et al.* [66]	Semi-arid	Daily, Monthly	T_{min}, T_{max}, R_a	MLP, GRNN, ELM, SVM, RF, XGBoost	T_{min}, T_{max}, R_a
Adamala *et al.* [67]	Semi-arid, Arid, Humid, Sub-humid	Daily	T_{min},T_{max} RH, R_s, WSP	GWNN, GANN, GWR, and GLR	T_{min}, T_{max} RH, R_s, WSP

Table 2.4: Summary of deep learning models for ET_o prediction

Author (s)	**Climate region**	**Time stamp**	**Input parameters**	**Models**	**Input parameters**
Saggi *et al.* [68]	Semi-arid	Daily	R_s, RH, T_{min}, T_{max}, WSP, SSH	DL, GBM, GLM, and RF	R_s, RH, T_{min}, T_{max}, WSP, SSH
Chen *et al.* [69]	Warm temperate	Daily	T_{min}, T_{max}, RH, R_s, R_a,	TCN, LSTM, DNN, RF, and SVM	T_{min}, T_{max}, T_{mean}, R_a ; T_{min}, T_{max}, T_{mean}, R_s,R_a
Yin *et al.* [70]	Arid	Daily	T_{min}, T_{max}, SSH, R_a, RH, VP, weather type	BiLSTM	T_{min}, T_{max}, SSH
Ferreira and da Cunha *et al.* [71]	Arid	Daily	T_{min}, T_{max}, RH, WSP, SSH, $ET_{0_{t-1}}$	CNN, LSTM, ANN, CNN-LSTM, RF	T_{min}, T_{max}, RH, WSP, SSH, $ET_{0_{t-1}}$
Lucas *et al.* [72]	Subtropical	Daily	T_{min}, T_{max}, SSH, RH, WSP	CNN, SARIMA	T_{min}, T_{max}, SSH, RH, WSP
Roy *et al.* [75]	Sub-tropical	Daily	T_{min}, T_{max}, RH, WSP, SSH	BiLSTM, LSTM, SSR-LSTM, ANFIS	T_{min}, T_{max}, RH, WSP, SSH
Nagappan *et al.* [73]	Tropical	Daily	T_{min}, T_{max}, RH, WSP, SSH	DLNN, RBFNN	T_{min}, T_{max}, WSP

Author (s)	Climate region	Time stamp	Input parameters	Models	Input parameters
Granata *et al.* [74]	Humid subtropical, Semi-arid	Daily	R_n,T, H, RH, $ET_{a_{t-1}}$, $ET_{a_{t-2}}$,	NARX, LSTM	R_n, T, $ET_{a_{t-1}}$,$ET_{a_{t-2}}$
Ferreira *et al.* [76]	Tropical	Daily	T_{min}, T_{max}, R_s, RH, WSP	RF, XGBoost, ANN and CNN*	T_{min}, T_{max}, RH

2.2.4 Hybrid Models for ET_o Predictions

The optimization models are effective methods for reducing uncertainties related to tuning the hyper-parameters of AI models. Meta-heuristic Optimization Algorithms (MOAs) are widely employed in tackling optimization problems because they can identify several optimum solutions in a single run. Different MOAs are coupled effectively with AI models to solve non-linear ET_o process modeling problems. Table 2.5 summarizes these hybrid models used in the literature for the ET_o process.

Gocic *et al.* [77] explored four AI models named GP, ANN, SVM-wavelet and SVM-fire-fly algorithm (SVM-FFA) to estimate monthly ET_o in humid continental climate region of Serbia. SVM model was coupled with wavelet and optimization algorithm for hyper-parameter tuning, and it was observed that SVM coupled with wavelet transform outperformed all other models. The success of wavelet transform was also repeated in [78]. Wavelet transform was coupled to ANN and ANFIS models to estimate daily ET_o values using different input combinations of meteorological data. The authors found that ANN-wavelet with limited input data (T_{min}, T_{max}, R_a and $(ET_o)_{t-1}$) provides reliable results as compared to other models. The wavelet transform-based optimization model was further explored by kisi, and Alizamir [79]. They investigated wavelet-based ELM (WELM) and ANN for the ET_o process using different input combinations of meteorological data. The comparison of obtained results to simple ELM, ANN, WANN, and online sequential ELM (OS-ELM) revealed the outstanding performance of WELM.

Other optimization models were also explored in past studies, e.g., Tikhamarine *et al.* [80] attempted to use Whale optimization, Ant Lion Optimizer (ALO), Multi-Verse Optimizer (MVO), Grey Wolf Optimizer (GWO), particle swarm-based hybrid model of ANN. A comparison of these models with the existing empirical model using limited data showed the remarkable performance of hybrid models. However, the ANN model coupled with the Grey wolf optimizer (ANN-GWO) outperformed all other proposed hybrid models using limited input data (T_{min}, T_{max}, and R_s). ANN-GWO model was further used by Maroufpoor *et al.* [81] in their study to overcome the two constraints of the unavailability of all meteorological data and comprehensive model for all types of climate regions in Iran. The Shannon entropy test was used to analyze the importance of each meteorological parameter. Results demonstrated that ANN-GWO with limited input data (T_{min}, T_{max}, and WSP) provide promising results as compared to stand-alone ANN and LS-SVR for all climate regions.

Dong *et al.* [82] performed the comparison of four bio-inspired algorithms (grasshopper optimization, grey wolf optimizer, particle swarm optimization, and salp swarm algorithm (SSA)) to optimize Kernel-based Non-linear Extension of Arps Decline (KNEA) for estimating monthly ET_o for seven different climate zones of China. Results revealed that GWO-KNEA performed excellent in all climate zones of China using input combination of T_{min}, T_{max}, and R_s. ANFIS model can integrate the benefit of fuzzy features and an adaptive neural network system to process non-linear and stochastic problems and has provided comparable results to ANN in many studies. It takes advantage of the fuzzy system's ability to handle ambiguity and imprecision of the dataset. However, ANFIS showed some limitations related to parameter tuning. As a result, many researchers have attempted to couple optimization algorithms to overcome this limitation.

Tao *et al.* [83] explored nature-inspired optimization model called firefly algorithm (FFA) for the first time to optimized the ANFIS model. They reported outstanding predictive ability of the hybrid ANFIS-FFA model for ET_o estimation in the dry tropical region of Burkina Faso compared to ANFIS. In another study, Roy *et al.* [84] investigated four optimization algorithms named FFA, Biogeography-based Optimization (BBO), Particle Swarm Optimization (PSO), and Teaching-Learning-based Optimization (TLBO) to tune ANFIS model's parameters for the estimation of ET_o in subtropical regions of different geographical locations (Bangladesh, south Florida, and the USA). They compared the results of these hybrid models to the classical ANFIS model, whose parameters were tuned using least square back propagation gradient descent. Results supported the findings of [83] and indicated that the FFA-ANFIS model outperforms other hybrid models.

AI models are recently coupled with a bio-inspired optimization algorithm to find the optimal solution to the problem and improve the computational speed. Wu *et al.* [85] coupled ELM with bio-inspired optimization models named GA, Ant Colony Optimization (ACO), Cuckoo Search Algorithm (CSA), and Flower Pollination Algorithm (FPA) for estimation of ET_o. The results indicated that using bio-inspired models, especially CSA and FPA, improved the performance of the ELM model in different climate zones of China. Mohammadi *et al.* [86] coupled whale optimization algorithm with SVM model. They also explored preprocessing approaches such as RL, RF, PCA, and COR to find optimal input parameters for different climate regions (arid, semi-arid, and hyper-arid) to obtain general results for ET_o modeling.

Table 2.5: Summary of hybrid models for ET_o prediction

Author (s)	**Climate region**	**Time stamp**	**Input parameters**	**Models**	**Input parameters**
Gocic´*et al.* [77]	Humid continental	Monthly	T_{min}, T_{max}, WSP, VP, SSH	GP, SVM-FFA, ANN, SVM–Wavelet	T_{min}, T_{max}, WSP, VP, SSH
Patil *et al.* [78]	Arid	Daily	T_{min}, T_{max}, R_a, $ET_{0_{t-1}}$, RH, WSP	ANN, ANFIS, Wavelet-ANN and Wavelet-ANFIS	T_{min}, T_{max}, R_a, $ET_{0_{t-1}}$
Kisi and Alizamir [79]	Semi-arid	Daily	T_{min}, T_{max}, RH, R_s, WSP	WELM, WANN, ANN, ELM and OS-ELM	T_{min}, T_{max}, R_s, RH
Tikhamarine *et al.* [80]	Temperate, Mediterranean	Monthly	T_{min}, T_{max}, WSP, R_s, RH	ANN-GWO, ANN-MVO, ANN-PSO, ANN-WOA, ANN-ALO	T_{min}, T_{max}, R_s
Maroufpoor *et al.* [81]	Sub-humid, humid, Arid, Semi-arid, Hyper-arid	Monthly	T_{min}, T_{max}, RH, WSP, SSH	ANN-GWO, ANN, LS-SVR	T_{min}, T_{max}, WSP

Author (s)	**Climate region**	**Time stamp**	**Input parameters**	**Models**	**Input parameters**
Dong *et al.* [82]	Arid desert, Semi-arid steppe, Semi-humid Cold-temperate, Semi-humid warm-temperate, Humid subtropical and tropical, the Qinghai-Tibetan Plateau (QTP)	Monthly	T_{min},T_{max} RH, WSP , R_s , R_a	GWO-KNEA, KNEA, PSO-KNEA, SSA-KNEA	T_{min}, T_{max}, R_s
Tao *et al.* [83]	Dry tropical	Daily	T_{min}, T_{max}, RH, R_s, WSP, VP	ANFIS, ANFIS-FA	T_{max}, T_{min}, RH_{max}, R_s, WSP
Roy *et al.* [84]	Subtropical	Daily	T_{min}, T_{max}, RH, R_s, R_n, latent heat, sensible heat flux	BBO-ANFIS, FA-ANFIS, PSO-ANFIS, and TLBO-ANFIS	T_{min}, T_{max}, RH, R_s, R_n, latent heat, sensible heat flux
Wu *et al.* [85]	Temperate continental, Temperate monsoon, Mountain plateau, Sub tropical monsoon	Daily	R_s, RH, T_{min}, T_{max}, WSP	ELM , ELM-GA, ELM-ACO, ELM-CSA, ELM-FPA	R_s, RH, T_{min}, T_{max}, WSP

Author (s)	**Climate region**	**Time stamp**	**Input parameters**	**Models**	**Input parameters**
Mohammadi *et al.* [86]	Arid, Semi-arid, hyper-arid	Daily	T_{min}, T_{mean}, T_{max}, RH, R_s, WSP, VP, R_a	SVR, RF-SVR-WOA	T_mean, R_a, WSP, T_{min}
Yan *et al.* [87]	Arid, Humdid	Daily	T_{min}, T_{max}, SSH, R_a, RH, WSP	WOA-XGB	T_{min}, T_{max}, R_a, RH, WSP, SSH
Gao *et al.* [88]	Continental monsoon	Monthly	T_{min},T_{max} RH, WSP , R_s , R_a P	BA-ANN, CSA-ANN, WOA-ANN	T_{min},T_{max} R_s, R_a
Wu *et al.* [89]	Arid	Daily	T_{min}, T_mean, T_{max}, R_a	Kmeans-FFA-KELM, FFA-KELM, ANFIS, RF, M5P	T_{min}, T_{max}, R_a
Zhu *et al.* [90]	Arid	Daily	T_{min}, T_{max}, RH, R_s, WSP, Pr	PSO-ELM, ANN, RF	T_{min}, T_{max}, R_s
Gong *et al.* [91]	Temperate monsoon climatic zone, Temperate continental climatic zone, Mountain plateau climatic zone, and Subtropical and tropical monsoon climatic zone	Daily/ Monthly, Annually	T_{min}, T_{max}, RH, , R_s , R_a ,WSP	GA-ELM and PSO-ELM	T_{min},T_{max}

This study is also followed by Yan *et al.* [87], WOA optimizer was coupled to XGB to estimate daily ET_o in arid and humid climate regions of China. The findings showed that in the arid region, the relevance of meteorological data for forecasting daily ET_o was WSP >SSH >RH, while in the humid region, SSH >RH >WSP, with XGB-WOA providing outstanding performance in both the climate regions.

Whale optimization was further evaluated by Gao *et al.* [88] in their study. They coupled three bio-inspired optimization algorithms, named bat algorithm, cuckoo search, and whale optimization algorithm, with the ANN model for the prediction of ET_o in the continental monsoon region of China. Statistical comparison indicated that temperature-based ANN coupled with Whale Optimization Algorithm (ANN-WOA) provided more accurate results. The ELM model has proved its applicability for ET_o estimation in recent studies [32]. However, the ELM model's input weights and hidden biases are randomly set, which may result in non-optimal solutions. Therefore, tuning the model's parameters with optimization algorithms can provide a more accurate and robust ET_o estimation.

Wu *et al.* [89] proposed the coupling of FFA and K-means clustering with kernel ELM model (Kmean-FFA-ELM) for the prediction of ET_o. The coupled model achieved better results than other models, such as the ANFIS, M5P model tree, RF, and FFA-ELM. Zhu *et al.* [90] recommended to use particle swarm optimization model to tune ELM (PSO-ELM) parameters for estimating daily ET_o values in arid region of China. The study showed that the PSO-ELM model outperformed the ELM, ANN, and RF model in three input combinations of input data(temperature data, radiation data, and mass-transfer data).

The PSO-ELM model was further evaluated for different climate zones of China in the study conducted by Gong *et al.* [91]. They attempted to tune the parameters of the ELM model using a GA and PSO for modeling ET_o using temperature-based and radiation-based input parameters. In contrast to the previous study, the result indicated that GA-ELM provided a more reliable estimation of ET_o in a different type of climate zone in China than the PSO-ELM model. An analysis of the numerous research articles covered in this subsection indicates the following:

Optimization algorithms have gained considerable attention in recent years due to their capacity to improve AI techniques in addressing complex non-linear problems. Several studies have indicated a significant improvement in their modeling accuracy using the optimization approaches in the literature, piqued researchers' curiosity. Therefore, much effort has been put into applying hybrid AI models and single AI model techniques for ET_o prediction. Related articles mainly focused on

comparing stand-alone AI models with hybrid AI models (coupled with optimized models).

The effective modeling outcomes of these investigations proved the usefulness of optimization models for enhancing single AI models in calculating ET_o. For instance, ANN and ANFIS models provided more reliable results when coupled with GWO and FFA optimization techniques for modeling the ET_o process. It has also been observed that bio-inspired optimization models were more vigorously explored and proved their efficiency in tuning hyper parameters than other optimization techniques. Moreover, instead of improving the model's performance, attention was paid to develope generalized models of ET_o for all climate regions using limited available meteorological data.

2.3 AI/ML Models for Remote Sensing Data to Predict *ET*

The development of new orbit sensors and the availability of free satellite images have encouraged the use of remote sensing (RS) data and techniques in agriculture and hydrology [92]. The main advantages of RS techniques are data availability, time and cost-effectiveness, and their potential to monitor hydrological and climate phenomena continuously. Remote sensing techniques have been widely used for estimating ET on a range of temporal and spatial scales and have massive potential for bridging the gap between point and large-scale ET measurements. The broad coverage of the spatiotemporal range is one of the critical advantages of remote sensing data over traditional ground observation data for ET estimation.

The ability to estimate ET using data from satellite sensors is improving, allowing researchers to understand better how ET behaves in space and time, lowering the parameter's uncertainty levels. Numerous surface energy balance algorithms for ET calculation using remote sensing data have been developed in this context. Surface Energy Balance Algorithm for Land (SEBAL) and its extended variant known as Mapping Evapotranspiration at High Resolution with Internalized Calibration (METRIC) are two widely accepted algorithms for mapping ET from satellite images and have been used in many parts of the world.

In addition, satellite images can offer a wide range of parameters that can be utilized to train AI for ET_o prediction. Moreover, several studies have focused on constructing a novel and widely applicable linear relationship between independent remote sensing metrics such as Albedo, Normalized difference vegetation index

(NDVI) emissivity, and a dependent parameter (ET) utilizing different AI techniques. Table 2.6 summarizes the related research studies in brief. ANN model provides reasonable accuracy for predicting ET using remote sensing parameters (NDVI, land surface temperature (LST), R_n) in the study conducted by Chen *et al.* [93]. NDVI was observed to have more influence on cropland ET than grassland ET. RF model has also provided more accurate results of ET prediction than the global MODIS ET product in [94]. Further, a comparison study of ten different machine learning models to observe their applicability to predict ET using the different combinations of remote sensing data was conducted in [95]. Dias also used ML models to predict ET_o MOD16 product and WorldClim data for a distant location.

Hybrid models that combine ML and PM model also shows the great potential of simulating surface conductance (Gs) and ET process [96]. Despite the numerous benefits of RS techniques to estimate spatial daily ET, there are certain limitations (s), such as the unavailability of satellite images or cloudy skies. These limitations were addressed in [97] by developing RVM trained on the output generated by the METRIC algorithm and weather data to predict spatial ET. Many attempts have also been made to identify fewer RS parameters that can be fed to ML models to achieve satisfactory performance.

Rahimikhoob *et al.* [98] investigated the use of leaf surface temperature for the estimation of ET_o using ANN and M5Tree models. Results revealed that this approach could act as an alternative approach in case of data unavailability. Zhang *et al.* [99] also investigated ML models (SVM, ANFIS and BP) to predict ET_o using fewer RS data such as LST and R_s. It had been observed that LST is an essential parameter for predicting ET_o.

Another attempt was made by Kim *et al.* [100] to use different R_s and meteorological data to estimate daily ET_o. The authors observed that LST and WSP were important parameters for the accurate prediction of ET_o. Another attempt was made to use meteorological variable and vegetation indexes to predict ET using different ML models by Mosre *et al* [101]. NDVI and surface energy had been observed as the main variables in estimating actual evapotranspiration.

Table 2.6: Summary of remote sensing with AI models for ET_o prediction

Author (s)	Climate region	Remote sensing data	Climate parameters	Sattelite	Land cover	AI/ML models
Chen *et al.* [93]	Continental	Latent heat flux, NDVI, LST, and R_n	-	MODIS	Grassland	ANN
Douna *et al.* [94]	Arid	LAI, LST, Short wave incoming radiation and outgoing radiation	Pr, WSP, T_{min}, T_{max}, RH	MOD15A2	cropland	RF
Carter *et al.* [95]	Continental	H, R_n, Downward surface radiation, Photosynthetically active radiation, NDVI, Enhanced Vegetation Index, LAI, Albedo	-	MODIS, GLASS	Grassland/ Cropland	Support vector, neural network, tree, linear, and kernal based models
Liu *et al.* [96]	-	NDVI, EVI, Near-infrared reflectance of vegetation (NIRv) and Short wave infrared (SWIR)	T, Pr, VP, R_s, Carbon dioxide concentration	MODIS43A	Cropland	ANN, LSTM, KNN, SVM, XG-Boost
Bachour *et al.* [97]	Semi-arid	T, LAI, NDVI, Soil Adjusted Vegetation Index (SAVI)	T, WSP, R_s, SSH	Landsat 5	Cropland	RVM

Author (s)	**Climate region**	**Remote sensing data**	**Climate parameters**	**Sattelite**	**Land cover**	**AI/ML models**
Rahimikhoob *et al.* [98]	Arid	T_s, R_a	T_{min}, T_{max}, R_s, RH, WSP, SSH	AVHRR/ NOAA sensor	Grassland	M5Tre, ANN
Zhang *et al.* [99]	Arid	LST, Surface reflectance	T, WSP, RH, SSH, Pr	MODIS	Grassland	SVM, BP, ANFIS
Kim *et al.* [100]	Temperate	NDVI, LAI, FPAR, LST, ST	RH, WSP	MODIS	Cropland	RF, GBM, and XGBoost
Mosre *et al.* [101]	Arid cold	NDVI, SAVI, EVI, Normalized Difference Greenness Index (NDGI), Normalized Difference Water Index (NDWI), ST	T_{min}, T_{max}, Pr, T_{mean}, RH, VPD, WSP	Landsat 7	Cropland	Linear Regression
Käfer *et al.* [102]	Subtropical humid	NDVI, LST, TR, R_n, albedo	T, RH, WSP, Pr	Landsat-8	Grassland	ANN
Neissi *et al.* [103]	Humid continental	Albedo, emissivity, NDWI	T_{min}, T_{max}, WSP, SSH, RH	Landsat 8	Cropland	M5Tree

Author (s)	**Climate region**	**Remote sensing data**	**Climate parameters**	**Sattelite**	**Land cover**	**AI/ML models**
Barzkar *et al.* [104]	Temperate-Warm, Wet-Warm, Arid-Cold, and Arid-Warm	NDVI, LAI, LST	T_{min}, T_{max}, T_{dew}, VP, RH, SSH, WSP	Landsat 8	Grassland	GEP
Brant Dias *et al.* [105]	Tropical	Precipitation of Coldest Quarter and Wettest Month, Temperature, Precipitation Seasonality, Altitude, WorldClim, Mean Diurnal range	PET, R_s, Pr, WSP	MOD16	grassland	RF, partial least squares (PLS), Principal Components Regression (PCR), Adaptive Forward-Backward Greedy, GBM, GLM, Cubist
Liu *et al.* [106]	Arid/ Semi-arid	Carbon dioxide concentration, NDVI, EVI, NIRv	T, Pr, VP, R_s	MODIS43A	Cropland	ANN

2.4 AI/ML enabled ET_c Prediction Models

Recently, research on modeling the ET process using AI models has been concentrating on directly predicting ET_c values instead of ET_o. However, ET_c is heavily dependent on crop types (different k_c), and the conducted studies are quite particular regarding crops and geographical areas. Table 2.7 provides the brief contribution of such studies. For instance, Abyaneh *et al.* [107] obtained lysimeter readings from a case study in Hamedan Province, Iran. They compared the performance of the ANN and ANFIS model with the PM method to estimate ET_c for garlic crops and observed that both AI models achieve better performance. Aghajanloo *et al.* [108] and Tabari *et al.* [109] also investigated different AI models for the prediction of potato ET_c in semi-arid regions of Iran. Shrestha and Shukla [110] identified the need to estimate k_c values using local conditions for the reliable estimation of ET_c. They predict k_c values for vine and standing crops using the SVM model hydro-climate data and then further compared estimated ET_c values with lysimeter and FAO-56 based k_c values. Results show that SVM outperforms ANN and RVM models and has better accuracy than FAO-PM based ET_c method. Feng *et al.* [111] examined the predictive capability of ELM and GRNN models for maize ET_c based on meteorological data, leaf area index (LAI) and h_c in continental temperate climate region of China. The results indicated that crop and meteorological data models produced maize ET_c accurately.

A similar case study for maize ET_c was conducted using meteorological parameters, LAI, and plant height by Tang *et al.* [112] in arid region of China. They identified that SVM and GANN models with combined meteorological and maize crop data produced more accurate ET_c predictions than models with only meteorological data. Abrishami *et al.* [113] also explored different combinations of LAI, h_c crop parameters with meteorological data to estimate wheat and maize ET_c values against lysimeter and FAO-PM method using ANN. They found that five inputs: T_{min}, T_{max}, R_n, LAI, and h_c achieve satisfactory performance closer to lysimeter values.

Another study conducted by Saggi *et al.* [114] examined AI models (fuzzy-genetic and regularization random forest (FG-RRF)) for predicting wheat and maize ET_c values. k_c values of both the crops were also simulated using local meteorological parameters, and the results depicted the suitability of this approach for modeling ET_c process of both the crops. Yamaç and Todorovic [115] employed KNN, ANN, and AdaBoost models with four different input combinations of meteorological data and k_c values to estimate the daily ET_c of potatoes in the Mediterranean region of Italy.

The results demonstrated that the KNN model gave the best ET_c estimates under limited meteorological data scenarios, whereas the ANN model produced somewhat better ET_c predictions when all data were available.

DL models, as an extension to traditional ANN models, have recently gained much attention in many fields such as image classification, autonomous driving, and regression problems due to their capability to learn the most complex relationship between the data using multiple hidden layers. Chen *et al.* [116] recently used deep learning models (Temporal Convolutional Networks (TCN), LSTM, DNN) to predict ET_c of maize crop based on meteorological, soil, and crop data. It was observed that the TCN model using the seven most critical input parameters (h_c, T_{mean}, T_{max}, Rh, R_s, LAI, and ST) identified by PCA and MIC method predicted maize ET_c with excellent accuracy. Hashemi and Sepaskhah [117] compared the performance of MLP model with the FAO-PM model and RBF model to estimate barely ET_c against the lysimeter measurements. The MLP and RBF models outperformed the PM model using SSH, RH, T_{mean}, and WSP as input. This finding eliminated the requirement for time-consuming data collection for k_c calculation. Fan *et al.* [118] explored the effect of different combinations of plant, soil, and meteorological data on the transpiration process of maize using AI models (SVM, Xgboost, DNN, and ANN). They found that LAI and soil water content (SWC) improve the performance of AI models than using only meteorological data to simulate the transpiration process. Yamaç [119] employed AI models (RF, SVM, KNN, Adaptive Boosting) to obtain the minimum required input parameters to estimate sugarbeet ET_c in the semi-arid region of Turkey. All AI models with T_{min} ,T_{max}, WSP, R_s and k_c as input parameters gave satisfactory results.

Ohana-Levi *et al.* [120] compared the performance of linear and non-linear AI models for predicting Cabernet Sauvignon ET_c values. Furthermore, ET_c were estimated using two approaches: direct estimation of ET_c using meteorological and crop parameters and another approach including simulation of k_c values and multiplying them by ET_o values. Results demonstrated that both approaches yield similar performance, non-linear AI models perform better, and LAI improves the important performance parameter for ET_c estimation. Shan *et al.* [121] investigated the ability of the MARS model to estimate maize ET_c using limited meteorological data in the semi-arid region of China and highly recommend the MARS model in data-scarce situations.

Table 2.7: Summary of AI/ML models for ET_c prediction

Author (s)	**Climate region**	**Crop**	**Time stamp**	**Crop parameters**	**Climate parameters**	**Models**
Abyaneh *et al.* [107]	Humid continental	Garlic	Daily	k_c	T_{max}, T_{min}, RH_{max}, RH_{min}, SSH, WSP	ANN, ANFIS
Aghajanloo *et al.* [108]	Semi-arid	Potato	Daily	k_c	T, R_n, RH, WSP, Pr	ANN, neural network–genetic algorithm (NNGA), Multivariate Nonlinear Regression (MNLR)
Tabari *et al.* [109]	Semi-arid	Potato	Daily	k_c	T, R_s, RH, WSP, P	SVM and ANFIS
Shrestha and Shukla [110]	Sub-tropical	Vine and Erect	monthly	k_c	T_{max}, T_{min}, P, RH,WSP, R_s	SVM, RVM, ANN
Feng *et al.* [111]	Continental temperate	Maize	Daily	LAI, h_c	T, RH, WSP, R_s	ELM, GRNN

Author (s)	**Climate region**	**Crop**	**Time stamp**	**Crop parameters**	**Climate parameters**	**Models**
Tang *et al.* [112]	Continental temperate	Maize	Daily	LAI, h_c	T, RH, WSP and R_s ,	SVM, GANN
Abrishami *et al.* [113]	Arid	Wheat, Maize	Daily	LAI, h_c	T_{min}, T_{max}, R_n, RH, WSP	ANN
Yamaç and Todorovic [115]	Mediterranean	Potato	Daily	k_c	T, R_s, WSP, RH	ANN, AdaBoost, KNN
Chen *et al.* [116]	Continental	Maize	Daily	LAI, h_c	T_{min}, T_{max}, T_{mean}, R_a, R_s, RH, WSP, ST,	TCN, LSTM, DNN
Hashemi *et al.* [117]	Continental	Barley	Daily	k_c	T, Pr, RH, WSP, wind velocity, SSH, Ep	MLP-ANN, RBF-ANN
Fan *et al.* [118]	Arid, Semi-arid	Maize	Daily	LAI	T_{max}, T_{min}, RH, WSP and R_s	SVM, Xgboost, DNN, ANN

Author (s)	Climate region	Crop	Time stamp	Crop parameters	Climate parameters	Models
Yamaç *et al.* [119]	Semi-arid	Sugarbeet	Daily	k_c	T_{max}, T_{min}, RH, WSP, R_s	RF, SVM, KNN, Adaptive Boosting
Ohana-Levi *et al.* [120]	Semi-arid /Mediterranean	Grapevine	Daily	LAI	T_{min}, T_{max}, RH,	MARS
Shan *et al.* [121]	Semi-arid	Maize	Daily	LAI, h_c, Ground cover	T, RH, WSP, SSH,	MARS
Saggi *et al.* [114]	semi-arid	wheat, Maize	Daily	k_c	T_{min}, T_{max}, R_s, SSH, WSP, RH	FG and RRF
Elbeltagi *et al.* [122]	Mediterranean	Wheat, Maize	Monthly	k_c	T_{min}, T_{max}, R_s, Pr	DNN

2.5 Research Gaps

After analyzing the aforementioned existing research work, the following research gaps have been identified.

- India has about 4the world's population. However, some of its major agricultural commodities need 2-4 times more water than other countries, such as China and USA due to poor irrigation techniques. Therefore, advanced technologies based on smart strategies and systems need to be developed to effectively use freshwater.

- Climate change, which has become more and more intense these days, is also strongly affecting crop water needs. It has raised irrigation demand, putting more pressure on available freshwater for agricultural production in many areas that already have water scarcity. Therefore there is a need to mitigate this issue by designing new efficient irrigation strategies.

- With recent developments in computational capacity in terms of parallel processing, software, and hardware, a new AI paradigm known as deep learning is now viable to address large amounts of data. The adoption of DL for irrigation scheduling is still minimal. It should be explored more for irrigation scheduling strategies. Also, AI models with the integration of metaheuristic optimization algorithms have enhanced performance. Deep learning models should also be hybridized to optimize model parameters for modeling complex hydrological processes.

- The development of the evapotranspiration model using the AI approach faces the unavailability of required data, especially in underdeveloped nations or remote areas. Therefore, the AI-enabled evapotranspiration modeling process's major challenge is to provide reliable accuracy using less meteorological data. Further, research studies are required to use only temperature as input data. Also, studies on evapotranspiration prediction for data-scarce stations using meteorological data of another station with a similar climate should be explored.

- FAO-PM has been widely accepted to estimate evapotranspiration in all climate regions. Although AI models have been used to simulate the evapotranspiration process, the biggest challenge for modeling evapotranspiration using AI is to develop a procedure/model that can be applied to all climate regions.

Chapter 3

Study Areas, Data and Theoretical Background

This chapter presents the geographical conditions of study areas and a description of the meteorological and crop dataset used in the research work. The research area of the conducted study includes the Ludhiana, Amritsar, and Patiala stations of the Punjab region of India. The statistical observations and cross-correlation of meteorological parameters of these stations and crop characteristics (wheat and rice) are provided in this chapter.

3.1 Overview

The agriculture sector has a significant role in the economy and culture of Punjab. The wheat-rice crop system (WRCS) is India's dominant cropping system, occupying around 12.3 million ha area [123]. The continuous groundwater withdrawal for the cultivation of this water-intensive cropping system has led to a dramatic fall in Punjab's groundwater level. For this reason, precise estimation of rice and wheat crop evapotranspiration is required to successfully monitor crop water requirements to prevent over or under irrigation problems. This study selects wheat and rice crops to model the crop evapotranspiration process. The required meteorological and crop datasets are obtained from India meteorological department (IMD) Pune, India. The crop coefficient values of rice and wheat crops are adopted from the case study of Punjab Agriculture University, Ludhiana.

3.2 Study Area

Punjab, known as India's 'food bowl', has 80% agricultural land and located between north latitude (29°32′ and 32°32′) and east longitude (73°55′ and 76°50′) with an altitude between 230 m and 700 m. It occupies around 50,362 km^2 geographical area of India. The study area map is shown in Figure 3.1. There are five

Agro-Climatic Zones: Western Plain, Central Plain, Western, Sub-Mountain, and Undulating Plain.

Wheat is the primary cereal of India, and Punjab alone contributes 40% of the wheat to the central pool. The state has a 3.51 million ha area under wheat cultivation [124]. Rice is one of India's largest export grains, and more than one-third of it is exported from the Punjab state alone. It is cultivated on a 2.6 million ha area in Punjab and is mainly flood irrigated [125].

This unsustainable use of groundwater has led many blocks of Punjab towards zero groundwater level as per the report of the Central Ground Water Board Department of Water Resources [126]. Therefore, it is urgent to optimally pay attention to the use of water resources to minimize the adverse effects caused by this cropping pattern in Punjab and achieve a sustainable agricultural system.

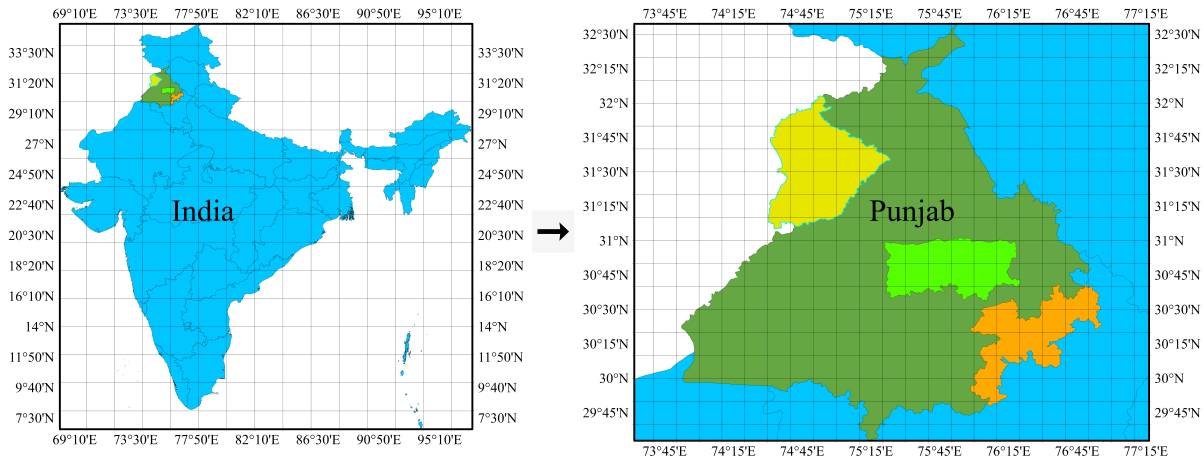

Figure 3.1: Punjab

3.2.1 Ludhiana

Ludhiana station is situated between north latitude (30°34′ and 31°01′) and east longitude (75°18′ and 76°20′) with an altitude of 262 m. The study area map is shown in Figure 3.2 The climate of Ludhiana can be categorized as tropical steppe, hot, and semi-arid, often dry with hot summer and cold winter except in the monsoon season. The station has an average annual and monsoon rainfall of 680 mm and 528 mm, respectively, and rainy days are limited to 34 days. The temperature varies from the lowest, 5.8°C in winter, to the highest, 45°C in summer. The soil type is

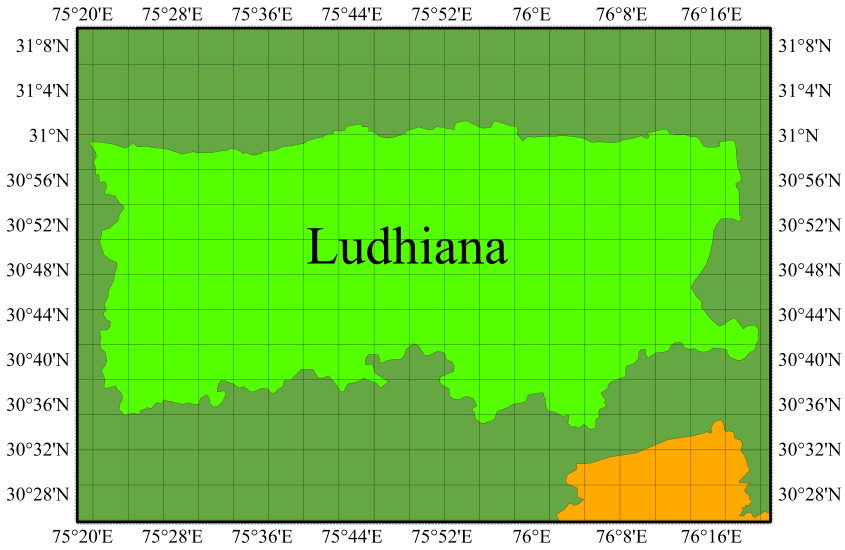

Figure 3.2: Ludhiana station

alkaline and classified as clayey loam and sandy. Ludhiana is the primary producer of wheat and paddy crops. Canal irrigation occupies 90 sq. km out of 3600 sq. km of the total area under irrigation. The rest of the area is irrigated using groundwater.

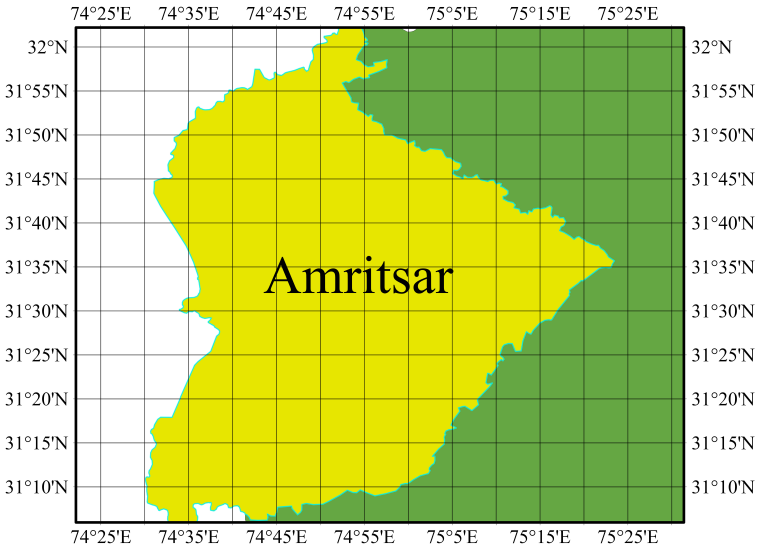

Figure 3.3: Amritsar station

3.2.2 Amritsar

Amritsar station is situated between north latitude (31°28′ and 32°30′) and east longitude (74°29′ and 75°24′) with an altitude of 234 m. The study area map is shown in Figure 3.3. The climate of Amritsar is also semi-arid, with a very hot

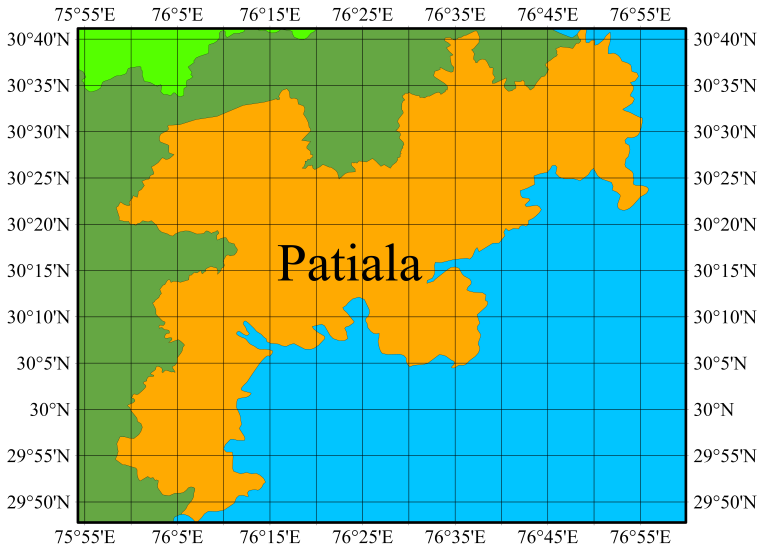

Figure 3.4: Patiala station

summer and freezing winter season. The average annual and monsoon rainfall of the station is approximately 703 mm and 570 mm, respectively. The average lowest temperature in winter is approximately $3.4°C$, and the highest temperature is $44°C$ in summer. This station's western part's soil type is coarse loamy, whereas the soil's nature is fine loamy in the central part. The major crops of this station are wheat and paddy. The 15% of the total irrigation area of 2180 sq. km is canal irrigated, and irrigation relies on groundwater in the rest of the area. The groundwater level of this station is dropping due to insufficient irrigation strategies. It has declined at the rate of 0.27 - 0.75 m/year over the last decade.

3.2.3 Patiala

Patiala station is situated between latitude $29°49'$ and $30°40'$ North and longitude $75°58'$ and $76°48'$ East with an altitude of 351 m. Figure 3.4 depicts the area map of Patiala station. This station also falls under a semi-arid tropical ecosystem characterized by dry and hot summers and cold winters. The average annual and monsoon rainfall is approximately 677 mm and 547 mm, respectively. The average minimum temperature in winter is $7.1°C$, and the maximum temperature is $40.4°C$. Most of the area of this station is covered with arid brown and tropical arid brown soils, and the soil in this area is poor in potassium, phosphorus, and nitrogen. Paddy, maize, and wheat are major crops of this station.

3.3 Dataset Description

This section presents a detailed description of the meteorological and crop data used in this research work.

3.3.1 Meteorological Dataset

A set of daily observations of meteorological parameters is retrieved from the India meteorological department in Pune, India. The meteorological parameters used in the study are maximum temperature (T_{max}), minimum temperature (T_{min}), wind speed measured at the height of 2 m (WSP), solar radiation (R_s), relative humidity (RH), vapor pressure (VP), and sunshine hours (SSH). The aforementioned daily meteorological parameters dataset covers data from 2003 to 2015 of Ludhiana station, 2000 to 2016 of Amritsar station, and from 2000 to 2015 of Patiala station located in the Punjab region of India. Actual ET_o values are calculated by the FAO-PM method using CROPWAT 8.0 software.

The statistical properties of meteorological parameters such as max (X_{max}), min (X_{min}), mean (X_{mean}), standard deviation (X_{std}), skewness (X_{skew}), kurtosis (X_{kurt}), and coefficient of variation ($C.V.$) for training and testing data are provided in Tables 3.1, 3.2, and 3.3 of Ludhiana, Amritsar and Patiala stations, respectively. It is observed from these tables that the statistical properties of training and testing datasets are somewhat similar for developing the best possible model. The cross-correlation of each variable and ET_o is provided in Tables 3.4, 3.5 and 3.6 of Ludhiana, Amritsar and Patiala stations, respectively.

3.3.2 Crop Dataset

Wheat and rice crops are considered in the research study to estimate crop evapotranspiration values. Wheat crop is sown in Punjab state during sowing windows from late October to December and harvested in April. The optimal temperature range for ideal wheat seed germination is $20°C$-$25°C$, and the optimal temperature for vegetative growth is $16°C$-$22°C$ [127]. The rice crop is sown from late June to August and harvested in October. It is a tropical plant that needs a lot of heat and humidity to survive. The temperature should be $16°C - 30°C$ during the sowing period, $20°C - 30°C$ at the time of the growth period, and $16°C - 27°C$ when harvesting [128].

The planting and harvesting dates of wheat and rice crop from the time duration of 2003-2015 are also obtained from IMD Pune, along with the meteorological data

Table 3.1: Statistical observation of the meteorological data of Ludhiana station

Training Dataset							
M.D.	X_{min}	X_{max}	X_{mean}	X_{std}	X_{skew}	X_{kurt}	*C.V.*
T_{min}	-1.6	34.5	17.4	8.1	-0.2	-1.2	0.5
T_{max}	7.8	46.2	29.8	7.5	-0.4	-0.6	0.3
RH	20.5	100	66.9	15.6	-0.7	0.04	0.2
WSP	0	3.3	1.1	0.6	0.9	0.7	0.6
VP	3.6	29.95	14.7	6.4	0.46	- 1.14	0.43
SSH	3.6	30	14.7	6.4	0.46	-1.1	0.4
R_s	4.8	29.7	17.5	6.3	-0.1	-0.91	0.4
ET_0	0.6	9.5	3.8	1.9	0.4	-0.8	0.5
Testing Dataset							
M.D.	X_{min}	X_{max}	X_{mean}	X_{std}	X_{skew}	X_{kurt}	*C.V.*
T_{min}	-1	31.2	17.9	8	-0.2	-1.2	0.5
T_{max}	8.6	44.2	30.1	7.1	-0.4	-0.3	0.3
RH	23	100	67.4	15.5	-0.7	0.03	0.2
WSP	0	3.2	1.1	0.6	0.9	0.6	0.6
VP	4.2	28.4	15.2	6.52	0.46	- 1.32	0.43
SSH	4.2	28.4	15.2	6.52	0.5	-1.3	0.4
R_s	4.8	29.5	17.7	6.3	-0.1	-0.97	0.4
ET_0	0.6	9.4	3.8	1.9	0.4	-0.8	0.5

Table 3.2: Statistical observation of the meteorological data of Amritsar station

Training Dataset							
M.D.	X_{min}	X_{max}	X_{mean}	X_{std}	X_{skew}	X_{kurt}	*C.V.*
T_{min}	- 2.6	30.4	15.97	8.37	- 0.29	- 1.22	0.52
T_{max}	7.8	48	30	7.54	- 0.39	- 0.45	0.24
RH	13	98.5	63	17.0	- 0.69	- 0.15	0.27
WSP	0.0	5	1.29	1.15	0.86	0.19	0.89
VP	1.35	42	18.8	9.09	0.43	- 0.98	0.48
SSH	0.0	12.0	6.71	3.28	- 0.73	- 0.50	0.48
R_s	0.0	28.0	16.15	6.16 -	0.15	- 0.85	0.38
ET_0	0.52	11.97	3.87	2.40	0.77	0.11	0.62
Testing Dataset							
M.D.	X_{min}	X_{max}	X_{mean}	X_{std}	X_{skew}	X_{kurt}	*C.V.*
T_{min}	- 1.4	31.5	15.87	8.53	- 0.33	- 1.19	0.54
T_{max}	8.4	47	30.5	7.64	- 0.45	- 0.50	0.25
RH	15	98	15	3.27	- 0.62	- 0.34	0.28
WSP	0.0	5	1.27	1.15	0.91	0.31	0.90
VP	1.4	40.9	18.8	9.12	0.44	0.99	0.48
SSH	0.0	12	6.69	3.27	- 0.74	- 0.48	0.49
R_s	- 1.0	27	16	6.27	- 0.20	- 0.84	0.38
ET_0	0.52	11	3.92	2.40	0.69	- 0.02	0.61

Table 3.3: Statistical observation of the meteorological data of Patiala station

Training Dataset							
$M.D.$	X_{min}	X_{max}	X_{mean}	X_{std}	X_{skew}	X_{kurt}	$C.V.$
T_{min}	-2.1	31.4	15.6	8.4	-0.3	-1.2	0.5
T_{max}	7.4	48.0	30.2	7.8	-0.3	-0.6	0.3
RH	13.0	99.0	66.0	18.0	-0.6	-0.1	0.3
WSP	0.0	8.6	1.4	1.3	1.1	1.3	0.9
SSH	0.0	12.4	6.5	3.2	-0.7	-0.4	0.5
R_s	4.9	28.4	16.5	5.9	-0.2	-0.8	0.4
ET_0	0.6	13.2	4.0	2.4	0.9	0.3	0.6
Testing Dataset							
$M.D.$	X_{min}	X_{max}	X_{mean}	X_{std}	X_{skew}	X_{kurt}	$C.V.$
T_{min}	-2.6	29.6	15.7	8.3	-0.3	-1.2	0.5
T_{max}	7.8	46.4	30.3	7.9	-0.5	-0.4	0.3
RH	19.0	99.0	66.1	18.5	-0.7	-0.1	0.3
WSP	0.0	7.2	1.4	1.3	1.0	1.0	0.9
SSH	0.0	12.4	6.6	3.2	-0.7	-0.5	0.5
R_s	4.9	28.3	16.5	5.9	-0.2	-0.8	0.4
ET_0	0.7	12.9	3.9	2.4	0.8	0.2	0.6

Table 3.4: Cross-correlation among meteorological data and ET_o of Ludhiana station

Ludhiana Station								
$M.D.$	T_{min}	T_{max}	RH	WSP	VP	SSH	R_s	ET_0
T_{min}	1	0.85	-0.23	0.35	0.85	0.17	0.57	0.8
T_{max}	0.85	1	-0.62	0.25	0.55	0.46	0.76	0.9
RH	-0.2	-0.62	1	-0.16	0.24	-0.5	-0.57	-0.6
WSP	0.35	0.25	-0.16	1	0.26	-0.07	0.17	0.5
VP	0.85	0.55	0.24	0.26	1	- 0.02	0.32	0.46
SSH	0.17	0.46	-0.5	-0.07	-0.02	1	0.86	0.5
R_s	0.57	0.76	-0.57	0.17	0.32	0.86	1	0.9
ET_0	0.77	0.87	-0.62	0.48	0.46	0.54	0.86	1

Table 3.5: Cross-correlation among meteorological data and ET_o of Amritsar station

Amritsar Station								
$M.D.$	T_{min}	T_{max}	RH	WSP	VP	SSH	R_s	ET_0
T_{min}	1	0.86	- 0.36	0.27	0.65	0.30	0.70	0.54
T_{max}	0.86	1	- 0.64	0.31	0.42	0.53	- 0.80	0.61
RH	- 0.36	- 0.64	1	- 0.34	0.05	- 0.46	- 0.57	- 0.52
WSP	0.26	0.31	- 0.34	1	0.15	0.10	0.31	0.51
VP	0.65	0.42	0.05	0.15	1	0.10	0.35	0.24
SSH	0.30	0.53	- 0.46	0.10	0.10	1	0.82	0.45
R_s	0.70	- 0.80	- 0.57	0.31	0.35	0.82	1	0.55
ET_0	0.54	0.61	- 0.52	0.51	0.24	0.45	0.55	1

Table 3.6: Cross-correlation among meteorological data and ET_o of Patiala station

Patiala Station							
$M.D.$	T_{min}	T_{max}	RH	WSP	SSH	R_s	ET_0
T_{min}	1	0.87	-0.44	0.12	0.34	0.67	0.8
T_{max}	0.87	1	-0.71	0.14	0.56	0.80	0.8
RH	-0.44	-0.712	1	-0.24	-0.50	-0.63	-0.7
WSP	0.12	0.14	-0.24	1	0.05	0.14	0.5
SSH	0.34	0.56	-0.50	0.053	1	0.89	0.6
R_s	0.67	0.80	-0.63	0.14	0.89	1	0.8
ET_0	0.77	0.83	-0.68	0.50	0.58	0.82	1

of growing durations of these two crops. The crop phenological stages are generally divided into four stages: initial stage, development stage, mid-stage, and late-stage, with different duration lengths. The length of each stage is calculated from growing degree days (GDD) which is determined using eq. (3.1).

$$GDD = \frac{T_{max} + T_{min}}{2} - T_t \tag{3.1}$$

where T_{max} , T_{min} and T_t represents maximum, minimum, and base temperature. The base temperature for wheat is $5°C$ and $10°C$ for rice crop [127] [129].

Table 3.7 and 3.8 provide the growth stage duration details of wheat and rice crop, respectively. The k_c values of wheat and rice are adopted from the research conducted at the Punjab Agricultural University's School of Climate Change, and Agricultural Meteorology in Ludhiana that aims to calculate k_c values of both the crops [130]. The k_c values for the wheat crop used in the study are k_c init = 0.39, k_c mid = 1.26, and k_c late = 0.36, and for rice crop, k_c init = 1.15, k_c mid = 1.36, and k_c late = 0.86.

Actual crop evapotranspiration values are calculated by multiplying the reference evapotranspiration with a single crop coefficient (k_c) that integrates the characteristics of the crop during different phenological stages [131], given in eq. (3.3). The study considered T_{min}, T_{max}, T_{mean}, and R_s meteorological parameters of Ludhiana station for the prediction of ET_c of wheat and rice crops. The correlation between above mentioned meteorological parameters and ET_c of wheat and rice crops is provided in Table 3.9 and 3.10 respectively. The mean values of T_{min}, T_{max}, T_{mean}, and R_s of Ludhiana station from 2003 to 2015 for wheat and rice crops growing period are provided in Table 3.11.

Table 3.7: Wheat growth stages duration from 2003-2016

Crop Variety	Sowing date	Harvesting date	Initial stage	Development stage	Mid Stage	Late Stage
PBW-343	19-11-2003	16-04-2004	27	69	23	30
HD-2329	20-11-2004	16-04-2005	25	59	32	31
HD-2329	21-11-2005	19-04-2006	26	54	33	36
PBW-502	02-11-2006	10-04-2007	24	71	40	24
PBW-502	05-11-2007	16-04-2008	27	85	27	24
PBW-343	22-11-2008	16-04-2009	27	60	29	29
DBW-17	25-11-2010	19-04-2011	37	59	23	26
PBW-550	15-11-2011	01-05-2012	28	71	28	41
PBW-550	28-11-2012	23-04-2013	36	56	23	31
PBW-550	14-11-2014	21-04-2015	33	66	30	29
PBW 621	08-11-2015	15-04-2016	30	66	30	33

Table 3.8: Rice growth stages duration from 2003-2015

Crop Variety	Sowing date	Harvesting date	Initial stage	Development stage	Mid Stage	Late Stage
PR-118	01-07-2003	23-10-2003	33	28	34	19
PR-118	28-05-2004	17-09-2004	28	36	36	12
PR-118	26-05-2005	27-09-2005	28	40	40	16
PR-115	14-06-2006	28-09-2006	32	28	30	16
PR-114	16-06-2007	25-10-2007	29	33	51	18
PR-116	28-06-2008	15-10-2008	33	26	35	15
PAU-201	05-06-2009	17-10-2009	32	33	51	18
PR-118	25-06-2010	25-10-2010	31	34	43	14
PR-116	30-07-2011	14-11-2011	28	28	35	16
PR-118	16-07-2012	30-10-2012	29	27	35	17
PR-116	16-07-2013	19-11-2013	31	32	47	16
PR-118	19-06-2015	24-10-2015	31	27	51	18

Table 3.9: Cross-correlation among meteorological data and ET_c of wheat crop

Wheat crop					
M.D.	T_{min}	T_{max}	T_{mean}	R_s	ET_0
T_{min}	1	0.75	0.9	0.38	0.53
T_{max}	0.75	1	0.96	0.77	0.7
T_{mean}	0.9	0.96	1	0.65	0.67
R_s	0.38	0.77	0.65	1	0.86
ET_0	0.53	0.7	0.67	0.86	1

Table 3.10: Cross-correlation among meteorological data and ET_c of rice crop

Rice crop					
M.D.	T_{min}	T_{max}	T_{mean}	R_s	ET_0
T_{min}	1	0.7	0.87	0.2	0.5
T_{max}	0.7	1	0.7	0.66	0.7
T_{mean}	0.87	0.7	1	0.5	0.75
R_s	0.2	0.66	0.5	1	0.86
ET_0	0.5	0.7	0.75	0.86	1

Table 3.11: Mean values of meteorological data of wheat and rice growth duration

Crop	Month	T_{min}	T_{max}	T_{mean}	R_s
Wheat	Nov	8.9	24.6	16.8	12.2
	Dec	7.1	20.9	14	10.2
	Jan	6.8	17.7	12.3	10.3
	Feb	9.4	22.6	16	15.2
	March	13.8	28.6	21.2	19.5
	Apr	17.3	35.5	26.4	19.5
Rice	July	27	34	30.5	19
	Aug	26.2	33.3	29.8	19.2
	Sep	24	33	28.5	19.5
	Oct	19.9	32.4	26.2	16.2

3.4 Methods of Irrigation Scheduling

Irrigation scheduling (IS) determines when and how much water to apply to an agricultural field. Developing efficient irrigation scheduling needs better knowledge of the biophysical processes of soil root water absorption and crop canopies' transpiration process. The primary goal of efficient irrigation scheduling is to minimize yield reduction, irrigation cost, and excess groundwater withdrawal, preventing aquifer exploitation, water logging problems, and water wastage. The precise estimation of water demand is critical for irrigation scheduling.

Various irrigation scheduling techniques may be used to determine the appropriate time of Irrigation and depth for crop development. Numerous methods for scheduling and estimating the required depth of different irrigation treatments have been introduced during the last few decades. These developed and suggested irrigation scheduling techniques can be categorized into three categories according to factors upon which scheduling depends, i.e., the evapotranspiration process, soil moisture, and plant water status.

3.4.1 Evapotranspiration based Irrigation Scheduling

"*Evapotranspiration (ET) is defined as the total amount of water lost by evaporation and transpiration via soil and plant canopy, is the primary route by which plants lose water and interchange energy with the environment.*"

The amount of solar radiation that reaches the soil surface determines how much evaporation occurs. The effects of solar radiation on the surface decrease as crops mature and get denser. At this time, transpiration through crops governs and becomes the primary process. Crops lose around 99% of the water they absorb through transpiration, with only 1% utilized for metabolic activity [132]. Thus accurate estimation of ET is one of the most significant steps in determining crop water requirements in the agricultural field and therefore acts as an important and necessary parameter in irrigation scheduling. It also gives decision-makers the information they need to figure out how to reduce water usage and ensure sustainable water management. The direct measurements of ET in the field is performed by isolating a portion of the crop from its surrounding using various instruments such as lysimeters, eddy covariance, sap flow gauge, and Bowen ratio. However, direct measurement of ET is costly, time-consuming, and difficult.

The alternative procedure is to estimate ET indirectly using empirical models that use local readily available meteorological variables. However, ET is influenced by a multitude of factors, including climatic variables such as air temperature, solar radiation, wind speed, and humidity; crop characteristics such as crop variety and type, development stage; environmental aspects including soil conditions, fertility, salinity, and crop disease [133]. Therefore, it is nearly impossible to develop an equation that can be utilized to estimate actual ET due to the interdependence of most of these parameters and their spatial and temporal variability. As a result, the concept of standardizing ET equations using reference evapotranspiration has been proposed in [134].

Reference Evapotranspiration

"*Reference Evapotranspiration is defined as the rate of ET from a large area of green grass of uniform height—8 to 15 cm, which is actively growing, entirely shading the ground, and not water stressed*" [135] [136].

The process of reference evapotranspiration is represented in Figure 3.5. Previously, grass and alfalfa have been employed as reference surfaces under different environmental situations. Numerous empirical models have been suggested in the

past to calculate reference evapotranspiration for grass surface (ET_o) and alfalfa surface (ET_r). These models can be classified into temperature-based, radiation-based, evaporation-based, and a combination of climate variables. Some of these models are provided in Table 3.12.

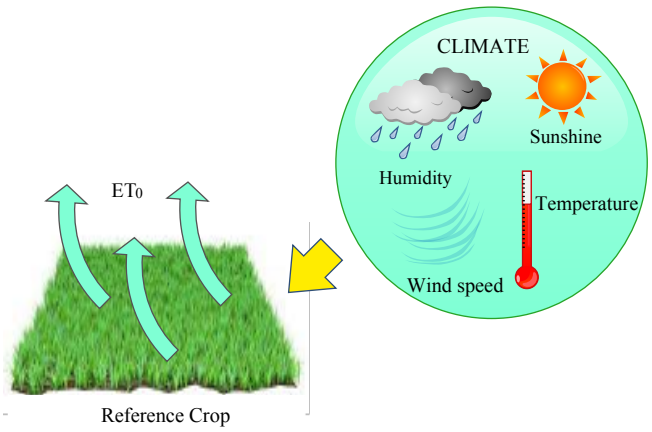

Figure 3.5: Reference evapotranspiration

The majority of researchers recommended to standardized Penman-Monteith equation for calculation of ET_o as this equation roughly approximates the observations made by lysimeter for ET calculations [136] [137]. Hence, for this reason, the standardized Penman-Monteith equation is selected in two versions. The first version, referred to as the American Society of Civil EngineersASCE-PM equation [162], has been suggested by the American Society of Civil Engineers Task Committee (ASCETC), while the second version, referred to as the Food Agriculture and Organization (FAO)-56 PM equation [161], has been recommended by the United Nations Food and Agriculture Organization (UNFAO). Food Agriculture and Organization has recommended FAO-56 Penman-Monteith (PM) as a reliable method to estimate ET_o that has been proved to provide consistent performance in different climate regions [163] [164]. This method is accepted worldwide and used by agronomists, researchers, and irrigation engineers as a standard method for ET_o calculation. The equation of FAO-56 PM is provided in eq. (3.2).

$$ET_0 = \frac{0.408 \triangle (R_n - G) + \gamma \frac{900}{T_{mean}+273} U_2 (e_s - e_a)}{\triangle + \gamma(1 + 0.34U_2)} \tag{3.2}$$

Here, R_n, G, γ, T_{mean}, and $\triangle$ are radiation ($MJm^{-2}day^{-1}$), soil heat flux density ($MJm^{-2}day^{-1}$), psychrometric constant ($kPa°C^{-1}$), mean air temperature ($°C$), and slope of saturation vapor pressure function ($kPa°C^{-1}$), respectively. U_2, e_s represents the wind speed at $2m$ height (ms^{-1}), saturation vapor pressure (kPa),

Table 3.12: Empirical models for evapotranspiration

Classification	Methods	Ref.
Temperature	Thornthwaite	[138]
	SCS Blanery-Criddle	[139]
	FAO-24 Blanery- Criddle	[140]
	Hargreaves	[141]
	Turc	[142]
	Jensen-Haise	[143] [144]
	Priestly-Taylor	[145]
Radiation	FAO-24 radiation	[146]
	Makkink	[147]
	Ritchie	[148]
Evaporation	Christiansen Pan	[149] [150]
	FAO-24 Pan	[146]
Combination	Penman VPD #1	[151] [152]
	Penman VPD #3	[152]
	Businger- van Barvel	[153] [154]
	Penman-Monteith	[155]
	1972 Kimberly-Penman	[156]
	FAO-24 Corrected Penman	[157]
	FAO-24 Penman(c=1)	[140]
	FAO-PPP-17 Penman	[158]
	1982 Kimberly Penman	[159]
	CIMIS Penman	[160]
	FAO-56 Penman Monteith	[161]
	ASCE-PM	[162]

and e_a represents actual vapor pressure (kPa), respectively.

Crop Evapotranspiration

"*Crop evapotranspiration (ET_c) is the total water loss from the specific crop due to the evaporation and transpiration processes.*" FAO-56 PM method is the most popular and effective technique to estimate crop water requirements. It adopts a two-step crop coefficient (K_c) – reference evapotranspiration (ET_o) method for the realistic calculation of crop evapotranspiration. ET_o is the predominant climate effect on water intake, and the crop coefficient (K_c) scales the ET_o to provide crop-specific effects on evapotranspiration and their variation during the growing season, as shown in eq. (3.3).

$$ET_c = K_c \times ET_0 \tag{3.3}$$

Ideally, quantifying ET_c using grass-reference ET_o or alfalfa-reference ET_r should yield similar results. However, K_c values obtained using different reference surfaces can not be used interchangeably. The crop phenological stages are generally divided

into four stages: initial stage, development stage, mid-stage, and late-stage, with different durations as defined below.

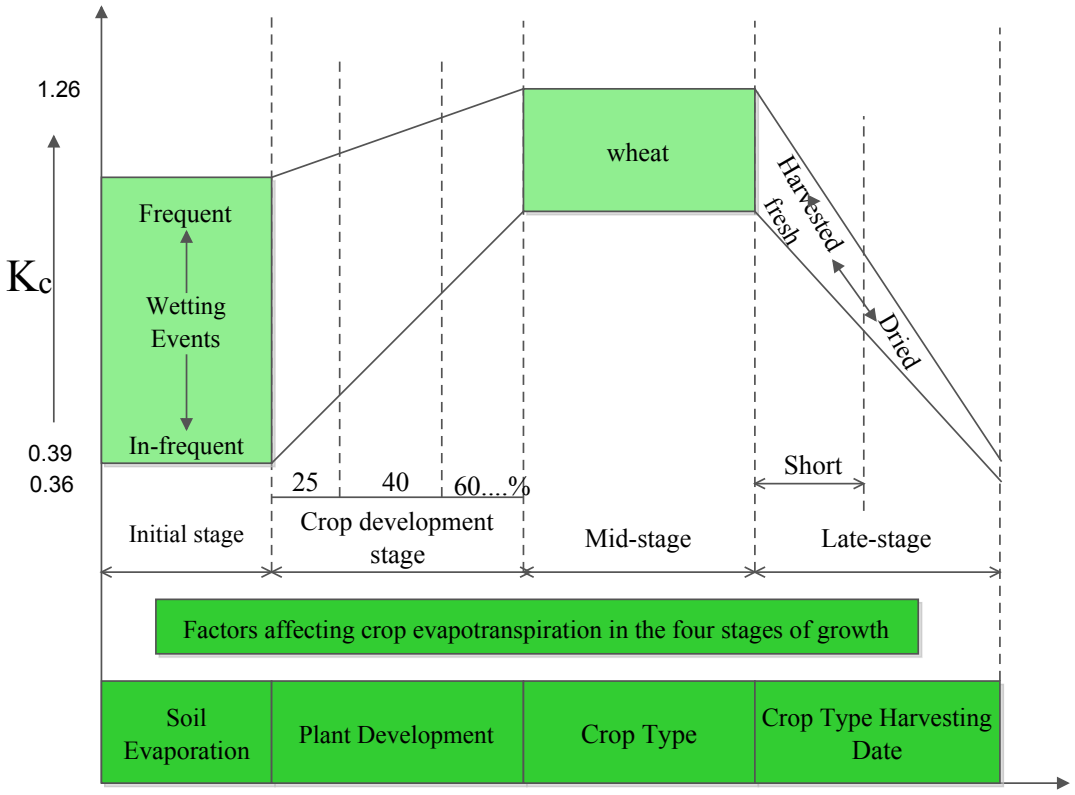

Figure 3.6: Growth stages of crop

- **Initial Stage**: This stage runs from the sowing date to 10% ground cover. This stage's duration depends on the crop type, variety of crops, and climate conditions. The leaf area is modest during this time, and soil evaporation accounts for most of the evapotranspiration process.

- **Development Stage**: This stage starts at the end of the initial stage and lasts until the effective ground cover of 70-80%. The crop matures and increasingly covers more area, hindering the evaporation process and transpiration, gradually replacing it as the primary process.

- **Mid Stage**: This stage represents the period between the effective complete cover and the beginning of maturity.

- **Late Stage**: The period between the beginning of maturity and harvest, or complete senescence, is the late stage of the crop.

The crop coefficient differs for each stage and varies with climatic conditions, as shown in Figure 3.6. Crop type, climate conditions, the growth stage of the crop, and soil evaporation are primary factors that determine the value of crop coefficient.

3.4.2 Crop Water Stress-based Irrigation Scheduling

Crop water stress is defined as insufficient water availability to crops. It can be identified from the physiological changes in the crop and the decrease in soil water content. In a water deficit situation, the crop leaves receive hydraulic and chemical signals via the xylem route, which changes crop physiological responses such as a decrease in photosynthetic process rate and stomata closure. This situation negatively impacts crop physiology (e.g., leaf area reduction, leaf wilting) and nutritional development, which leads to reduced crop biomass, yield, and quality.

The plant response to water stress depends on the environmental conditions and the need for crop evapotranspiration conditions as irrigation must replenish soil moisture losses due to evapotranspiration. Plant water status (PWS) measurements are necessary to better understand the processes of plant response to water stress adaptation and increase yield production through precision irrigation. It determines the response of the crop to available soil moisture, soil evaporation requirements, hydraulic resistance, and absorption capability of the plant-root interface. It is a more vulnerable stress indicator than soil moisture. Plant-based irrigation scheduling methods employ indices related to plant water status. A variety of plant-based stress measures have been suggested for irrigation scheduling.

The direct method involves pressure chambers and parameters to quantify crop water stress by measuring leaf water potential (LWP). Leaf water potential is considered to provide the average soil water potential next to the roots of the plant and gives a good indication of crop water status. However, the application of these instruments is limited as this is time-consuming and laborious to perform numerous measurements to quantify leaf water potential. Non-destructive and rapid onset monitoring of crop water stress is critical to precision irrigation management. Canopy temperature (T_c) has long been regarded as a good indicator of plant water status. The use of thermal infrared technology to measure canopy temperatures is a widely acknowledged method for monitoring plant water status and identifying the onset of water stressors [165].

Crop water stress index (CWSI), first introduced by Jackson *et al.* [166] and Idso *et al.* [167], is a method that uses infrared thermography (IRT) based T_c measurements and other climate parameters such as air temperature (T), solar radiation

(R_s), wind speed (WSP), and relative humidity (RH) to quantify water stress. It has been an extensively used index to identify water stress, schedule irrigation, and forecast yield in various crops under various agro-climatic scenarios due to its reliable and non-destructive nature [165] [168]. Ideally, CWSI has two limits: 0 and 1, 0 denotes a non-water stressed, and 1 denotes a highly water-stressed condition. Moreover, there exist two forms of CWSI, theoretical [167], and empirical approach [166]; both of these approaches have been successful in relating sap flow and leaf flow potential. However, CWSI computation require lower baseline temperature (T_{lb}) and upper baseline temperature (T_{ub}). In the theoretical approach, these baseline temperatures are generally computed by the mass-energy balance method, which is complex and infeasible to obtain in field conditions. On the other hand, the empirical method involves simple calculation and requires only temperature and relative humidity to determine baseline canopy temperature. Therefore, the empirical approach has been widely adopted to calculate CWSI and is defined in eq. (3.4).

$$CWSI = \frac{T_c - T_{lb}}{T_{ub} - T_{lb}} \tag{3.4}$$

Here, T_c denotes canopy temperature, T_{lb} represents canopy temperature in non-water-stressed conditions (lower baseline temperature), and T_{ub} represents canopy temperature in water-stressed conditions (upper baseline temperature). T_{lb} is estimated using linear regression of T_c – T and vapor pressure deficit (VPD) for no transpiring and possibly transpiring crops, respectively, and for estimating T_{ub}, constant values have also been suggested for different crops [169].

Although, this method yields accurate CWSI estimations and is easier to implement in the field. However, the direct measurement of these two baseline temperatures is practically very difficult while simultaneously measuring T_c as both baseline temperatures require undesirable and unattainable soil moisture conditions. The alternate methods for their estimation have been suggested that involves artificial reference surfaces [170], stressed and non stressed water treatments [171], numerical estimation using physical models [172], etc. However, their field application is limited due to the numerous parameters involved in the physical models and the extensive maintenance of artificial reference surfaces.

As a result, estimating the baseline temperature using parsimonious prediction models based on inadequate meteorological data would promote the use of CWSI as a tool for monitoring crop stress and scheduling irrigation. Thermal remote sensing techniques have been extensively adopted in measuring canopy temperature for

monitoring water stress. Recent studies have focused on utilizing AI-based models to estimate CWSI using thermal remote sensing techniques. Moreover, a section of researchers also focuses on directly using digital images to differentiate stressed and non-stressed plants using AI-based techniques.

3.4.3 Soil Moisture-based Irrigation Scheduling

Soil moisture (SM) is a key element in agricultural productivity and the hydrological cycle. The accurate prediction of SM is critical for the efficient use and management of water resources. Moreover, crop water requirement (CWR) using the soil water balance approach is highly recommended because it takes into account actual CWR and can result in considerable water savings in irrigated agriculture [173].

Applying this approach for irrigation scheduling involves understanding temporal fluctuations in SM at the field for crops grown under optimum or water-stress circumstances. However, SM is affected by soil properties, crop type, and meteorological parameters, and it is difficult to formulate ideal mathematical models for the prediction of SM. Therefore, methods for forecasting SM with low data requirements are needed to achieve optimized irrigation scheduling, especially for various water-saving irrigation strategies that are necessary to handle food and water security challenges under water scarcity.

Researchers have used a variety of ways to determine soil moisture (in gravimetric and volumetric forms), which may be classified into classical techniques (e.g., calcium carbide technique and thermo-gravimetric) and modern techniques (e.g., dielectric techniques, heat flux soil moisture sensors, infrared moisture balance, etc.). However, the inability to directly measure soil water content in the field at a low cost limits the applicability of the soil water balance equation for irrigation scheduling.

Over the last three decades, several models for modelling soil water content (SWC) in soil-crop systems have been developed e.g. HYDRUS [174], SWAP [175], EUROACCESS- II [176] [177], etc. Artificial intelligence models are also applied for simulating numerous hydrological processes, including soil moisture estimation. These models have a high prediction ability and do not need a thorough understanding of soil physical parameters. Further AI models with remotely sensed data have also been applied to simulate soil water dynamics.

Chapter 4

Hybrid Deep Learning Models for Reference Evapotranspiration

This chapter presents hybrid deep learning models to predict the daily reference evapotranspiration using meteorological parameters of Ludhiana and Patiala stations. CNN-LSTM and Conv-LSTM are investigated on different combinations of meteorological parameters to identify the minimum required meteorological parameters for the reliable prediction of ET_o. Further, the proposed hybrid models are compared to temperature and radiation-based empirical models.

4.1 Overview

Reference evapotranspiration (ET_o) plays an undeniably important role in irrigation management. Precise estimation of ET_o is essential for designing, planning, and effectively implementing irrigation scheduling particulars in water-scarce areas to increase agricultural productivity [178]. It can be measured directly using a lysimeter or eddy covariance. However, due to technical complexities [179] and high cost, it is calculated using some empirical equations such as FAO-PM [161] or American Society of Civil Engineers Penman–Monteith (ASCE-PM) equations [180].

These equations require meteorological data (solar radiation, temperature, vapor pressure, humidity, and wind speed) as inputs and are widely accepted worldwide. However, the availability of these meteorological data is a challenging issue in developing countries. So, many other empirical models have been developed that use limited climate data to estimate evapotranspiration, such as the temperature-based models: Hargreaves Samani model [141], and radiation-based models: Makkink [147], Ritchie [148]. The choice of these methods depends on the availability of data and the accuracy of these methods. However, it has been found that these models perform best for weekly and monthly data but not for daily data. Also, these equations have not able to provide comparable accuracy with the ob-

served ET_o equation [181]. So, there is a need to develop a model that uses limited available climate data as input to predict ET_o with no compromise on estimation accuracy.

There exists a complex non-linear regression process to calculate ET_o that depends on meteorological data. Many meteorological variables, such as air temperature, radiation, relative humidity, sunshine hours, etc., show seasonality and time dependency properties. Therefore, the process of evapotranspiration can be considered as a time series regression problem.

Deep learning models effectively address problems with massive amounts of data, multivariate with complex relationships, and multi-step time series forecasting tasks [182]. The problem of prediction of evapotranspiration values also exhibits the same characteristics, such as there exist complex non-linear relationships between multiple variables, and these variables follow time series behavior. Nevertheless, these methods are less widely applied to the evapotranspiration process. Therefore, in this chapter, an attempt is made to apply deep learning time series forecasting algorithms to model the process of reference evapotranspiration.

Convolution neural network (CNN) and long short-term memory (LSTM) are two popular deep learning algorithm. However, a literature review conducted in this study reveals that very little work has been reported for estimating reference evapotranspiration using these two models. It has also been reported that CNN and LSTM models can provide better performance when used as hybrid models such as CNN-LSTM and Conv-LSTM [183] [184]. In consideration of the foregoing, the present study proposes two-hybrid deep neural network models for the estimation of reference evapotranspiration: Convolution—Long Short Term Memory (Conv-LSTM), which performs the convolution operation in LSTM cells and Convolution Neural Network—LSTM (CNN-LSTM) that uses the convolution layer for feature extraction of input data, and then extracted features are fed to LSTM layers.

The study also focuses on climate data scarcity conditions, and thus, different input combinations of climate parameters have been used to investigate the minimum required parameters to model the ET_o process. Further, the proposed hybrid models are then compared with existing temperature and radiation-based empirical models such as Hargreaves, Makkink, and Ritchie. The next sections discuss the proposed hybrid models and methodology adopted for the prediction of daily ET_o values.

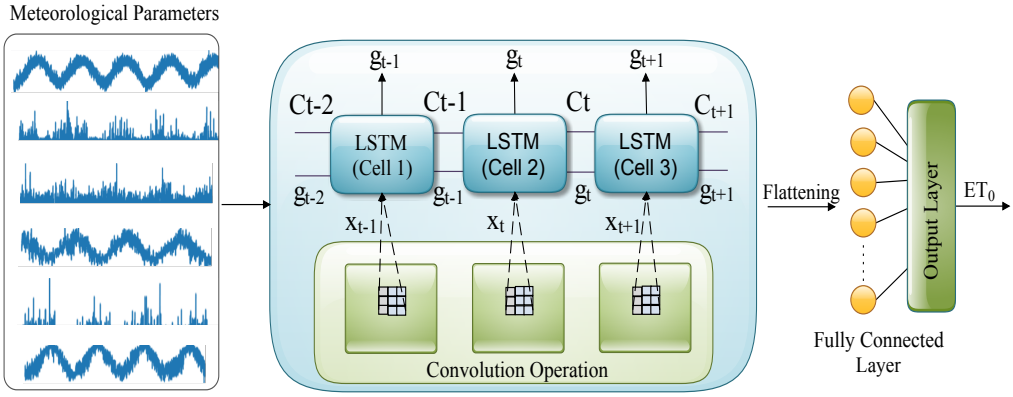

Figure 4.1: Architecture of Conv-LSTM

4.2 Conv-LSTM

Conv-LSTM [185] is a type of recurrent neural network. Its core working is similar to the LSTM model, but here the convolution operation is used to decide the input-to-state and state-to-state transitions. LSTM cells receive input x_t and hidden state output h_t at each time iteration t. The previous cell output state C_{t-1} and current cell output C_t are also taken into consideration to perform state updations using convolution operation and generating output. The key operations of Conv-LSTM are shownbelow in the eq. (4.1) to (4.6).

$$i_t = sigm(M_{ic} \circ C_{t-1} + M_{ih} * h_{t-1} + M_{ix} * x_t + b_i) \tag{4.1}$$

$$f_t = sigm(M_{fc} \circ C_{t-1} + M_{fh} * h_{t-1} + M_{fx} * x_t + b_f) \tag{4.2}$$

$$o_t = sigm(M_{oc} \circ C_{t-1} + M_{oh} * h_{t-1} + M_{ox} * x_t + b_i) \tag{4.3}$$

$$g_t = tanh(M_{gh} * h_{t-1} + M_{gx} * x_t + b_c) \tag{4.4}$$

$$C_t = C_{t-1} \circ f_t + g_t \circ i_t \tag{4.5}$$

$$h_t = tanh(C_t) \circ o_t \tag{4.6}$$

where $\circ$ represents convolution operation, $*$ represents Hadamard product, sigm and tanh represent the logistic sigmoid function and hyperbolic tangent function, respectively. i_t, f_t, o_t, and g_t represents the input, forget, output and input modulation gates, respectively. x_t, C_t and h_t are the input, cell state, and hidden state at t^{th} step of the model. M_i, M_o, and M_f are the weight matrix for input, output, and forget gates, respectively. The architecture of Conv-LSTM used in this study for modeling the process of evapotranspiration is shown in Figure 4.1.

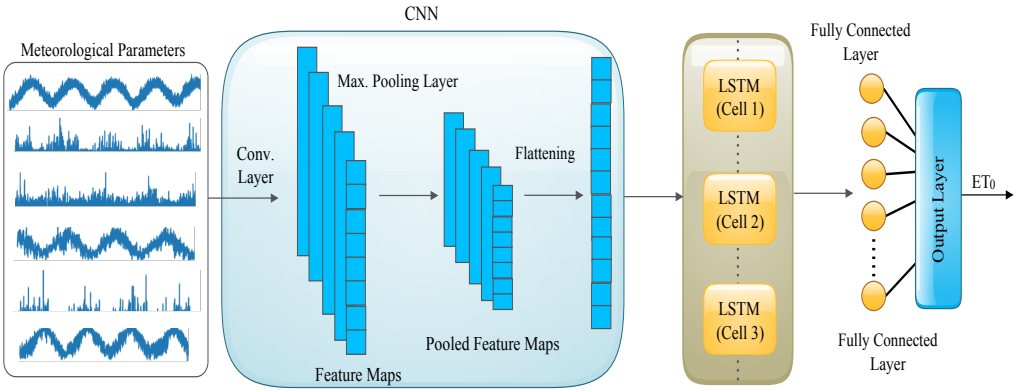

Figure 4.2: Architecture of CNN-LSTM

4.3 CNN-LSTM

CNN-LSTM [184] is a hybrid neural network model that combines the CNN layers and LSTM in one unified framework. It has been proved in the past that the performance of LSTM is improved if relevant features are provided [186].

In the present study, the CNN-LSTM model is used for predicting ET_o values, which consists of a CNN layer to extract relevant features from climate data and find a correlation among multivariate time series sequences that affect the evapotranspiration process. This layer's output is used as an input to the LSTM layer (after several other layers, such as pooling and flattening layers) that models the temporal information to predict the evapotranspiration values of the next timestamp.

Let $X_T = [X_1, X_2, X_3, X_4 \ldots . X_n]$ to be the input meteorological data vector, which is provided to CNN. Then the output of the CNN is passed to gate units of the LSTM layer. The LSTM cell updates its state using the operations shown in eqs. (4.7) to (4.14).

$$O_t = g(c \times X_{t-\frac{l}{2}:t+\frac{l}{2}} + b \forall t \in T) \tag{4.7}$$

$$i_t = sigm(w_i h_{t-1} \ + \ M_i x_t + \ b_i) \tag{4.8}$$

$$f_t = sigm(w_f h_{t-1} \ + \ M_f x_t + \ b_f) \tag{4.9}$$

$$o_t = sigm(w_o h_{t-1} \ + \ M_o x_t \ + \ b_o \ ) \tag{4.10}$$

$$g_t = tanh(w_g h_{t-1} \ + \ M_g x_t) \tag{4.11}$$

$$C_t = C_{t-1} \circ f_t \ + \ g_t * i_t \tag{4.12}$$

$$h_t = tanh\,(c_t) * \ o_t \tag{4.13}$$

$$y^n = \sum_j w_{ji}^{n-1}(relu(h_i^{n-1}) \quad + \quad b_i^{n-1}) \tag{4.14}$$

where ReLu is the rectified linear activation function which is a non-linear one, w is the weight from i^{th} node of layer n-1 to j^{th} node of layer n, and b represents bias. y^n is the final output of ET_o values. The dense layer is the last layer of this model that receives feature vector $h_T = [h_1, h_2, h_3, h_4, \ldots, h_n]$. The architecture of CNN-LSTM used in this study is shown in Figure 4.2.

4.4 Methodology

This section presents the proposed methodology used in the study. In the first subsection, a detailed analysis of the dataset is provided using statistical properties. Then, the criteria for selecting input parameters for developing the proposed hybrid deep learning models are discussed. The subsection 4.4.2 presents the model development strategy and flow chart of the conducted study. Finally, in the last subsection, the evaluation parameters used to assess the performance of the proposed models are provided.

4.4.1 Data Collection and Input Selection

The study is carried out at Ludhiana and Amritsar stations in the Punjab region of India. A detailed description of the geographical conditions of both the study areas is provided in section 3.2 of chapter 3. The daily meteorological parameters (T_{max}, T_{min}, WSP, R_s, RH, VP, and SSH) of both stations are retrieved from IMD Pune, India. The actual/observed ET_o values are calculated by the FAO-PM method using CROPWAT 8.0 software. The statistical observations of meteorological parameters show that the training and testing datasets are somewhat similar for developing the best possible model (Tables 3.1 and 3.2). The number and combinations of input variables affect the performance of the model [187].

This study selects the deep learning models' inputs based on the correlation of different meteorological variables with reference evapotranspiration. It is clear from these two tables that air temperature and solar radiation show the highest correlation with ET_o (Tables 3.4 and 3.5). Hence, these input variables must be included in selecting input variables with a combination of other climate variables to find the best model. Hereby, selecting only limited variables with reliable accuracy will also solve the problem of estimating reference evapotranspiration in the developing countries that do not have sensors deployed in every region to collect values of all climate variables.

4.4.2 Model Development

In this study, model development is carried out in Python programming language (3.6) using the following libraries: Keras (2.3.0-tf), Tensor Flow (2.2.0), Scikit Learn (0.22.2). All the computations are performed online using the graphical processing unit (GPU) provided by the cloud platform (Google Colab). Both Conv-LSTM and CNN-LSTM have been developed in the study to estimate the daily evapotranspiration of both stations. The meteorological dataset retrieved from IMD Pune, India is in the raw form and has some impurities such as missing values, outliers, etc. Hence, it cannot be directly fed to the deep learning models.

Missing data is one of the well-known research problems and can lead to inaccurate predictions and inconsistent results. The machine learning model's performance is also affected by the methods used to treat these missing values [188] [189]. Here, two missing data treatment methods are used to handle the climate dataset's missing values: Linear regression and K-nearest neighbor (KNN). Linear regression for missing data imputation has been widely adopted in past studies [190]. The only necessary condition is independent (X) and dependent (missing data variable) variables (y) must be correlated. Some of the climate parameters are highly co-related and can help in estimating the missing data (Table 3.4 and 3.5). Linear regression for missing data treatment is performed with the iterative imputer class of Python's scikit-learn package. The algorithm works in a round-robin fashion, and for each iteration, it tries to fit the regressor line (X, y), and loss is computed using equation (4.15).

$$loss = \frac{1}{n}\sum_{i=1}^{n}(y_p - y)^2 \tag{4.15}$$

where y_p is the predicted value of dependent variable y and is given as follows:

$$y_p = \alpha_1 X + \alpha_2 \tag{4.16}$$

here, the values α_1 and α_2 are coefficients of X and intercept, respectively. These values are updated to minimize the loss function to find the best fit line using gradient descent until convergence is reached.

The second method used in the study is KNN, where missing data is filled using the average or most common value of k-neighbors depending upon the type of data. The nearest neighbors are selected using distance matrices such as Euclidean distance, Minkowski's distance, and Manhattan distance. The KNN Imputer class in scikit-learn package of Python provides imputation of missing data using the K-nearest approach. The KNN imputation has been used in past studies and proved to

be a robust and sensitive method for missing data imputation [191]. Missing data of those climate parameters that are not correlated with other parameters are handled in the study using KNN. The value of k = 3 is used to provide the best trade-off between imputation error and data structure preservation [192].

The outliers present in the dataset due to instrument or human error are detected and eliminated in the study using the z-score method. The equation of the z-score method is provided in the following equation.

$$z = \frac{x_i - \bar{x}}{s} \tag{4.17}$$

where x_i is the data point, $\bar{x}$ is the mean, and s is the standard deviation; if the value of z exceeds 3, the corresponding data point is considered an outlier. z score () method of scipy library of Python is used in this study to detect and remove outliers present in the dataset. Normalization transforms the dataset in the standard range [0,1] to avoid convergence problems during the model's training. There are many methods to normalize the dataset, such as power transformer, quantile transformer (uniform/normal), robust scaler, max-abs scaler, and min-max scaler. However, the min-max scaler has been selected in this study as it is widely used in the literature and outperforms other techniques in some cases [193]. The min-max normalization equation is given as:

$$x_{norm} = \frac{x_i - x_{max}}{x_{max} - x_{min}} \tag{4.18}$$

where x_{norm} represents normalized value, x_{max} and x_{min} represents the maximum and minimum values of the dataset.

The pre-processed dataset is fed to deep hybrid learning models (CNN-LSTM and Conv-LSTM). The selection of hyper-parameters such as the number of filters, kernel size, activation function, number of neurons in fully connected layers, optimizer, batch size, etc., affects a given model's learning speed and performance. Therefore in this study, the model's hyper-parameter is defined using the Random search method of the Keras tuner library, as it has been observed that this approach is more efficient than grid search and manual hyper tuning methods [194].

The dataset is divided into two subsets: training data (70%) and testing data (30%). The dropout layer (with a probability of 0.1) is applied to dense layers to avoid overfitting and make the generalizable model. The random search method trains the model using this training data, and 10% of the training data is used for the validation process for hyper-parameters tuning. The hyper-parameters that minimize the error are selected to obtain the best model. Finally, the best obtained

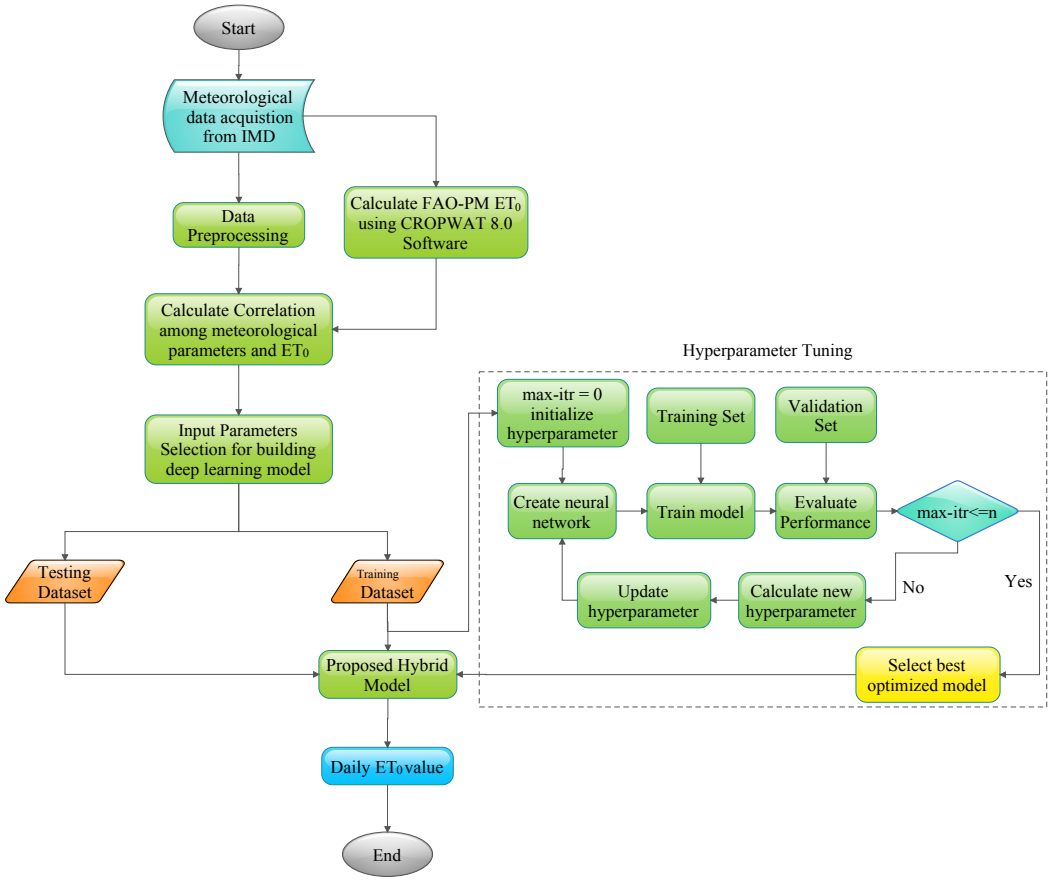

Figure 4.3: Flowchart of the proposed methodology of ET_o estimation

model is tested with testing data. The flowchart of the proposed methodology is shown in Figure 4.3.

4.4.3 Model Performance Evaluation Parameters

The performance evaluation is an essential step towards model development. It includes the comparison of models' estimated values with actual values using mathematical measurement to observe how efficiently the proposed model can simulate the actual output. In this study, deep learning models (CNN-LSTM, Conv-LSTM) are trained on different input combinations of climate data to estimate ET_o. The estimated ET_o values are compared to the observed/actual ET_o values calculated using the following statistical indicators: Mean absolute error (MAE), Root mean square error (RMSE), Percent bias (Pbias), Nash-Scuttle efficiency (NSE), Coefficient of determination (R^2) and Index of agreement (IA) which are calculated by the following equations.

$$MAE = \frac{1}{N}\sum_{i=1}^{N}(ET_{ob_i} - ET_{p_i}) \tag{4.19}$$

$$RMSE = \sqrt{\frac{\sum_{i=1}^{N}(ET_{ob_i} - ET_{p_i})^2}{N}} \tag{4.20}$$

$$Pbias = \frac{\sum_{i=1}^{N}(ET_{ob_i} - ET_{p_i})}{\sum_{i=1}^{N} ET_{ob_i}} \times 100 \tag{4.21}$$

$$NSE = 1 - \frac{\sum_{i=1}^{N}(ET_{ob_i} - ET_{p_i})^2}{\sum_{i=1}^{N}(ET_{ob_i} - \bar{ET_{ob}})^2} \tag{4.22}$$

$$R^2 = \frac{\sum_{i=1}^{N}(ET_{ob_i} - \bar{ET_{ob}})(ET_{p_i} - \bar{ET_p})}{(\sum_{i=1}^{N}(ET_{ob_i} - \bar{ET_{ob}})^2)(\sum_{i=1}^{N}(ET_{p_i} - \bar{ET_p})^2)} \tag{4.23}$$

$$IA = 1 - \frac{\sum_{i=1}^{N}(ET_{ob_i} - ET_{p_i})^2}{\sum_{i=1}^{N}(|ET_{p_i} - \bar{ET_{ob_i}}| + |ET_{ob_i} - \bar{ET_{ob_i}}|)} \tag{4.24}$$

Here ET_{ob_i} (mmd^{-1}) is observed or FAO-PM calculated value of ET_o, ET_{p_i} is the estimated value of ET_o, which is predicted by using the proposed deep learning models for the ith value of data point, $\bar{ET_{ob}}$ is mean of observed value, $\bar{ET_p}$ is the mean of predicted values of ET_o, and N is the number of data points considered in the study.

Mean absolute error is the average of absolute and predicted values without considering the directions, and it ranges between 0 to 1. The lower MAE value results in a perfect estimation by the model [195]. RMSE is a measure of residual error deviation that indicates how close the data is to the best fit line. The lower value of RMSE shows a better estimation of the model. Percent bias is an estimation error that is normalized by observation. The low-magnitude values of percent bias indicates accurate model simulation. R^2 shows the degree of correlation between ET_o values estimated by deep learning models and observed ET_o values. IA is a dimensionless measure to represent model quality, which ranges between 0 (worst fit) and 1 (best fit) [196]. NSE is a popular and potentially reliable metric for evaluating the predictive competency of hydrologic models. It ranges from 0 to 1 for unbiased models, with 1 representing a perfect model, and for biased models, it may be algebraically negative [197].

4.5 Results and Discussion

The essence of this study is to find out the minimum required input parameters and observe the feasibility of the proposed hybrid deep neural network models to model the complex non-linear relationship that exists between climate parameters and ET_o. This section provides insight into the obtained results from the conducted study. An experiment is conducted to examine two-hybrid deep neural network

models: CNN-LSTM and Conv-LSTM to estimate daily ET_o values of Ludhiana and Amritsar stations.

In the first subsection, the aforementioned models are implemented using different input combinations of the available meteorological dataset to estimate the ET_o values. The results obtained with these two-hybrid deep learning models are provided in Tables 4.1 and 4.2 using performance metrics such as NSE, MAE, and RMSE of training and testing datasets. In the second subsection, input combinations that give promising results are further comprehensively analyzed. In the third subsection, the proposed models' performance is compared with the existing temperature and radiation-based empirical models. Finally, in the last subsection, the strengths and limitations of the conducted study are analyzed.

The comparison of predicted ET_o values of proposed hybrid deep learning models are shown in Figures 4.4 and 4.5 of both stations. Table 4.3 summarizes the best-selected input combination's performance. Table 4.4 depicts the comparison of empirical models with proposed deep learning models. The scatter plots showing the hybrid models' performances with limited input data and empirical models are shown in Figures 4.6 and 4.7, respectively.

4.5.1 Performance Comparison of Hybrid Models under Various Input Combinations

Temperature is considered as the inseparable input data for the estimation of ET_o in many studies [53] [61] [198]. Solar radiation has also shown the highest correlation with ET_o, among other climate variables, as shown in Tables 3.4 and 3.5. Also, radiation has been used as one of the key input data in many empirical equations for calculating reference evapotranspiration. Therefore, in this study, temperature and radiation are considered as prime input parameters to estimate ET_o values. The different input combinations with these prime input parameters are fed to deep learning models (CNN-LSTM and Conv-LSTM). Tables 4.1 and 4.2 present the results of these models with 21 different input combinations. The input combinations used in the study are also consistent with many previous studies [28] [199]. Input combinations from 1–6 in Table 4.1 use air temperature and the combination of air temperature with other meteorological variables RH, R_s, WSP, VP, and SSH.

The correlation between the above mentioned meteorological parameters and ET_c of wheat and rice crops is provided in Table 3.9 and 3.10 respectively. The mean values of T_{min}, T_{max}, T_{mean}, and R_s of Ludhiana station from 2003 to 2015 for wheat and rice crop growing period are provided in Table 3.11. The obtained

results also support the decision to use other combinations using temperature and solar radiation as prime inputs for estimating reference evapotranspiration. The result is also consistent with the work of Traore [53], where improvement in results has been observed with the use of solar radiation along with air temperature.

Sunshine hour is also another input variable that shows the promising result with NSE ranges from 0.906 to 0.910 and 0.9078 to 0.9136, MAE ranges from 0.050 to 0.049, and 0.0494 to 0.0479, and RMSE varies from 0.068 to 0.066, and 0.0674 to 0.646 of training and testing data using CNN-LSTM and Conv-LSTM models, respectively of Ludhiana station and NSE ranges from 0.9039 to 0.9068 and 0.9087 to 0.9135, MAE ranges from 0.0491 mmd^{-1} to 0.0491 mmd^{-1}, and 0.0494 mmd^{-1} to 0.0488 mmd^{-1} and RMSE varies from 0.0691 mmd^{-1} to 0.0691 mmd^{-1} and 0.0674 $mmd^{-1}$to 0.0647 mmd^{-1} of training and testing data using CNN-LSTM and Conv-LSTM, respectively of Amritsar station.

The combination of relative humidity, wind speed, and vapor pressure does not provide good results. Also, Conv-LSTM outperforms the CNN-LSTM model in combinations from 1–6 as shown in Table 4.1. Table 4.2 demonstrates the performance of possible input combinations using temperature and radiation as prime input data along with other meteorological variables. It is clear from Table 4.2 that Conv-LSTM provides the most accurate results in almost every possible combination considered in the study. It can be observed from Table 4.2 that generally, the model's performance is increased with an increase in the number of input variables, but in some cases, it is also found that an increase in the number of input variables does not impact the model's performance. For example, combination 10, 12, and 14 provides comparable performance, and combination 11, 13, and 17 also shows similar performance.

Table 4.1: Performance of hybrid DL models using input combination with temperature variable

			Ludhiana Station				**Amritsar Station**			
S.	**Input**	**Performance**	**CNN-LSTM**		**Conv-LSTM**		**CNN-LSTM**		**Conv-LSTM**	
no	**Combination**	**metrics**	**Train**	**Test**	**Train**	**Test**	**Train**	**Test**	**Train**	**Test**
1	T_{max}, T_{min}	NSE	0.746	0.736	0.811	0.805	0.734	0.731	0.802	0.804
		MAE (mmd^{-1})	0.089	0.089	0.076	0.076	0.090	0.090	0.077	0.076
		RMSE (mmd^{-1})	0.112	0.113	0.097	0.097	0.115	0.114	0.099	0.097
2	T_{max}, T_{min}, RH	NSE	0.257	0.229	0.840	0.835	0.261	0.236	0.846	0.842
		MAE (mmd^{-1})	0.151	0.151	0.070	0.071	0.149	0.149	0.069	0.069
		RMSE (mmd^{-1})	0.192	0.193	0.089	0.089	0.192	0.192	0.088	0.088
3	T_{max}, T_{min}, R_s	NSE	**0.926**	**0.928**	**0.937**	**0.942**	**0.908**	**0.914**	**0.944**	**0.948**
		MAE (mmd^{-1})	0.043	0.042	0.039	0.038	0.054	0.052	0.035	0.035
		RMSE (mmd^{-1})	0.061	0.059	0.056	0.053	0.068	0.064	0.053	0.050
4	T_{max}, T_{min}, VP	NSE	0.83	0.825	0.832	0.828	0.831	0.829	0.832	0.823
		MAE (mmd^{-1})	0.072	0.072	0.072	0.072	0.072	0.073	0.071	0.073
		RMSE (mmd^{-1})	0.092	0.092	0.092	0.091	0.092	0.091	0.091	0.093
5	T_{max}, T_{min}, WSP	NSE	0.723	0.715	0.881	0.870	0.746	0.732	0.884	0.874
		MAE (mmd^{-1})	0.092	0.092	0.060	0.062	0.089	0.090	0.061	0.061
		RMSE (mmd^{-1})	0.117	0.117	0.077	0.079	0.112	0.114	0.078	0.078
6	T_{max}, T_{min}, SSH	NSE	0.906	0.91	0.908	0.914	0.904	0.907	0.909	0.914
		MAE (mmd^{-1})	0.05	0.049	0.049	0.048	0.049	0.049	0.049	0.049
		RMSE (mmd^{-1})	0.068	0.066	0.068	0.065	0.069	0.069	0.067	0.065

Table 4.2: Performance of hybrid DL models using the different input combinations

S. no	Input Combination	Performance metrics	Ludhiana Station				Amritsar Station			
			CNN-LSTM		Conv-LSTM		CNN-LSTM		Conv-LSTM	
			Train	Test	Train	Test	Train	Test	Train	Test
7	T_{max}, T_{min}, R_s, RH	NSE	0.949	0.947	0.956	0.956	0.939	0.94	0.955	0.957
		MAE (mmd^{-1})	0.036	0.035	0.032	0.032	0.041	0.04	0.033	0.032
		RMSE (mmd^{-1})	0.05	0.05	0.047	0.046	0.054	0.053	0.047	0.046
8	T_{max}, T_{min}, R_s. SSH	NSE	0.924	0.931	0.952	0.956	0.935	0.938	0.958	0.963
		MAE (mmd^{-1})	0.043	0.043	0.033	0.032	0.04	0.038	0.03	0.028
		RMSE (mmd^{-1})	0.062	0.058	0.049	0.046	0.056	0.055	0.046	0.042
9	T_{max}, T_{min}, R_s, WSP	NSE	0.952	0.939	0.983	0.983	0.953	0.94	0.983	0.984
		MAE (mmd^{-1})	0.034	0.037	0.019	0.019	0.03	0.034	0.018	0.017
		RMSE (mmd^{-1})	0.049	0.054	0.029	0.029	0.048	0.053	0.029	0.028
10	T_{max}, T_{min}, R_s, VP	NSE	0.862	0.857	0.949	0.948	0.82	0.815	0.946	0.949
		MAE (mmd^{-1})	0.057	0.057	0.036	0.036	0.063	0.062	0.039	0.037
		RMSE (mmd^{-1})	0.083	0.083	0.051	0.05	0.094	0.094	0.052	0.049
11	T_{max}, T_{min}, R_s, RH, SSH	NSE	0.96	0.959	0.96	0.957	0.935	0.938	0.938	0.937
		MAE (mmd^{-1})	0.031	0.031	0.03	0.031	0.04	0.038	0.039	0.039
		RMSE (mmd^{-1})	0.045	0.044	0.045	0.045	0.056	0.054	0.056	0.055
12	T_{max}, T_{min}, R_s, RH, VP	NSE	0.958	0.954	0.958	0.954	0.956	0.955	0.957	0.954
		MAE (mmd^{-1})	0.032	0.033	0.032	0.033	0.034	0.034	0.034	0.035
		RMSE (mmd^{-1})	0.046	0.047	0.046	0.047	0.046	0.046	0.046	0.047

			Ludhiana Station				Amritsar Station			
S.	**Input**	**Performance**	**CNN-LSTM**		**Conv-LSTM**		**CNN-LSTM**		**Conv-LSTM**	
no	**Combination**	**metrics**	**Train**	**Test**	**Train**	**Test**	**Train**	**Test**	**Train**	**Test**
13	T_{max}, T_{min}, R_s,	NSE	**0.988**	**0.989**	**0.989**	**0.99**	**0.981**	**0.98**	**0.989**	**0.989**
	RH, WSP	MAE (mmd^{-1})	**0.016**	**0.016**	**0.015**	**0.015**	**0.024**	**0.024**	**0.015**	**0.015**
		RMSE (mmd^{-1})	**0.024**	**0.023**	**0.024**	**0.022**	**0.03**	**0.03**	**0.024**	**0.023**
14	T_{max}, T_{min}, R_s,	NSE	0.959	0.962	0.96	0.962	0.914	0.916	0.959	0.958
	SSH, VP	MAE (mmd^{-1})	0.031	0.03	0.03	0.029	0.048	0.047	0.03	0.031
		RMSE (mmd^{-1})	0.045	0.043	0.045	0.043	0.066	0.064	0.045	0.045
15	T_{max}, T_{min}, R_s,	NSE	0.98	0.983	0.984	0.983	0.936	0.937	0.984	0.984
	SSH, WSP	MAE (mmd^{-1})	0.02	0.019	0.019	0.019	0.042	0.042	0.017	0.017
		RMSE (mmd^{-1})	0.032	0.029	0.029	0.029	0.056	0.055	0.028	0.028
16	T_{max}, T_{min}, R_s,	NSE	0.984	0.984	0.984	0.985	0.986	0.987	0.986	0.987
	VP, WSP	MAE (mmd^{-1})	0.02	0.02	0.019	0.019	0.017	0.017	0.018	0.018
		RMSE (mmd^{-1})	0.028	0.027	0.028	0.027	0.026	0.025	0.026	0.025
17	T_{max}, T_{min}, R_s,	NSE	0.929	0.917	0.959	0.959	0.932	0.907	0.961	0.956
	RH, SSH, VP	MAE (mmd^{-1})	0.044	0.047	0.03	0.03	0.039	0.043	0.031	0.032
		RMSE (mmd^{-1})	0.059	0.063	0.045	0.045	0.058	0.067	0.044	0.046

S.	Input	Performance	Ludhiana Station				Amritsar Station			
			CNN-LSTM		Conv-LSTM		CNN-LSTM		Conv-LSTM	
no	Combination	metrics	Train	Test	Train	Test	Train	Test	Train	Test
18	T_{max},T_{min}, R_s,	NSE	0.98	0.976	0.99	0.991	0.981	0.979	0.992	0.993
	RH, SSH, WSP	MAE (mmd^{-1})	0.02	0.022	0.014	0.014	0.021	0.022	0.011	0.011
		RMSE (mmd^{-1})	0.031	0.034	0.022	0.021	0.031	0.032	0.02	0.018
19	T_{max}, T_{min}, R_s,	NSE	0.966	0.954	0.987	0.989	0.965	0.953	0.988	0.989
	RH, WSP, VP	MAE (mmd^{-1})	0.029	0.031	0.017	0.016	0.031	0.034	0.016	0.016
		RMSE (mmd^{-1})	0.041	0.047	0.025	0.024	0.042	0.048	0.024	0.023
20	T_{max}, T_{min}, R_s,	NSE	0.978	0.977	0.989	0.989	0.976	0.975	0.99	0.991
	WSP, VP, SSH	MAE (mmd^{-1})	0.023	0.023	0.016	0.016	0.024	0.025	0.013	0.013
		RMSE (mmd^{-1})	0.033	0.033	0.024	0.023	0.034	0.035	0.022	0.021
21	T_{max}, T_{min}, R_s,	NSE	**0.989**	**0.989**	**0.991**	**0.992**	**0.991**	**0.991**	**0.991**	**0.991**
	WSP, VP, WSP,	MAE (mmd^{-1})	**0.015**	**0.016**	**0.013**	**0.012**	**0.012**	**0.013**	**0.013**	**0.013**
	RH	RMSE (mmd^{-1})	**0.022**	**0.023**	**0.021**	**0.02**	**0.02**	**0.019**	**0.021**	**0.021**

4.5.2 Comprehensive Evaluation of Best Input Combination for Proposed Hybrid Models

The value of NSE indicates the predictive power of hydrological models. The value closer to 1 shows the model's efficiency. Thus, based on the value of NSE, eight promising input combinations are selected to predict the value of ET_o. The values of IA, R^2, and *Pbias* during the training and testing period of the considered models are given in Table 4.3.

It is clear from Table 4.3 that the Conv- LSTM has IA and R^2 values closer to 1 and *Pbias* closer to zero, which shows that the model is not under or overestimated. However, a *Pbias* value greater than zero in some input combinations for the CNN-LSTM model has been observed, indicating the overestimation.

The other important information that can be derived from Table 4.3 is that wind speed when combined with prime input data, gives satisfactory results. From the selected best eight input combinations, number 13 (T_{max}, T_{min}, R_s, WSP, and RH) is able to achieve reliable performance with R^2 values from 0.989 to 0.991 with possible limited input combinations.

The line graph visualizes daily ET_o values predicted by proposed deep learning models during the testing period in Figures 4.4 and 4.5 of Ludhiana and Amritsar stations, respectively. It is clear from Figures 4.4 and 4.5 that the estimation of ET_o values by CNN-LSTM and Conv-LSTM are somewhat similar to the observed ET_o values. However, the estimated ET_o values by Conv-LSTM are closer to the observed ET_o values and indicate that Conv-LSTM performs better in eight selected combinations.

In the following subsection, empirical models are compared to CNN-LSTM and Conv-LSTM models with the same input combination as used by these empirical models.

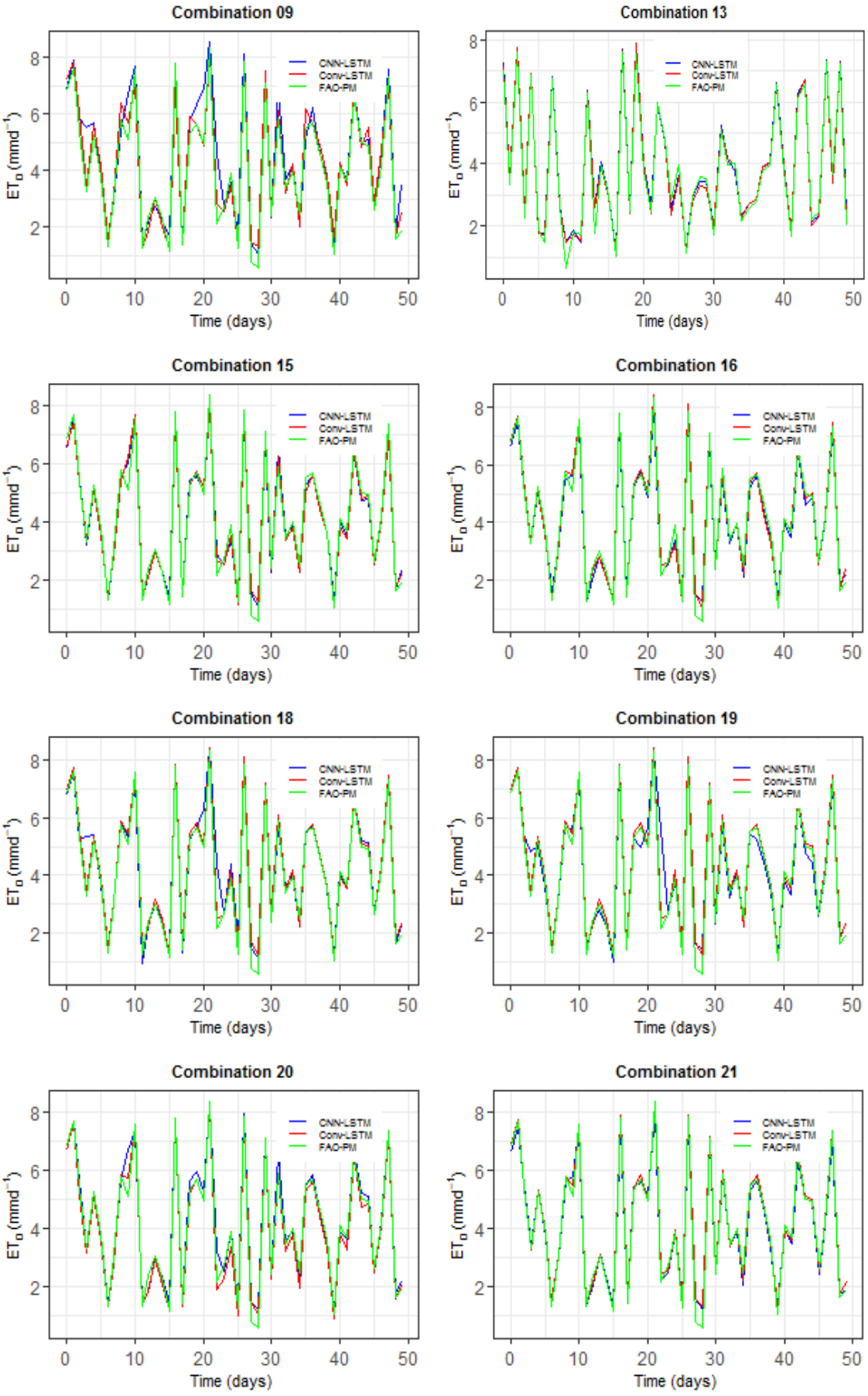

Figure 4.4: Comparison of ET_o values predicted by hybrid DL models for Ludhiana station

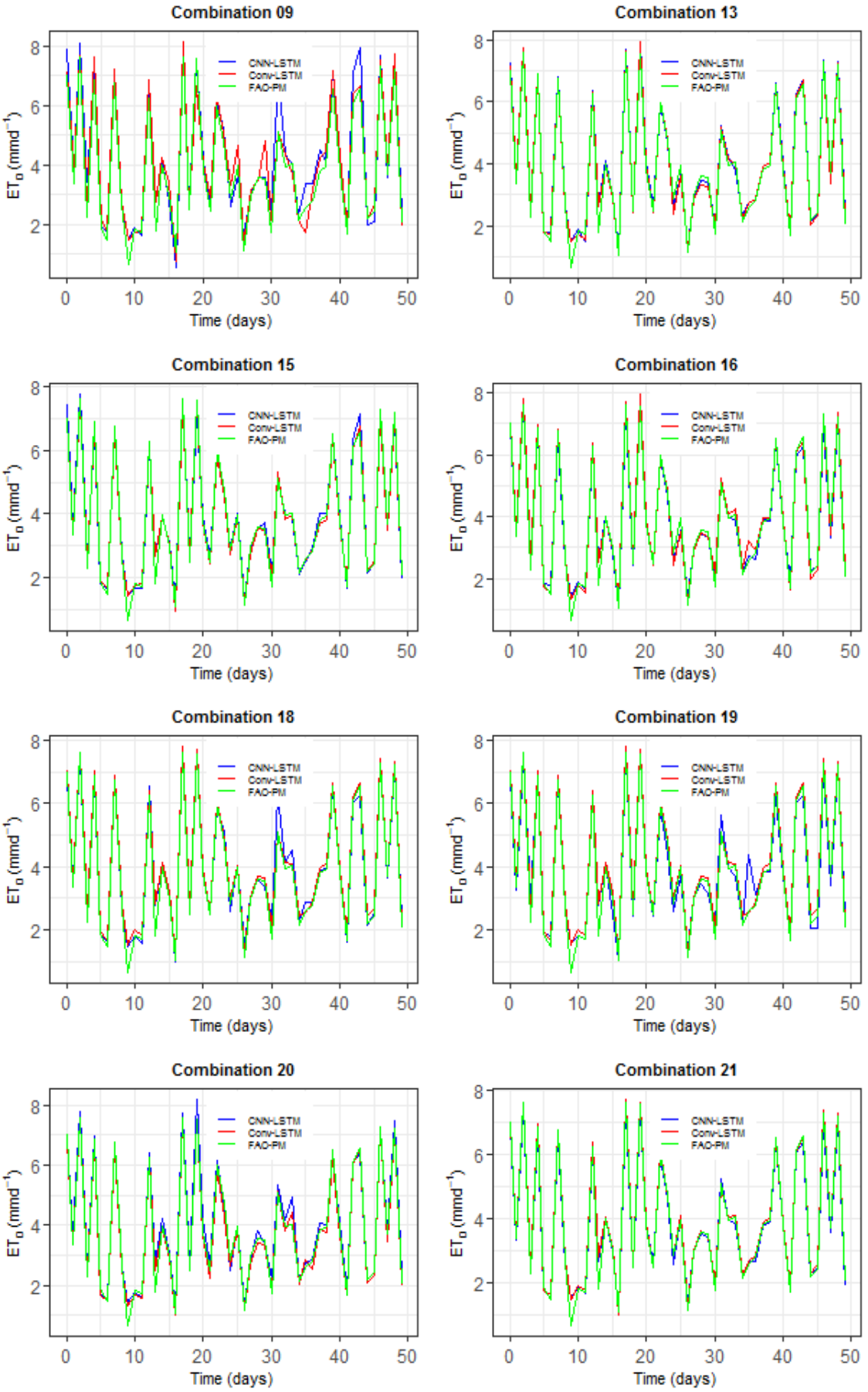

Figure 4.5: Comparison of ET_o values predicted by hybrid DL models for Amritsar station

Table 4.3: Performance of hybrid DL models using promising input combination

Input	Performance	Ludhiana Station				Amritsar Station			
		CNN-LSTM		Conv-LSTM		CNN-LSTM		Conv-LSTM	
Combination	metrics	Train	Test	Train	Test	Train	Test	Train	Test
Combination 9	IA	0.988	0.985	0.996	0.996	0.987	0.985	0.995	0.996
	R^2	0.957	0.945	0.984	0.984	0.956	0.945	0.983	0.984
	Pbias	-0.489	-0.995	-0.388	-0.302	-1.465	-1.978	-0.090	0.112
Combination 13	IA	0.997	0.997	0.997	0.997	0.995	0.987	0.989	0.997
	R^2	0.989	0.991	0.989	0.991	0.987	0.990	0.989	0.990
	Pbias	-0.163	0.066	0.420	0.722	-0.009	0.152	1.566	1.757
Combination 15	IA	0.995	0.996	0.996	0.996	0.987	0.988	0.996	0.995
	R^2	0.982	0.986	0.986	0.985	0.952	0.952	0.985	0.985
	Pbias	-0.017	-0.198	-0.431	-0.414	0.419	0.078	-0.670	-0.639
Combination 16	IA	0.996	0.996	0.996	0.996	0.996	0.996	0.996	0.996
	R^2	0.987	0.988	0.987	0.988	0.986	0.987	0.988	0.988
	Pbias	0.334	0.523	0.188	0.442	1.429	1.673	2.090	2.050

		Ludhiana Station				Amritsar Station			
Input	**Performance**	**CNN-LSTM**		**Conv-LSTM**		**CNN-LSTM**		**Conv-LSTM**	
Combination	**metrics**	**Train**	**Test**	**Train**	**Test**	**Train**	**Test**	**Train**	**Test**
	IA	0.995	0.994	0.997	0.998	0.995	0.981	0.998	0.998
Combination 18	R^2	0.983	0.980	0.993	0.993	0.984	0.980	0.992	0.993
	Pbias	-0.495	-0.812	1.013	1.118	0.987	0.930	-0.896	-0.659
	IA	0.991	0.988	0.997	0.997	0.991	0.988	0.997	0.997
Combination 19	R^2	0.970	0.958	0.989	0.991	0.967	0.958	0.989	0.990
	Pbias	0.025	-0.366	-0.668	-0.284	2.563	1.776	1.658	1.891
	IA	0.995	0.994	0.997	0.997	0.994	0.994	0.997	0.998
Combination 20	R^2	0.981	0.980	0.991	0.991	0.979	0.978	0.990	0.992
	Pbias	-0.886	-1.201	0.465	0.667	-0.606	-0.744	-0.297	-1.933
	IA	0.997	0.997	0.998	0.998	0.997	0.997	0.996	0.997
Combination 21	R^2	0.992	0.992	0.993	0.994	0.992	0.992	0.991	0.992
	Pbias	1.087	1.288	0.792	1.054	-2.221	-1.933	-0.358	-0.057

4.5.3 Performance Comparison with Empirical Models

The comparison of the proposed deep learning models (CNN-LSTM and Conv-LSTM) with temperature-based empirical models: Hargreaves model (HG) and radiation-based models: Makkink (MK) and Ritchie (RC) are provided in Table 4.4. Hargreaves equation uses T_{min}, T_{max}, and R_a as the input parameters to predict ET_o values.

Table 4.4 shows that CNN-LSTM and Conv-LSTM provide better results than the Hargreaves model with similar input datasets. These hybrid algorithms improve the performance of the Hargreaves model by increasing R^2 by 6% and decreasing RMSE by 92%. Figure 4.6 presents the scatter plot of Hargreaves, CNN-LSTM, and Conv-LSTM with respect to observed ET_o values. The highest accordance with 1:1 is observed with Conv-LSTM and CNN-LSTM models. The evaluation of regression lines shows that the value 'a'(slope value) and value of 'b'(intercept value) have a small difference with ideal values (a = 1 and b = 0) of both hybrid models. It indicates these models' ability to predict ET_o using only temperature and extra-terrestrial radiation (R_a) data with more reliability than the existing temperature-based empirical Hargreaves model. Makkink and Ritchie used T_{max}, T_{min}, and R_s as input combinations.

Table 4.4: Comparisons of empirical models with hybrid DL models

Temperature Based Model				
Input data	**Model**	R^2	**MAE** (mmd^{-1})	**RMSE** (mmd^{-1})
T_{min}, T_{max}, R_a	CNN-LSTM	0.87	0.0553	0.0749
	Conv-LSTM	0.88	0.0534	0.0735
	Hargreaves	0.83	0.8274	1.0047
Radiation Based Model				
Input data	**Model**	R^2	**MAE** (mmd^{-1})	**RMSE** (mmd^{-1})
T_{min}, T_{max}, R_s	CNN-LSTM	0.94	0.0427	0.0607
	Conv-LSTM	0.95	0.0383	0.053
	Makkink	0.84	0.8233	1.1632
	Ritchie	0.86	0.6577	0.8188

A similar input dataset is used in combination 3, as shown in Table 4.1. Both CNN-LSTM and Conv-LSTM improve the results of these empirical models by decreasing the MAE and RMSE values by 94% to 95% and increasing the R^2 score by 9% to 12%, as shown in Table 4.4. The scatter plots of CNN-LSTM, Conv-LSTM,

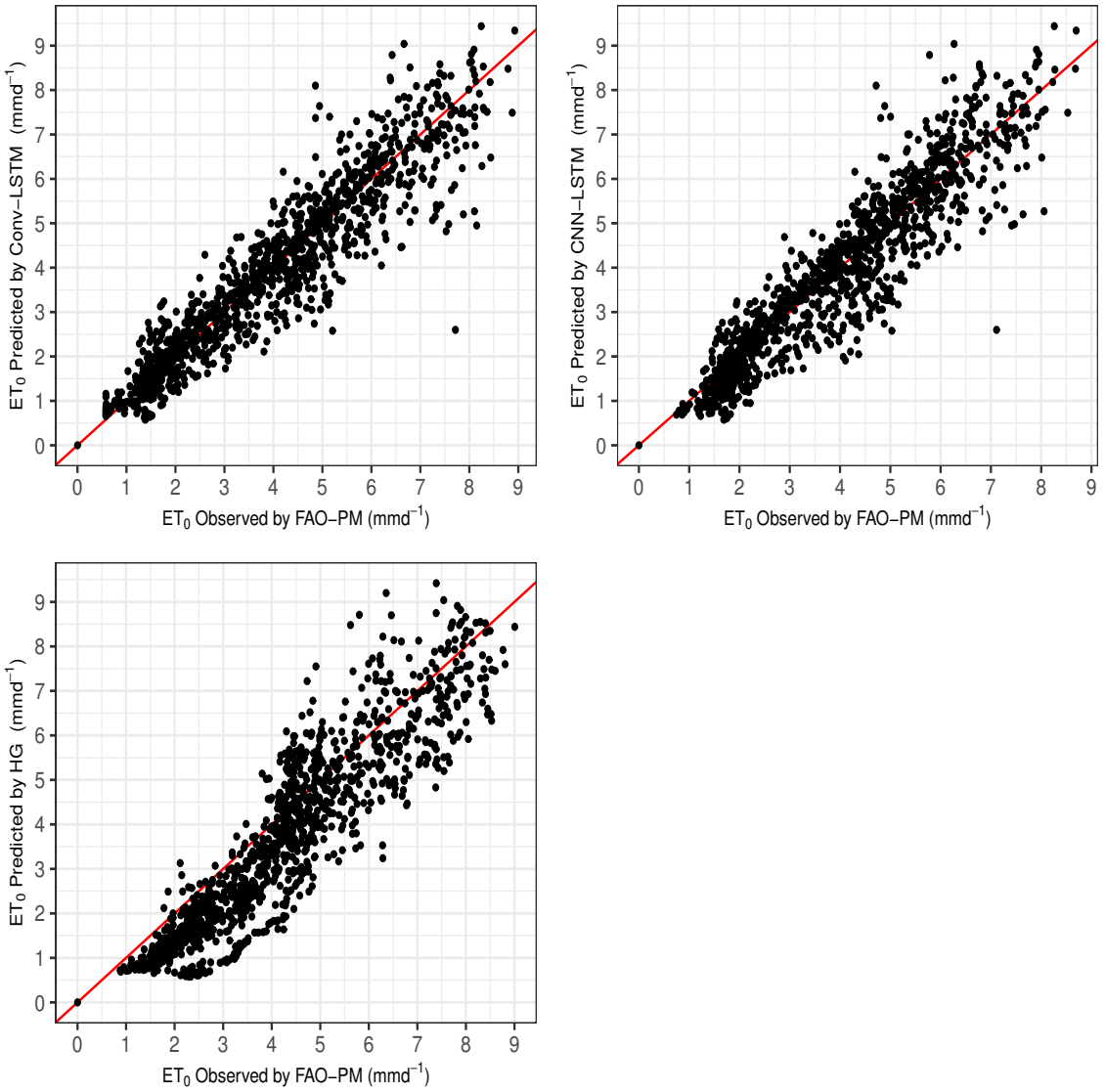

Figure 4.6: Comparison of ET_o prediction by hybrid DL and Hargreaves models

Makkink, and Ritchie methods for the same input dataset with respect to the observed ET_o values are shown in Figure 4.7. It is evident from Figure 4.7 that CNN-LSTM and Conv-LSTM are consistent with the 1:1 line as compared to Makkink and Ritchie method and closely follow observed ET_o values, and generate less scatterness. The evaluation of the regression line (ax+b) shows that Conv-LSTM is closer to the best fit line with a slope value equal to 1 and a lower intercept value equal to 0.0183, indicating its superiority over other algorithms to predict ET_o values.

Another key information that can be gleaned from Table 4.4 is that the radiation-based model used in the study performs better than the temperature-based model. This could be because both stations are in the semi-arid region, where other climate conditions are more favorable to the evapotranspiration process.

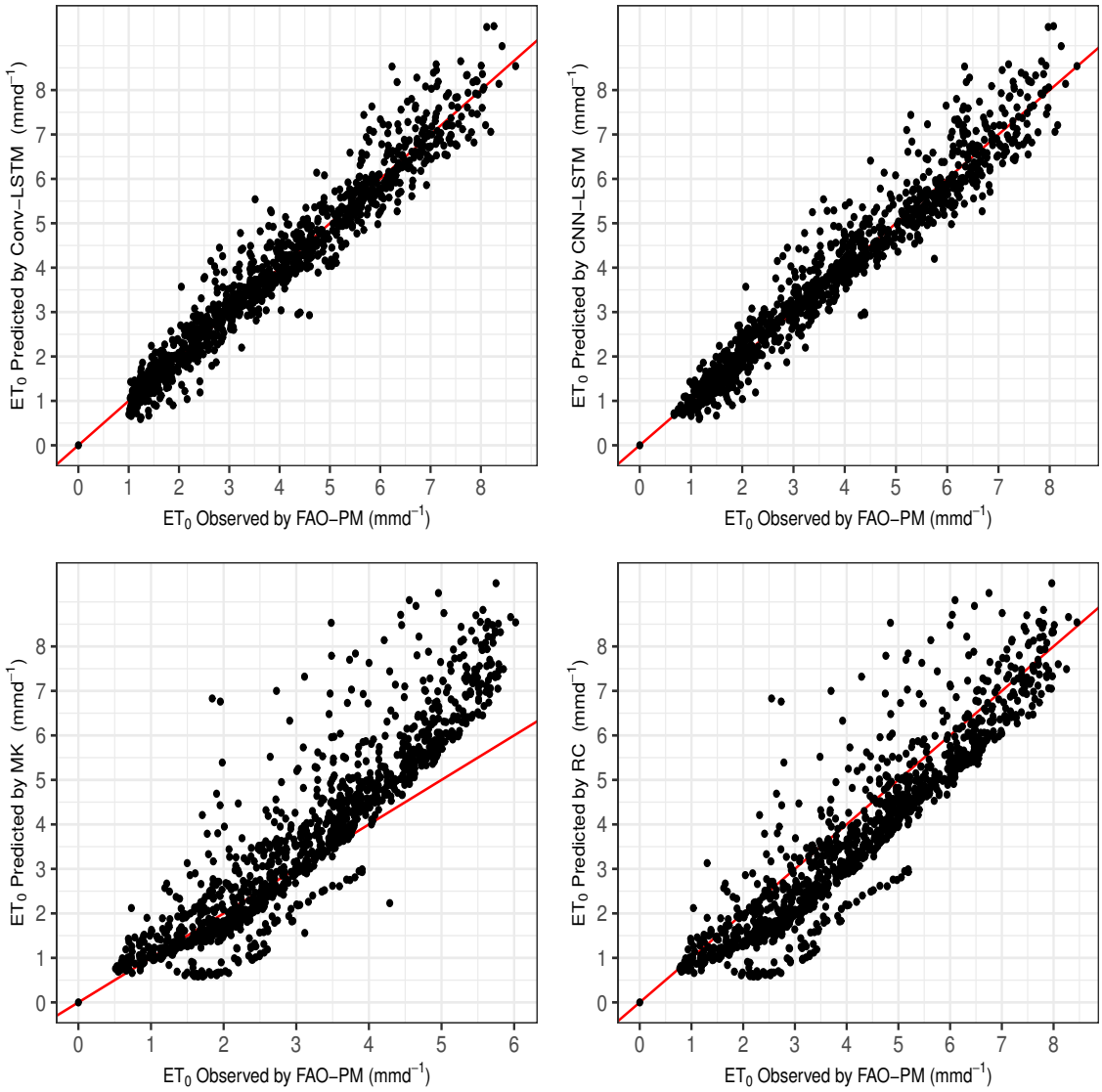

Figure 4.7: Comparison of ET_o prediction by hybrid DL, Makkink, and Ritchie models

Patil *et al.* [61] also used the combination of T_{max}, T_{min}, and R_a to predict ET_o values and compare the results with the Hargreaves equation. RMSE = 0.70 mmd^{-1} to 0.72 mmd^{-1} for Pali and Jodhpur stations of India using extreme learning machine was achieved in this study. However, in the current study, RMSE = 0.075 mmd^{-1} has been obtained for the same input combination.

Traore *et al.* [53] estimated ET_o values using the different sets of T_{max}, T_{min}, R_a, and R_s and obtained the highest performance using T_{max}, T_{min}, and R_s using MLP with MAE = 0.708 mmd^{-1} and MSE = 0.770 mmd^{-1}. In the present study, combination 3, as shown in Table 4.1, uses a similar input set and gives improved results by providing MAE = 0.0365 mmd^{-1} and MSE = 0.002938 mmd^{-1}. Traore *et al.* [25] used Gene expression programming to model the reference evapotranspiration process of one station in China using limited input data, and only minimum

and maximum temperatures were considered. They obtained $R^2 = 0.77$, MAE = 0.902 mmd^{-1}, and RMSE = 1.207 mmd^{-1} on average.

In the current work, combination 1, as presented in Table 4.1, uses both minimum and maximum temperatures to predict ET_o values, and the improved result has been obtained using Conv-LSTM which provides the maximum result with $R^2 = 0.8111$, MAE = 0.076 mmd^{-1}, and RMSE = 0.0969 mmd^{-1}. This comparison reveals the effectiveness of Conv-LSTM in modeling the process of ET_o.

Chapter 5

Deep Reinforcement Learning based Ensemble Approach for ET_o

This chapter presents a Deep Reinforcement Learning (DRL)-based ensembling approach to predict daily ET_o values of Ludhiana and Patiala stations. Four deep learning-based models, i.e., CNN-LSTM, Conv-LSTM, CNN-XGB, and CNN-SVR, act as baseline models for the proposed ensembling approach. The ET_o process is represented as a mixed integer non-linear programming (MINLP) problem with an objective to minimize the mean square error (MSE) using the DRL-based ensembling approach.

5.1 Overview

The past few decades have experienced the development of various artificial intelligence (AI) based techniques to model, predict, and optimize the ET_0 process. These AI-based techniques mainly include artificial neural network (ANN) based models, e.g., multi-layer perceptron (MLP), radial basis function (RBF) neural networks, and generalized regression neural networks (GRNN) [59] [34], genetic programming (GP) based models [77] [200], tree-based models, e.g., random forest (RF) and M5 model tree (M5Tree) [34] [37], kernel-based models, e.g., support vector machine (SVM) and least-squares support vector machine (LSSVM) [110] [42] and other AI models such as multivariate adaptive regression splines (MARS) [201] [202], adaptive neuro-fuzzy inference system (ANFIS) [83] [203]. Although these AI-based techniques may provide reliable results; the main concern is that for a particular problem, different models produce different outputs [49] [204].

Ensemble learning is a technique that deals with other models to solve a specific problem [205]. It has been observed that an ensemble of different models results in improved forecasting accuracy and low error variance as compared to individual models [206] [207] and hence effective in real-world scenarios [208] [209]. However, as

per the authors' knowledge, very few works have been reported in the literature to model ET_o process using the ensemble learning technique. Weighted average-based and stack-based ensembles are two prominent ensemble learning techniques [210]. Stack ensemble technique considers baseline models' output as input features for another high-level model and trains it to generate the final output [49] [211].

The weighted average-based ensemble approach calculates and combines the contribution weights of each baseline model to the final output by minimizing the mean square error (MSE) of ensemble outputs. However, these ensemble learning techniques suffer certain limitations. For example, the stack-based ensemble technique is time-consuming, expensive to deploy, and does not perform better as compared to the best individual baseline model in some situations [212].

In the weighted ensemble technique, the baseline models' contribution weights remain the same and do not take into account the time-varying features of the input dataset (e.g., climate dataset). Therefore, to overcome the stated limitations, this study proposes a novel ensemble technique based on the concept of DRL. It uses hybrid deep learning models as baseline models and agents of deep-Q-network (DQN) ensemble these models to ensure effective estimation of ET_o values.

5.2 Overview of Deep Reinforcement Learning (DRL)

DRL integrates a neural network with a reinforcement learning framework to help agents reach their targets. This learning technique is gaining popularity in many fields, especially in dynamic decision-making systems. This technique is used to ensemble DL models to estimate ET_o values in the present study. This section presents the underlying theory to understand the proposed solution better. In particular, an overview of reinforcement learning is provided in subsection 5.2.1, the introduction of Q learning is given in subsection 5.2.2, and an illustration of the Deep Q Network is presented in subsection 5.2.3.

5.2.1 Reinforcement Learning

Reinforcement Learning (RL) is a machine learning paradigm that works on the principle of dynamic programming that builds and trains algorithms using a reward and punishment strategy. It is different from other ML paradigms, so there is no need to provide an explicit recommendation to execute the task; instead, it solves the problem independently.

There exists a set of states $s = \{s_0, s_1 \ldots\ldots s_t\}$, set of actions $a = \{a_0, a_1 \ldots\ldots a_t\}$, and reward R in RL environment. The agent interacts with an environment and at time t, performs an action a_t, and move from state s_t to a new state s_{t+1} with some defined reward r_t. The next action of the agent for the specific state is defined by policy function $\pi(s_t|a_t)$, which maps states and actions. The agent receives a reward for the right actions and punishment for the wrong actions.

The main objective of RL is to identify the optimized policy π^* that maximizes the discounted rewards by minimizing the punishment so that agent can take corrective action in the future for a particular state [213]. Mathematically, this process is formulated as Markov Decision Process (MDP) and represented in eq. (5.1).

$$P(s_{t+1}, a_{t+1}|s_t, a_t) = P(s_{t+1}, a_{t+1}|s_0, a_0 \ldots\ldots\ldots s_t, a_t) \tag{5.1}$$

Here, $P(s, a)$ is a transition probability that can be described as the probability of state that move from one state (s_t) to another state (s_{t+1}) by taking an action a_t. The value function $(V(s, a))$ for each state and action (s, a) pair is the expected scalar reward in given state s if agent performs an action a, by following policy π, and is mathematically represented in eq. (5.2).

$$V^{\pi}(s, a) = E[\sum_{t=0}^{\infty} y^t r(s, a)] \tag{5.2}$$

Here $r(s, a) \in R$ is reward function that defines the goals to be achieved by the agent. The optimal value function $(V^{\pi^*}(s, a))$ derived using the optimal policy (π^*) provides the maximum reward achieved from all states by obeying the Bellman equation. This is given in eq. (5.3).

$$V^{\pi^*}(s, a) = r(s, a) + max\varpi \sum P(s', a) V\pi^*(s', a) \tag{5.3}$$

The graphical representation of the reinforcement learning process is shown in Figure 5.1.

5.2.2 Q Learning

Q-Learning is a value-based, model-free Reinforcement Learning algorithm that evaluates the quality of the action to be performed by the agent based on the action-value function. It determines the value of being in a particular state and performing a specific action.

The basic Q learning version maintains a q-table containing $Q(s, a)$ values for each state-action pair. The two inputs: current state (s) and action (a), are provided to the Q function, and it returns a reward as an output for that state-action pair. This Q value function $Q^{\pi}(s, a) : S \times A \rightarrow R$ satisfies the Bellman equation and is represented as MDP in eq. (5.4):

$$Q^{\pi}(s, a) = \sum_{s \in S} P(s', a) r(s, a) + \varpi Q^{\pi}(s', a') \tag{5.4}$$

Here, ϖ is a discount factor that denotes the importance of future rewards compared to current rewards and ranges between 0 and 1. A discount factor of 0 means that the system prioritizes the current reward, whereas a value of 1 means that the system prioritizes future rewards. Initially, this function returns random fixed values before analyzing the environment. Afterward, with further analysis, the Q function provides a more accurate estimate of the value function for the action $'a'$ in the state $'s'$.

The Q function is constantly updating to provide the optimal value. The optimized policy can easily be obtained after obtaining the optimum Q value for each state-action pair, corresponding to the maximum $Q(s, a)$ value. This directs the agent on the optimum course of action a^* to take in a particular state s.

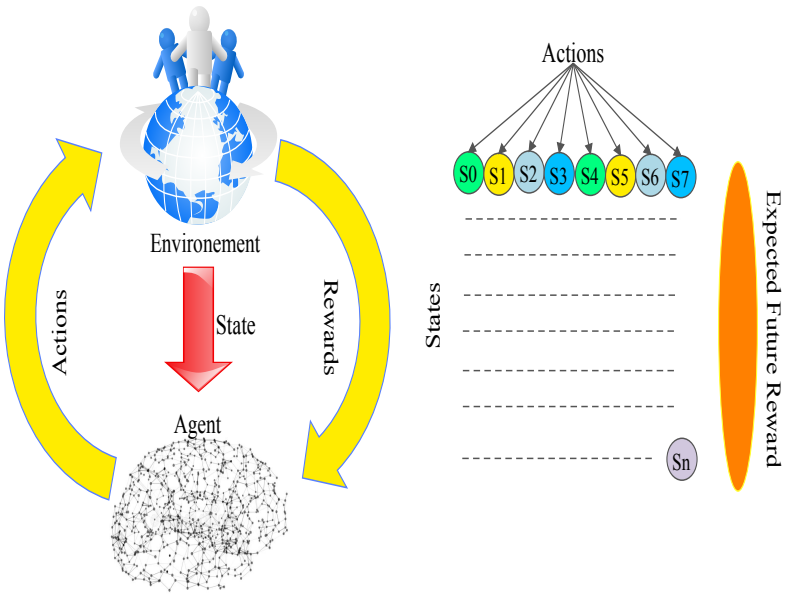

Figure 5.1: Reinforcement learning

5.2.3 Deep Q Network

DQN is a reinforcement learning technique that combines deep neural networks and Q-Learning to enable RL to operate in complicated, high-dimensional, and dynamic environments [214]. The concept was first introduced to remove the shortcoming of Q learning, such as the curse of dimensionality caused by increased memory size for storing Q-table of a huge set of state-action and the unrealistic amount of time required for exploring a large number of states to create Q-table [215]. It also removes the possibilities of overestimation due to the max operator present in the Q learning algorithms by using a neural network to approximate the Q value function [216].

DQN uses two strategies: replay memory [217] and the target network. In replay memory, the experience (s_t, a_t, r_t, s_{t+1}) of the last $X_{replay} \in X$ time steps is collected using ϵ greedy policy and stored in memory with size M.

The main objective of replay memory is to apply a set of experiences (s_t, a_t, r_t, s_{t+1}) called a mini-batch to train selected neural networks randomly from replay memory to approximate the Q function. In target network the Q function $Q(s, a)$ is replaced by $Q(s, a; \Theta)$,where Θ represents parameters of network. This parameter is only updated after i iterations to minimize the possibility of divergence as the target value Y^{DQN} is kept constant for i iterations. The target value can be given in eq. (5.5)

$$Y^{DQN} = r_{t+1} + \varpi max_a Q(s_t, a_t; \Theta) \tag{5.5}$$

The Loss (ΔL) is calculated using the squared difference between the target and updated Q value and represented in eq. (5.6). Stochastic Gradient descent (SGD) is used to minimize the loss.

$$\Delta L(s_t, a_t; \Theta_t) = ((r_t + \varpi max_a Q^*(s_t, a_t; \Theta' t)) - Q(s_t, a_t; \Theta_t))^2 \tag{5.6}$$

The Θ_t value is updated by minimizing the mean square error in the Bellman equation using the eq. (5.7).

$$\Theta_{t+1} = \Theta_t + \alpha(Y_t - Q(s_t, a_t; \Theta_t))\Delta L(s_t, a_t; \Theta_t) \tag{5.7}$$

where α is the learning rate.

5.3 Problem Formulation

The process of ET_o prediction can be formulated as a mixed-integer non-linear programming problem (MINLP) which consists of input data (climate parameters), a set of constraints followed by an objective function to predict the ET_o values. The input training data can be formulated as a tuple: (T_{min}, T_{max}, R_s), where T_{min}, T_{max}, and R_s are the daily average minimum and maximum temperature and solar radiation. In any prediction problem, the actual observed value can be represented in eq. (5.8).

$$y = r(x) + n \tag{5.8}$$

where y is the observed value, $r(x)$ denotes the real value of true predicted function and n is noise.

In this study, Deep Learning (DL) models are used as prediction models that try to find the r' function closer to the true function r. The main aim of the prediction model is to minimize the distance between predicted and actual values to reduce errors. The mean square error is the expected value of the square difference of c. It can be mathematically represented in eq. (5.9).

$$MSE = E[(y - r'(x))^2] \tag{5.9}$$

This MSE can be further decomposed to the sum of bias and variance present in the predicted function. Bias is defined as the difference between the expected value of $r'(x)$ to the true predicted function $r(x)$. The bias can be represented in eq. (5.10).

$$bias[r'(x)] = E[r'(x)] - r(x) \tag{5.10}$$

Variance is calculated as the average square deviation of $r'(x)$ from its expected value and mathematically represented in eq. (5.11).

$$var[r'(x)] = E[(r'(x) - E[r'(x)])^2] \tag{5.11}$$

Now, MSE can be rewritten as the sum of bias, variance, and non-reducible error (ψ^2) as shown in eq. (5.12).

$$E[(y - r'(x))^2] = E[bias[r'(x)]^2] + E[var(r'(x))] + \psi^2 \tag{5.12}$$

Because of the bias-variance issue, balancing bias and variance as optimization goals is logical. Thus, the objective function for the stated problem can be formulated as shown in eq. (5.13).

$$min(MSE) = minE[(y - r'(x))^2] \tag{5.13}$$

The core of ensemble learning is to minimize bias and variance. Thus ensemble approach has been adopted to minimize the objective function. Four hybrid DL models, such as CNN-LSTM, Conv-LSTM, CNN-XGB, and CNN-SVR, act as the baseline models for the ensemble approach.

5.4 Methodology

The framework of the methodology used to conduct the study is shown in Figure 5.2. It includes four parts: a collection of the meteorological dataset, prediction of ET_o by baseline models, ensembling baseline models using DRL, and prediction of the final output. This section elaborates on the proposed DRL-based ensemble ET_o prediction model. The subsection 5.4.1 provides the description of the meteorological dataset of Ludhiana and Patiala stations. Then, the subsection 5.4.2 introduces the baseline models used to predict ET_o values. The prediction of these models serves ensemble learning. In the subsection 5.4.3, the proposed Ensemble Approach using the DQN algorithm is discussed in detail.

5.4.1 Data Collection and Preprocessing

The research study is conducted in the Ludhiana and Patiala stations of Punjab, India. The geographical conditions of these study areas are discussed in chapter 3. Daily meteorological inputs, e.g., minimum temperature (T_{min}), maximum temperature (T_{max}), relative humidity (R_H), windspeed (U_2), sunshine hours (SSH), and solar radiation (R_s) covering a period of 13 years (2003 to 2015) and 17 years (2000 to 2015) of Ludhiana station and Patiala station respectively, is retrieved from India meteorological department (IMD) Pune, India to evaluate the proposed technique. Table 3.1 and Table 3.3 show the statistical observations of meteorological data of both stations. The cross-correlation among meteorological data of Ludhiana and Patiala stations is provided in Table 3.4.

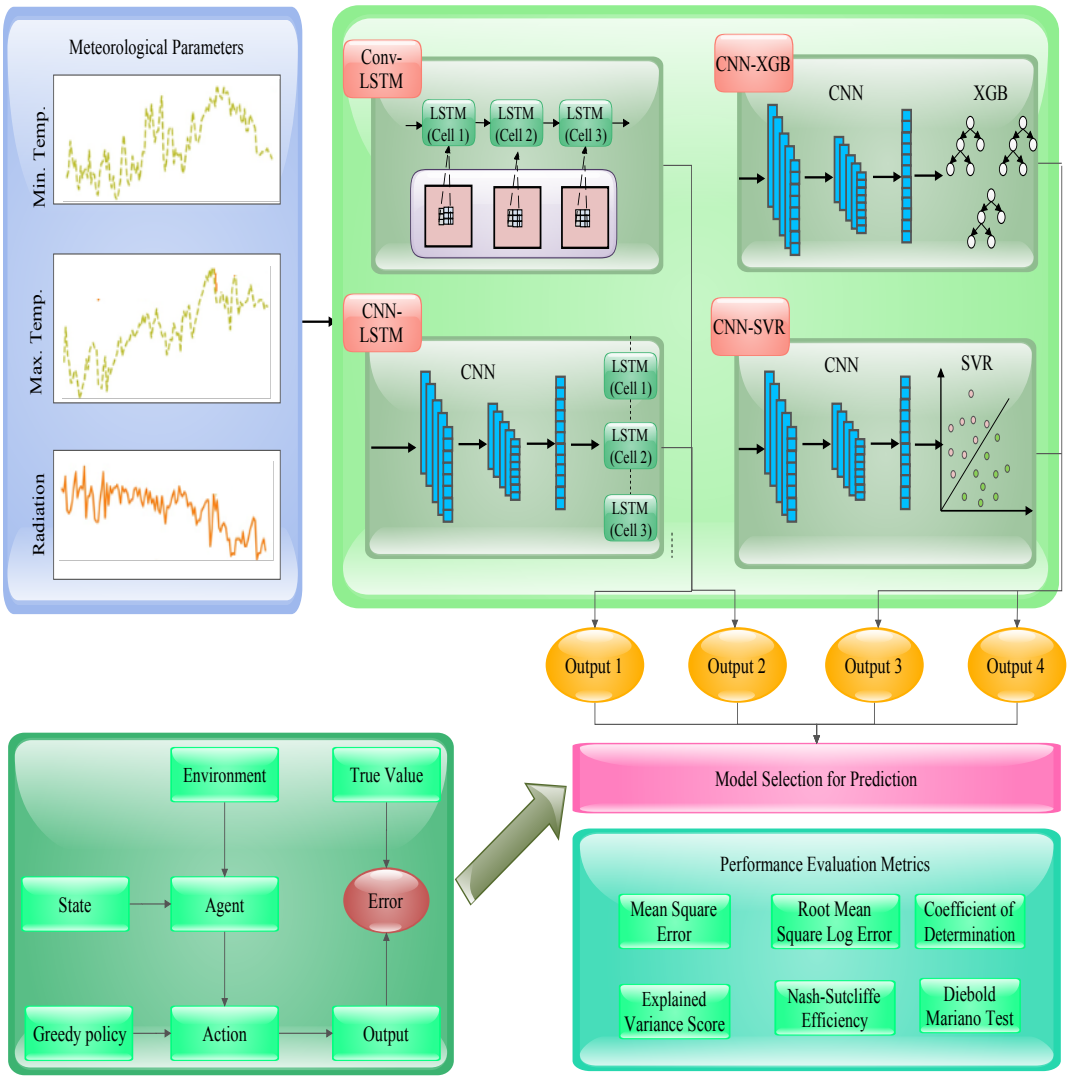

Figure 5.2: Framework of proposed approach

FAO-56 PM equation is used to compute ET_o values to obtain the benchmark dataset to compare the ET_o values estimated by proposed models. The conducted study considers limited climate parameters such as T_{min}, T_{max}, and R_s to estimate ET_o values and then evaluate how close it can get to actual observations made by the FAO-56 PM equation.

The meteorological dataset is preprocessed to transform the data into a useful and efficient format. Data preprocessing includes missing data treatment, outlier detection, and normalization. In this study, the mixgb package of R programming language, proposed by Deng *et al.* [218], is used to handle missing values. Outlier detection is performed using the z-score method, whereas normalization of data is done using min-max scaler [193].

5.4.2 Baseline Prediction Models

The selection of baseline models for the ensemble approach is critical. The conducted study explores ten AI regression algorithms and their hybrid versions with Convolution Neural Network (CNN). These algorithms belong to a different paradigm and have been proven effective in modeling the evapotranspiration process and regression problems in past studies.

These algorithms are Support Vector Regressor (SVR), eXtreme Gradient Boosting (XGboost), RF, ANN, Long Short-term memory (LSTM), CNN, CNN-LSTM, CNN-XGB, CNN-SVR, and CNN-RF. Thus, the study uses four hybrid deep neural network models (CNN-LSTM, Conv-LSTM, CNN-XGB, and CNN-SVR) to construct baseline models for ensemble learning. Each hybrid deep neural network model use historical data to obtain the prediction results of ET_o. The principle of these baseline models is discussed in the following subsections.

These algorithms are applied to the dataset used in the study and ranked in order of their performance as shown in Table 5.1. Among these algorithms, we have opted top 4 algorithms for ensemble techniques that provide higher performance than other models.

Table 5.1: Performance comparison of different AI algorithms

Model	R^2	**RMSLE** (mmd^{-1})	**MSE** (mmd^{-1})
Conv-LSTM	0.948262	0.001226	0.002502
CNN-XGB	0.943238	0.001301	0.002745
CNN-SVR	0.942897	0.001294	0.002762
CNN-LSTM	0.93656	0.001432	0.003068
LSTM	0.927483	0.001639	0.003507
CNN-RF	0.905995	0.002352	0.004534
ANN	0.903026	0.002418	0.004558
XGB	0.894868	0.002714	0.004941
SVR	0.886865	0.002844	0.005456
RF	0.877211	0.003142	0.005921

5.4.2.1 CNN-LSTM

CNN-LSTM is a hybrid neural network model that integrates the layers of Convolutional Neural Networks (CNN) and long short-term memory (LSTM) into a single framework. This model was firstly proposed by Sainath *et al.* [184]. It has already been proven that relevant features improve the performance of LSTM. CNN algo-

rithm is widely known to extract relevant features from input data. The architecture of CNN-LSTM consists of a CNN layer, LSTM layer, and dense layer to produce the final output. The extracted relevant features from CNN layers are fed to corresponding LSTM layers. Finally, after performing temporal modeling, the output of the LSTM is passed to a fully connected layer to provide sequential output [219] The detailed architecture of CNN-LSTM used in the study is explained in section 4.3 of chapter 4.

5.4.2.2 Conv-LSTM

Shi *et al.* [220] proposed convolution LSTM network firstly in 2015. It is a type of recurrent neural network (RNN). Its basic operation is identical to the LSTM model, except that the convolution operation instead of matrix operation is applied to determine the input and state-to-state transitions. At each iteration t, LSTM cells receive input x_t and h_t output of hidden state. The convolution operation is performed to generate output and state update using input x_t, the output of hidden state h_t, the output state of current cell C_t, and output state C_{t-1} of the previous cell. The detailed architecture of CNN-LSTM used in the study is explained in section 4.2 of chapter 4.

5.4.2.3 CNN-XGB

CNN has several notable milestones in the fields of image processing and Natural Language Processing (NLP). The primary reason for the success of CNN is its ability to extract relevant and essential features automatically. XGBoost is an integrated learning approach based on gradient boosting that provides accurate results via repetitive processing of weak learners. It has been employed in many research works due to its outstanding performance and efficiency [221] [222].

This study proposes a hybrid model of CNN and XGboost, i.e., CNN-XGB, to model the reference evapotranspiration process. Firstly, convolution layers are used to learn relevant input features automatically, and then the XGBoost regression model is employed to extract a high dimensional feature set to predict ET_o. The architecture of the proposed CNN-XGB model consists of a convolution layer and a pooling layer (max) followed by flattening.

Then, finally, the fully-connected layer's output is passed through the XGBoost algorithm for regression analysis, i.e., to predict the values of ET_o for wheat and rice crops. Figure 5.3 visualizes the proposed architecture of the CNN-XGB hybrid model. The mathematical representation of convolution operation in 1D CNN is eq.

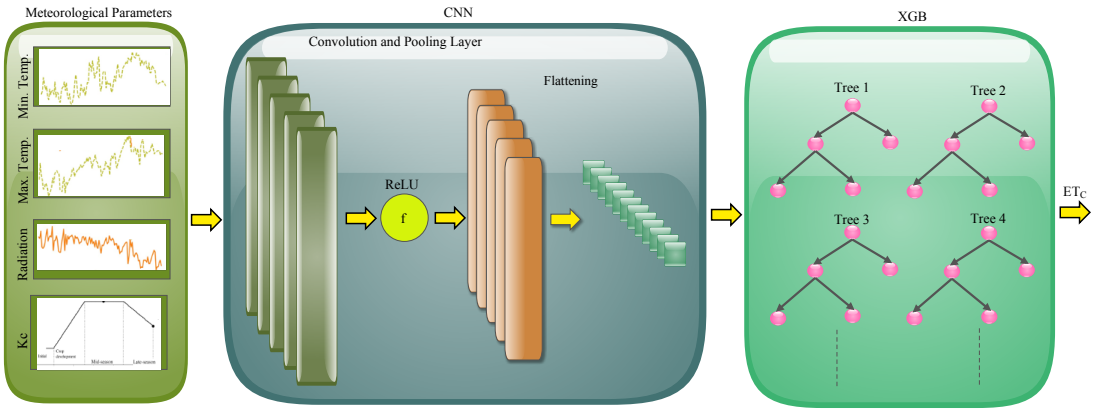

Figure 5.3: Architecture of CNN-XGB

(5.14).

$$x_j = g\left(\sum_{n=1}^{M} x_i.k_{ij} + b_j\right) \tag{5.14}$$

where n denotes the size of filters, k indicates the total number of filters, M represents the channel input numbers, and b is the kernel bias. Then the max pooling operation is used, and then finally, the output of the fully connected layer is fed to XGBoost. The mathematical expressions for the XGBoost algorithm are discussed in eq. (5.15).

$$D = \{(x_j, y_j)\}\,(|D| = m, x_j \epsilon R^n, y_j \epsilon R) \tag{5.15}$$

where D represents the dataset, m denotes the total number of input samples, n represents the total number of features associated with those samples, x_j is the eigenvalue, and y_j is the true value. Finally, the XGBoost algorithm adds up the results of K-trees to get the final predicted value which can be given as shown in eq. (5.16).

$$y'_j = \sum_{k=1}^{K} g_k\left(x_j\right), g_k \epsilon G \tag{5.16}$$

where g_k is the leaf score of k^{th} tree and G denotes the set of all the K scores.

5.4.2.4 CNN-SVR

CNN-SVR is a hybrid deep learning model that merges two powerful algorithms, i.e., CNN and SVR, into a single framework. CNN extracts the essential features of the input data, and then SVR is substituted at the place of the output layer to perform the regression analysis to generate the output. The architecture of CNN-

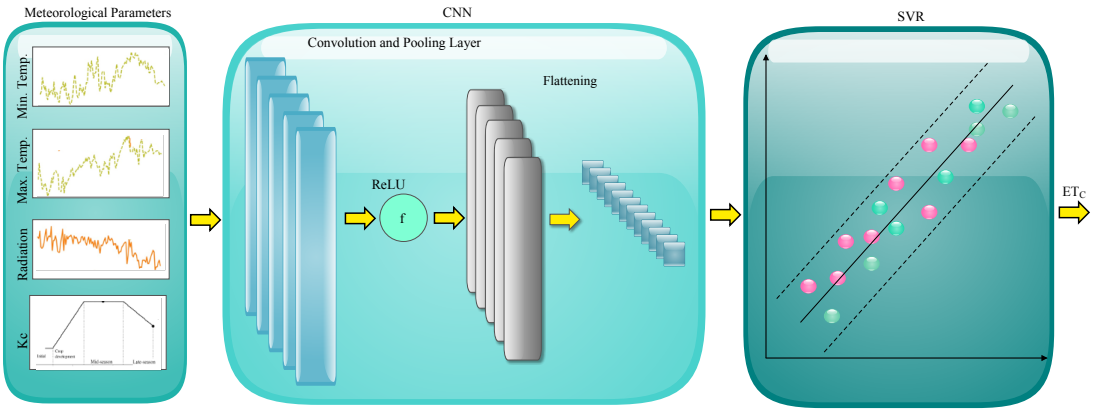

Figure 5.4: Architecture of CNN-SVR

SVR used in the present study consists of a convolution layer, a pooling layer (max), and flattening. SVR is employed as the final output layer to produce output. The proposed architecture of the CNN-SVR hybrid model is illustrated in Figure 5.4.

Algorithm 1 Ensembling using DQN for ET_o estimation

Input:
N-Total number of episodes.
M-Capacity of replay memory.
ϵ - the probability of random action.
ϖ - discount rate.
$\bar{M}$ - size of mini-batch
$\triangle$ - a smoothening function of target critic.
T- number of iterations in DQN episodes.
Initialize a deep neural network.
Initialize replay memory buffer with the capacity M.
Initialize the action-value function as Q(s,a,θ)
Initialize the target-value function as Q(s,a,θ') with some random weights $\theta' = \theta$

for $(episode = 1; episode \leq N; episode{+}{+})$ **do**
  for $(t = 1; t \leq T; t{+}{+})$ **do**
    Observe environment conditions and generate the state s.
    Using ϵ- greedy policy, select action a in A $=\{a_1, a_2, a_3, a_4\}$.
    $a_t = \begin{cases} random\ action & \epsilon\ probability \\ max_a Q(s_t, a; \theta) & (1-\epsilon)\ probability \end{cases}$
    Execute the action a_t and calculate the prediction results.
    Observe the reward r_t and next state s_{t+1}
    Save the experience (s_t, a_t, r_t, s_{t+1}) in replay memory.
    Extract random mini-batch $\bar{M}$ (s_t, a_t, r_t, s_{t+1}) from replay memory.
    set target value function as:

    $y_i = \begin{cases} r_i & for\ terminal\ s_{i+1} \\ r_i + \varpi max_{a_{i+1}} Q'(s'_t, a'; \theta') & otherwise \end{cases}$
    Perform a gradient descent on $(y_i - Q(s_i, a_i; \theta))$ to minimize the loss.
    Update target critic function by
    $\theta' = \triangle\theta + (1 - \triangle)\theta'$.
  end for
end for

The meteorological parameters are passed through layers of the CNN for the feature extraction process, and then these features are fed to SVR to predict the value of ET_c for wheat and rice crops. The CNN operation is the same as discussed in the previous section. The output of CNN is treated as an input feature vector to

train the SVR model, which can be mathematically formulated as (5.17).:

$$\sum_{i=1}^{m} wx_i + b = 0 \tag{5.17}$$

where x_i is the input sample, w is the corresponding weight, and b denotes the bias.

5.4.3 Ensemble Approach based on DRL

The downside of existing ensemble techniques is that the chosen solution is implemented every time step, and thus it makes the combination of the baseline models invariant. However, distinct baseline models exhibit different accuracy rates for distinct observations. The predictions of each baseline model are unstable for all time steps. Therefore, a deep reinforcement learning-based framework is proposed to dynamically choose the best model for each time step to tackle this problem. There are five components of the constructed reinforcement learning framework: state, action, reward, agent, and environment. These components are described in the following subsections.

5.4.3.1 State

The state space for the defined problem is represented as observations of real-world environment parameters, such as climate parameters used to estimate ET_o values. Here, only limited climate parameters are used to develop a technique that can handle data-scarce situations without compromising prediction accuracy. The state is described in eq. 5.18.

$$S = \{T_{min}, T_{max}, R_s\} \tag{5.18}$$

The abovementioned state includes three climate parameters : minimum temperature (T_{min}), maximum temperature (T_{max}), and, solar radiation (R_s). All the state parameters are normalized to $[0, 1]$ scale to remove the effect of amplitude.

5.4.3.2 Action

The action space is the option of baseline models that the agent will select for estimating ET_o process.

$$A = \{a_1, a_2, a_3, a_4\} \tag{5.19}$$

In this case, there are four possible actions in terms of hybrid DL models such as a_1 for CNN-LSTM, a_2 for Conv-LSTM, a_3 for CNN-XGB, and a_4 for CNN-SVR

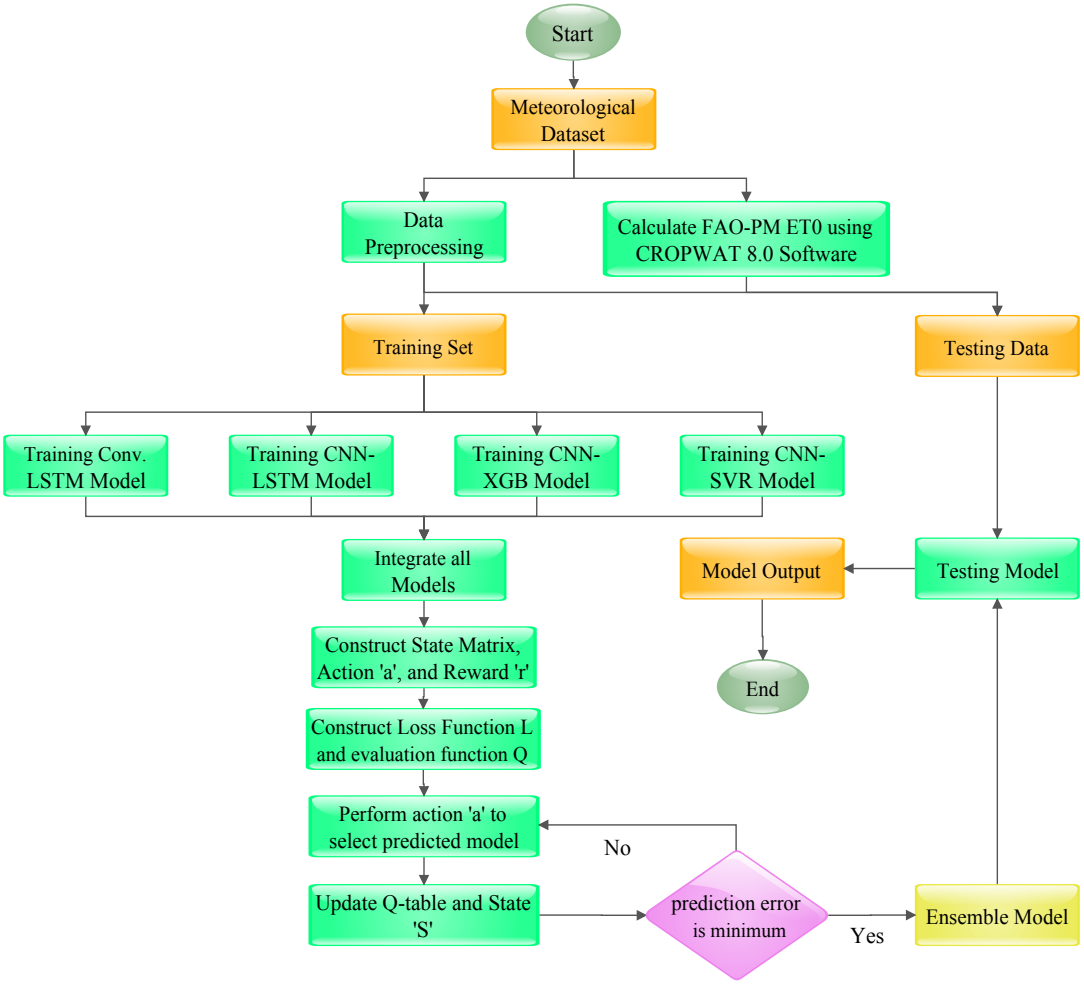

Figure 5.5: Flowchart of proposed approach

model is performed. The selection of these actions that are to be performed by an agent is determined by a greedy policy.

5.4.3.3 Reward

The aim of the reward design is to minimize the prediction error over all time steps. The reward for the action is calculated by observing the prediction error made by the selected hybrid DL model. If prediction error is minimum among all other models, the reward is positive; otherwise, a negative reward is awarded. The current action at time t selects model m from a set of ensembled models M={CNN-LSTM, Conv-LSTM, CNN-XGB, CNN-SVR} and the prediction result of the ensembled model is given in eq. (5.20).

$$f(t) = Ens_D[m(t; D)] \tag{5.20}$$

where f(t) is output of proposed ensembling approach for datapoint D at time step t by selecting model m. Also, the absolute prediction error of the prediction

result from the actual value is given in eq. (5.21).

$$\Phi(t) = f(t) - a \tag{5.21}$$

This prediction error is compared to the prediction error of the static selected model with minimum prediction error among all other models at time t to design reward architecture. If the prediction error Φ is the same as the error of the static selected model M^*, the reward is positive, otherwise negative. The agent is trained to gradually select the optimum model for time step t by following the direction of reward. The mathematical representation of the reward function is given in eq. 5.22.

$$r_t = \begin{cases} +1 & if\ \Phi(t)=\Phi(t,M^*) \\ -1 & else \end{cases} \tag{5.22}$$

5.4.3.4 Agent

The agent's main objective is to develop an optimum policy that chooses actions to achieve maximum cumulative future rewards. It interacts with the environment using actions, rewards, and observations. In this research study, the DQN agent is used to determine an action to select an optimal hybrid DL model using ϵ-greedy approach for the estimation of ET_o values.

5.4.3.5 Environment

The reinforcement environment (Env) can be expressed as shown in eq. (5.23).

$$Env = \{S, A, r, P\} \tag{5.23}$$

where S denotes a set of state-space, A denotes the action-space set, r indicates the reward function, and P indicates the transition probability of state. Algorithm 1 depicts the DQN-based ensembling for ET_o prediction. The flowchart of the proposed approach is presented in Figure 5.5.

5.4.4 Model Performance Evaluation Criteria

Prediction accuracy is an essential parameter in the assessment of predictive models. In the study, five model performance evaluation metrics are employed in terms of mean square error (MSE), root means square log error (RMSLE), error variance score (EVS), and coefficient of determination (R^2) (see eq. 4.23). Further, Diebold–Mariano (DM) test is also used to assess the predicting ability of the proposed ensemble technique. The mathematical representation of performance evalu-

ation metrics is as follows:

$$MSE = \frac{\sum_{i=1}^{N}(ET_{ob_i} - ET_{p_i})^2}{N} \tag{5.24}$$

$$RMSLE = \sqrt{\frac{\sum_{i=1}^{N}(log(ET_{p_i}+1) - log(ET_{ob_i}+1))^2}{N}} \tag{5.25}$$

$$EVS = 1 - \frac{var(ET_{ob_i} - ET_{p_i})}{var(ET_{ob_i})} \tag{5.26}$$

where ET_{ob} (mmd^{-1}) is FAO-56 PM estimated or observed ET_o value, ET_{ob} is the predicted value of ET_o for the i^{th} value of data point, $\bar{ET_{ob}}$ is mean of observed value of ET_o and N is the number of data points considered in the study. MSE is the mean of the squared difference between observed and estimated values and lies between 0 to ∞. The lower MSE value shows that model makes a better estimation. RMSLE calculates the root of squared differences between the model's log-transformed observed and predicted values, and the optimal value of this metric is 0.0.

Explained Variance Score (EVS) indicates how efficiently the given model can explain the variations in the dataset or measure the discrepancy between predicted and actual values. The value closer to 1.0 indicates that the model makes better predictions [223]. R^2 represents the degree of correlation between predicted values of ET_o by proposed models and observed values estimated by FAO-56 PM.

Diebold-Mariano Test

The standard evaluation metrics, such as MSE, R^2, etc., are useful for comparing the performance of two models. However, these metrics cannot determine the significant difference in the prediction of the two predictive models. Hypothesis testing is a statistical inference technique to determine the significant difference between the two predictive models by quantifying confidence levels. In the present study, Diebold-Mariano (DM) hypothesis test [224] is employed to assess the performance of the proposed DRL-based ensemble model. Let ET_{ob_n} denotes the observed value and $ET_{p_n}^{(1)}$ and $ET_{p_n}^{(2)}$ denote the estimated value of ET_o by two predictive models for time series climate data. The objective is to determine if these two models are significantly different. The errors between observed and predicted values of these two models are defined in eq. (5.27) and (5.28).

$$E^{(1)} = ET_{ob_n} - ET_{p_n}^{(1)} \tag{5.27}$$

$$E^{(2)} = ET_{ob_n} - ET_{p_n}^{(2)} \tag{5.28}$$

where $E^{(1)}$ and $E^{(2)}$ denote the error between the observed and predicted values of model 1 and model 2, respectively. The loss function (L(E)) is used to determine the precision of each prediction. Two widely used loss functions are absolute deviation error as shown in eq. (5.29)

$$L(E) = \sum_{i=1}^{n} |E_{(i)}| \tag{5.29}$$

and squared error loss as shown in eq. (5.30)

$$L(E) = \sum_{i=1}^{n} (E_i)^2 \tag{5.30}$$

Here E_i is error of prediction of i^{th} input. In this study, an equal accuracy hypothesis is tested to examine if one model predicts better than another. The null hypothesis for the study is represented in eq. (5.31).

$$H_0 = L(E^{(1)}) = L(E^{(2)}) \tag{5.31}$$

against the alternative hypothesis is represented in eq. (5.32).

$$H_1 = L(E^{(1)}) \neq L(E^{(2)}) \tag{5.32}$$

Here, $L(E^{(1)})$ and $L(E^{(2)})$ denotes the loss functions of model 1 and model 2 respectively.

The null hypothesis (H_0) states that the prediction accuracy of the two models is the same, whereas the alternative hypothesis (H_1) states that the accuracy of the models varies. DM test statistic can be formulated as shown in eq. (5.33).

$$DM = \frac{\frac{1}{n}\sum_{i=1}^{n}(L(E^{(1)}) - L(E^{(2)}))}{\sqrt{s^2/n}} \tag{5.33}$$

Here, s^2 represents the variance of $d = L(E^{(1)}) - L(E^{(2)})$. The null hypothesis will be rejected for the present study if the DM test score is not in the range of [-1.96, 1.96] at 5% confidence level.

5.5 Results and Discussion

This section analyzes the four baseline models' performance using the meteorological dataset of Ludhiana and Patiala stations. Then, the estimation ability of the proposed DRL-based ensemble model is evaluated and compared to the baseline models' estimation abilities using four performance metrics, i.e., MSE, R^2, RMSLE, and EVS, followed by the Diebold-Mariano test. To further assess the performance of the proposed DeepEvap approach, the estimation results of alternative existing ensemble models (stacked and weighted ensemble models) are also added as a contrast.

5.5.1 Prediction of ET_o by Baseline Models

The CNN-LSTM, Conv-LSTM, CNN-SVR, and CNN-XGB deep neural networks are evaluated in this section to observe the effectiveness of these models in ET_o prediction. The bar-graph representation of prediction results of these four baseline models for Ludhiana and Patiala stations is shown in Figure 5.6. The performance

Table 5.2: Performance comparison of baseline models for Ludhiana station

Model	Train			
	MSE (mmd^{-1})	$\boldsymbol{R^2}$	**RMSLE** (mmd^{-1})	**EVS**
CNN-LSTM	0.003354	0.932629	0.001568	0.935775
Conv-LSTM	0.002940	0.940930	0.001441	0.942152
CNN-XGB	0.002943	0.940875	0.001389	0.941625
CNN-SVR	0.003015	0.939441	0.001417	0.940024
Model	**Test**			
	MSE (mmd^{-1})	$\boldsymbol{R^2}$	**RMSLE** (mmd^{-1})	**EVS**
CNN-LSTM	0.003068	0.936560	0.001432	0.940903
Conv-LSTM	0.002502	0.948262	0.001226	0.948746
CNN-XGB	0.002745	0.943238	0.001301	0.943425
CNN-SVR	0.002762	0.942897	0.001294	0.944099

comparison of these models for training and testing datasets is provided in Table 5.2 and Table 5.3 for Ludhiana and Patiala stations, respectively. The meteorological dataset of Ludhiana and Patiala stations is divided into a training dataset (70%) and a testing dataset (30%), 10% of the training dataset is further used as a validation set for the hyperparameter tuning process.

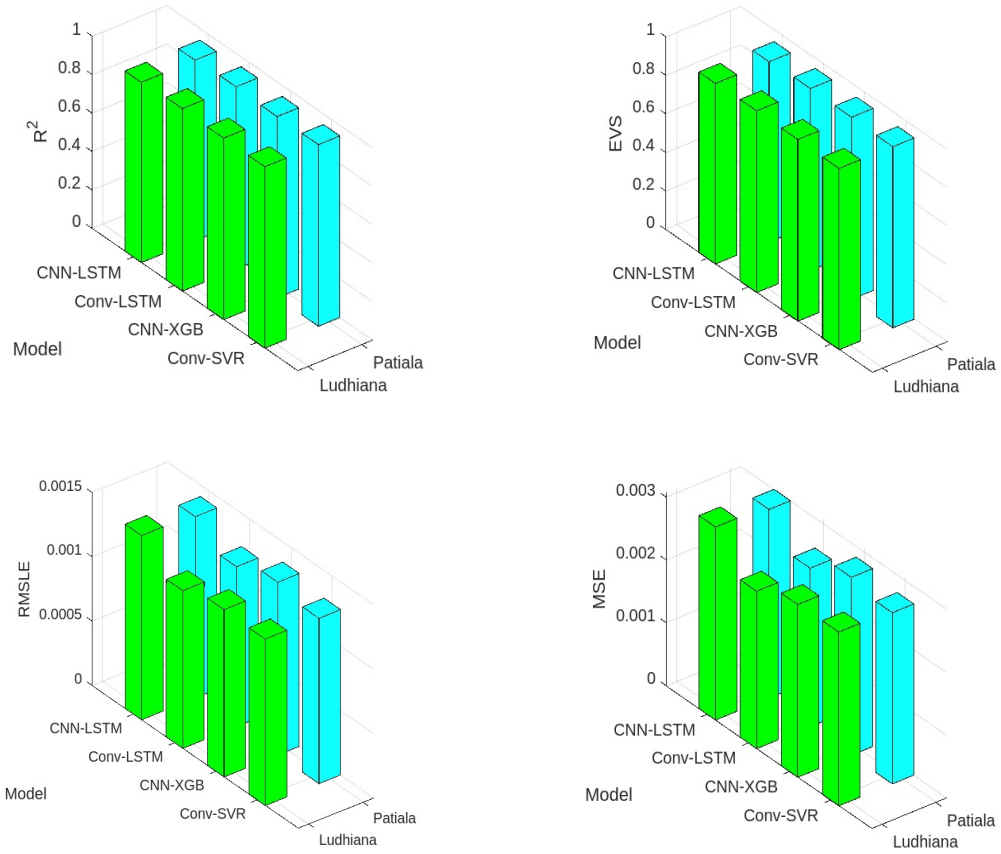

Figure 5.6: Performance measures of baseline models

The hyperparameters of these models, such as the number of filters, learning rate, activation function, batch size, number of hidden nodes, number of epochs, etc., are selected using the random search algorithm of the Keras tuner library. Minimization of the MSE is the objective function during neural network training that represents the degree to which the neural network approximates the ET_o prediction.

It is noteworthy that if these hyper-parameters are not selected carefully, the performance of these baseline models gets affected and can even lead to worst performance. However, this phenomenon helps in building a more powerful ensemble model since the baseline models with different hyper-parameters are naturally diverse.

It can be observed from the Table 5.2 and Table 5.3 that Conv-LSTM shows best overall prediction, with MSE, R^2, RMSLE, and EVS values as 0.002502 $(mmd^{-1})^2$, 0.948262, 0.001226 mmd^{-1}, and 0.948746 for Ludhiana Station and 0.002519 $(mmd^{-1})^2$, 0.947927, 0.001241 mmd^{-1}, and 0.949443 for Patiala Station respectively. According to experimental results, CNN-LSTM provide worst performance with MSE =

Table 5.3: Performance comparison of baseline models for Patiala station

Model	Train			
	MSE (mmd^{-1})	R^2	**RMSLE** (mmd^{-1})	**EVS**
CNN-LSTM	0.003330	0.933110	0.001571	0.934357
Conv-LSTM	0.002919	0.941369	0.001464	0.943999
CNN-XGB	0.002813	0.943485	0.001384	0.94352
CNN-SVR	0.003080	0.938126	0.001454	0.938807
Model	**Test**			
	MSE (mmd^{-1})	R^2	**RMSLE** (mmd^{-1})	**EVS**
CNN-LSTM	0.002998	0.938004	0.001408	0.938779
Conv-LSTM	0.002519	0.947927	0.001241	0.949443
CNN-XGB	0.002829	0.941516	0.001343	0.941733
CNN-SVR	0.002721	0.943738	0.001285	0.945095

$0.003354\ (mmd^{-1})^2$ to $0.003330\ (mmd^{-1})^2$.

It has been further noted that a single deep neural network is not capable of adequately estimating ET_o for different meteorological datasets. The primary reason for this could be that different deep neural networks have varied hidden layer structures, resulting in recognition abilities for different meteorological datasets. Therefore, a technique (e.g., ensemble learning) that can increase the model's flexibility and resilience is required. In the following subsection, the performance of the proposed DeepEvap approach is discussed.

5.5.2 Results of Proposed Ensemble Model

This subsection provides the results of the proposed DRL-based ensemble model. The line graph represents the relationship between two sets of values, where one set is always dependent on the other. The line graph representation of ET_o prediction values over time by the proposed ensemble model versus actual ET_o values is shown in Figure 5.7. It is evident from Figure 5.7 that the proposed model can simulate the actual values of ET_o. In order to prove that the ensemble model shows better performance than baseline models, the proposed DRL-based ensemble model is compared to the CNN-LSTM model, the Conv-LSTM model, the CNN-SVR model, and the CNN-XGB model. Table 5.4 shows the performance comparison of baseline models (CNN-LSTM, Conv-LSTM, CNN-SVR, and CNN-XGB) with the proposed model.

Table 5.4: Performance comparison of DeepEvap with baseline models

Station	**Models**	**MSE** (mmd^{-1})	$\boldsymbol{R^2}$	**RMSLE** (mmd^{-1})	**EVS**
Ludhiana	CNN-LSTM	0.003068	0.936560	0.001432	0.940903
	Conv-LSTM	0.002502	0.948262	0.001226	0.948746
	CNN-SVR	0.002745	0.943238	0.001301	0.943425
	CNN-XGB	0.002762	0.942897	0.001294	0.944099
	DeepEvap approach	0.001889	0.960948	0.000909	0.961137
Patiala	CNN-LSTM	0.002998	0.938004	0.001408	0.938779
	Conv-LSTM	0.002519	0.947927	0.001241	0.949443
	CNN-SVR	0.002829	0.941516	0.001343	0.941733
	CNN-XGB	0.002721	0.943738	0.001285	0.945095
	DeepEvap approach	0.001864	0.961452	0.000880	0.962270

Further, to examine the effectiveness of the proposed DRL-based ensemble model, the Diebold-Mariano test is conducted with these baseline models. This test is conducted to determine if there is a significant difference in the prediction performance of the two models. A detailed discussion of this model is presented in section 5.4.4.

Table 5.5 represents the DM statistics values using absolute deviation error as loss function. The results indicate that DM values of CNN-LSTM, Conv-LSTM, CNN-SVR, and CNN-XGB models are above the upper limits of 5% significance level. Thus, the study's null hypothesis: the prediction accuracy of the two models is the same, is rejected. Table 5.4 and Table 5.5 indicate that the proposed ensemble model (DeepEvap) substantially outperforms the baseline models and is significantly better than these models. For instance, the MSE, R^2, RMSLE, and EVS of proposed DeepEvap are 0.001889 $(mmd^{-1})^2$, 0.960948, 0.000909 mmd^{-1}, and 0.961137 respectively for Ludhiana station and the MSE, R^2, RMSLE, and EVS of the proposed ensemble model are 0.001864 $(mmd^{-1})^2$, 0.96145, 0.000880 mmd^{-1}, and 0.962269, respectively.

The scatter plot of the baseline models and the proposed model is presented in Figure 5.8 and Figure 5.9 of Ludhiana and Patiala stations, respectively. The highest accordance with the 1:1 line is observed with the proposed ensemble model (DeepEvap). The examination of regression lines reveals that the slope value ("a") and intercept value ("b") of the proposed DeepEvap approach deviate slightly from their ideal values (a=1 and b=0) as compared to the four baseline models. It shows that the proposed ensemble model is more reliable than the baseline models.

Moreover, the study aims to minimize the objective function, i.e., MSE. It is clear from Table 5.4 that the proposed DeepEvap approach has achieved minimum

Table 5.5: Diebold-Mariano test of baseline models with DeepEvap approach

Model	DM Statistics	
	Ludhiana	**Patiala**
CNN-LSTM	7.97	8.58
Conv-LSTM	6.85	6.75
CNN-XGB	7.10	6.88
CNN-SVR	7.10	7.82
Proposed DeepEvap approach	-	-

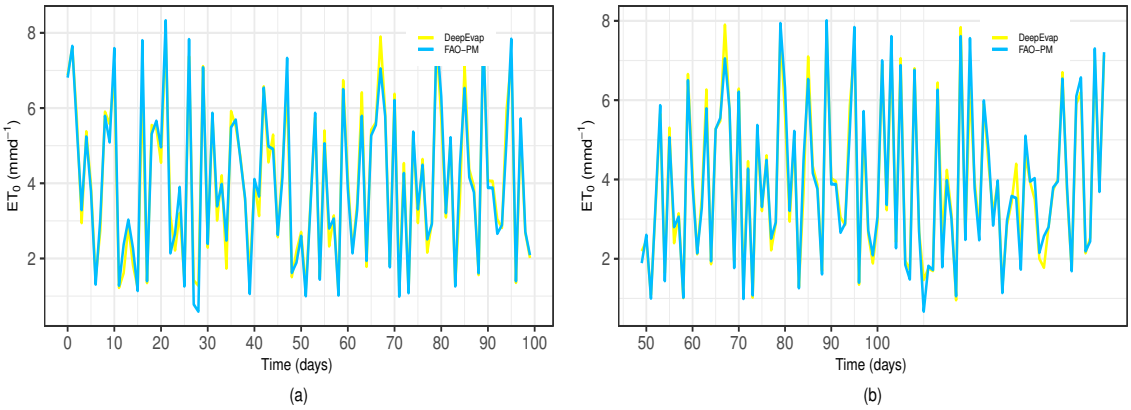

Figure 5.7: ET_o Prediction results of: (a) Ludhiana station (b) Patiala station

MSE as compared to four baseline models. The MSE value of CNN-LSTM, Conv-LSTM, CNN-XGB, CNN-SVR, and proposed DeepEvap approach for Ludhiana station is 0.003068, 0.002502, 0.002745, 0.002761, and 0.001888 respectively and for Patiala station MSE value of CNN-LSTM, Conv-LSTM, CNN-XGB, CNN-SVR, and proposed DeepEvap approach is 0.002998, 0.002518, 0.0028286, 0.002721, and 0.0018644, respectively.

5.5.3 Comparision with Alternative Ensemble Approaches

Deep Reinforcement Learning (DRL) works best in decision-making problems in a dynamic environment. An agent learns via repeated interactions with the environment to attain a goal. Such interaction generates information regarding the agent's behavior outcomes and helps improve performance. The proposed ensemble technique uses a deep reinforcement approach to dynamically select models for prediction by interacting with the environment and incorporating the time-varying input characteristics. However, other approaches, such as weighted and stacked ensemble approaches, are static and do not deploy time-varying environment characteristics.

In this subsection, a comparative study is carried out to validate the effectiveness of the proposed DeepEvap approach. The Proposed model (PM), DeepEvap, is

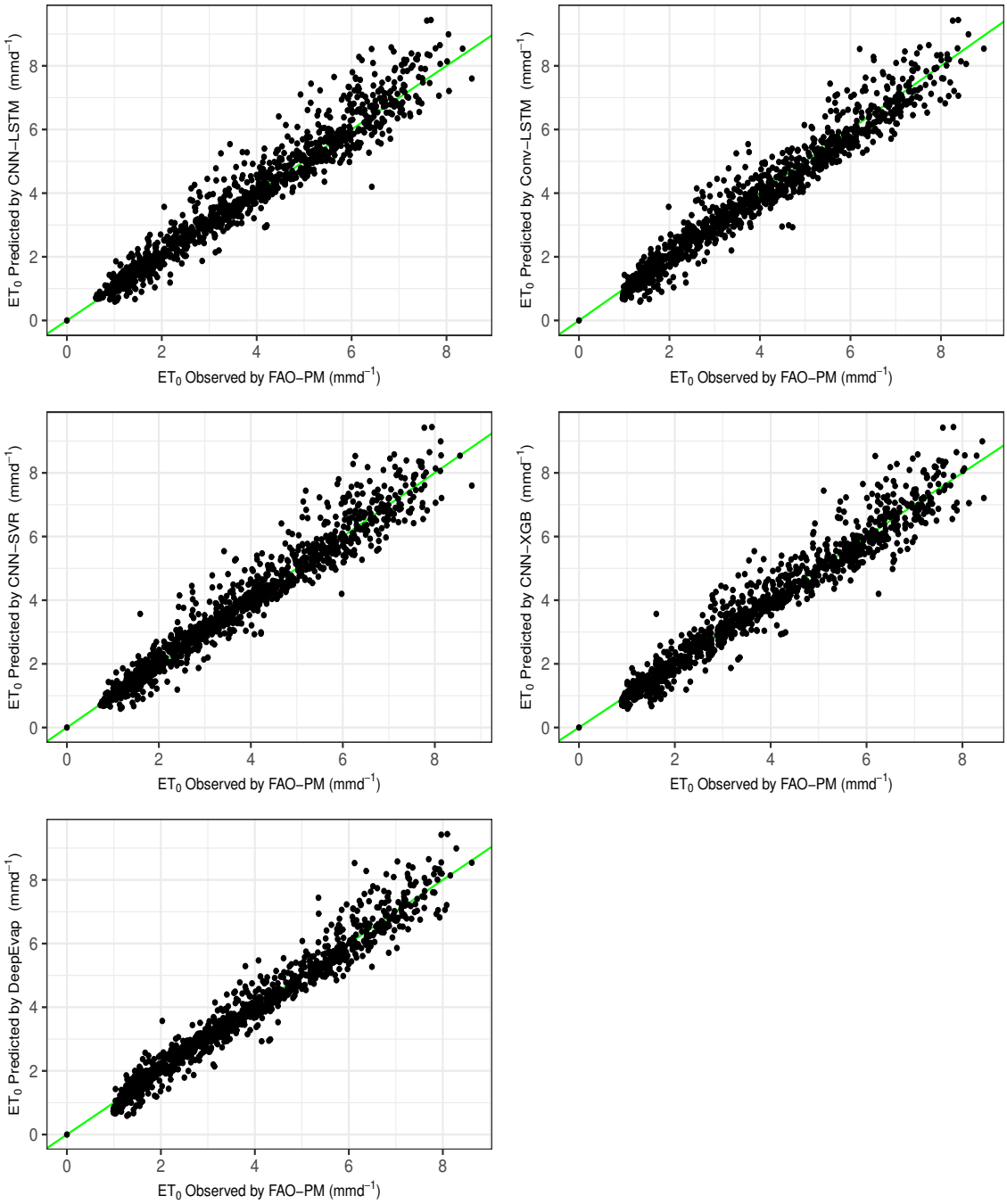

Figure 5.8: Comparison of baseline models and DeepEvap for Ludhiana station

compared to the best baseline model and two existing ensemble approaches, the weighted ensemble model (WM) and the stacked ensemble model (SM). Table 5.6 summarizes the performance comparison of the proposed DeepEvap approach with the best baseline, weighted, and stacked ensemble model. It can be gleaned from Table 5.6 that the presented DRL-based ensemble model, DeepEvap improves the result by decreasing the MSE value of the best baseline model by 25%, weighted ensemble model by 22% and stacked ensemble model by 20% for Ludhiana station and Patiala station the MSE value is decreased by 26%, weighted ensemble model

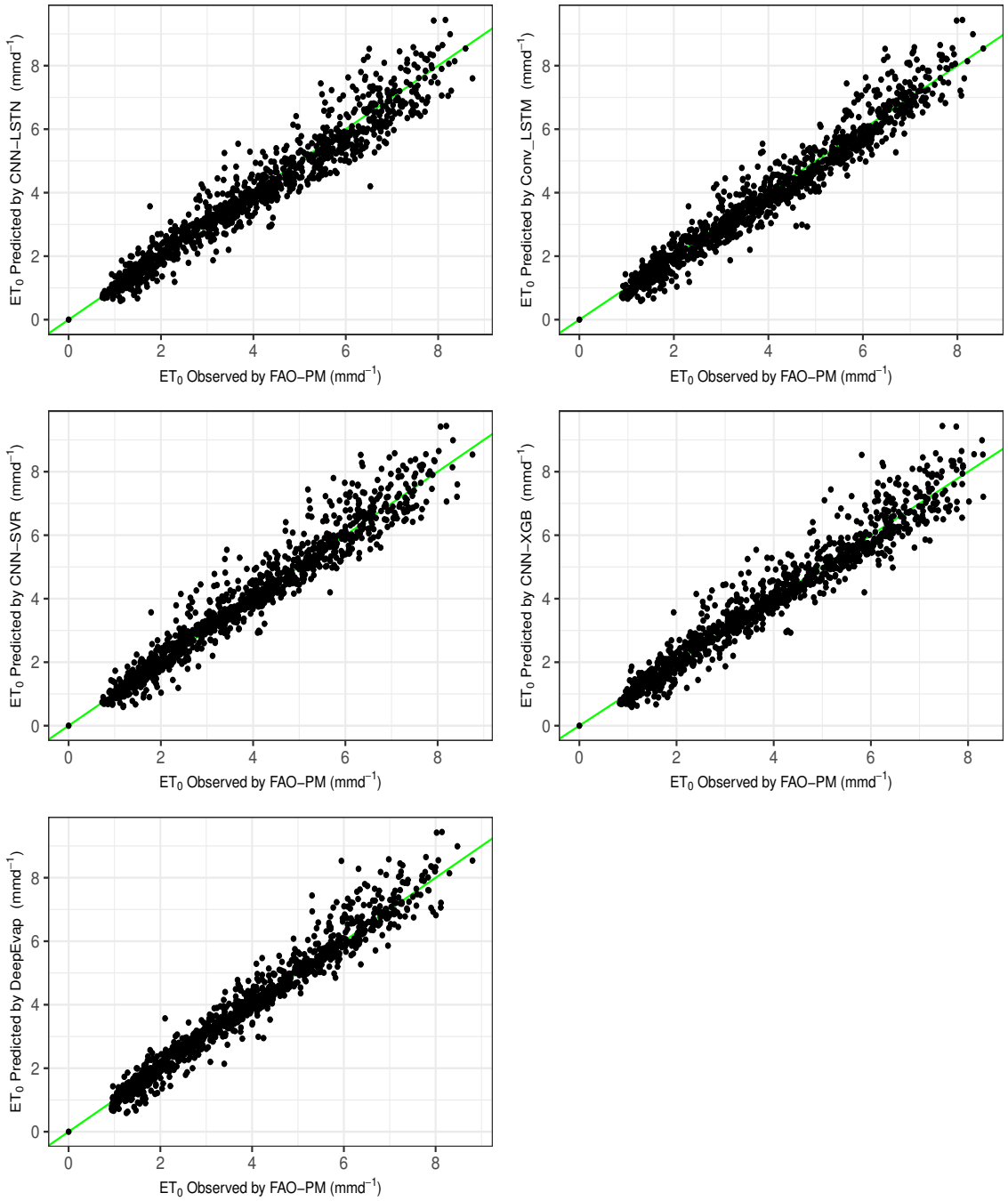

Figure 5.9: Comparison of baseline models and DeepEvap for Patiala station

by 22% and stacked ensemble model by 19%. Figure 5.10 and Figure 5.11 show the absolute prediction error of the weighted ensemble model, stacked ensemble model, and the proposed ensemble model of the Ludhiana and Patiala stations, respectively. It can be observed that the prediction error of the proposed ensemble model is lower than that of the other two ensemble models. Thus it shows the superiority of the proposed model over existing ensemble approaches. The heat map of Diebold Mariano test values for each pair of models used in the study is represented in Figure 5.12 (a) and Figure 5.12 (b) for both stations.

Table 5.6: Performance comparison of DeepEvap with baseline and ensemble models

Station	Models	MSE (mmd^{-1})	R^2	RMSLE (mmd^{-1})	EVS
Ludhiana	Best baseline model	0.002502	0.948262	0.001226	0.948746
	Weighted ensemble model	0.002406	0.950257	0.001165	0.950316
	Stacked ensemble model	0.002365	0.951098	0.001142	0.952603
	Proposed DeepEvap approach	0.001889	0.960948	0.000909	0.961137
Patiala	Best baseline model	0.002519	0.947927	0.001241	0.949443
	Weighted ensemble model	0.002391	0.950558	0.001155	0.950702
	Stacked ensemble model	0.002296	0.952528	0.001109	0.952855
	Proposed DeepEvap approach	0.001864	0.961452	0.000880	0.962270

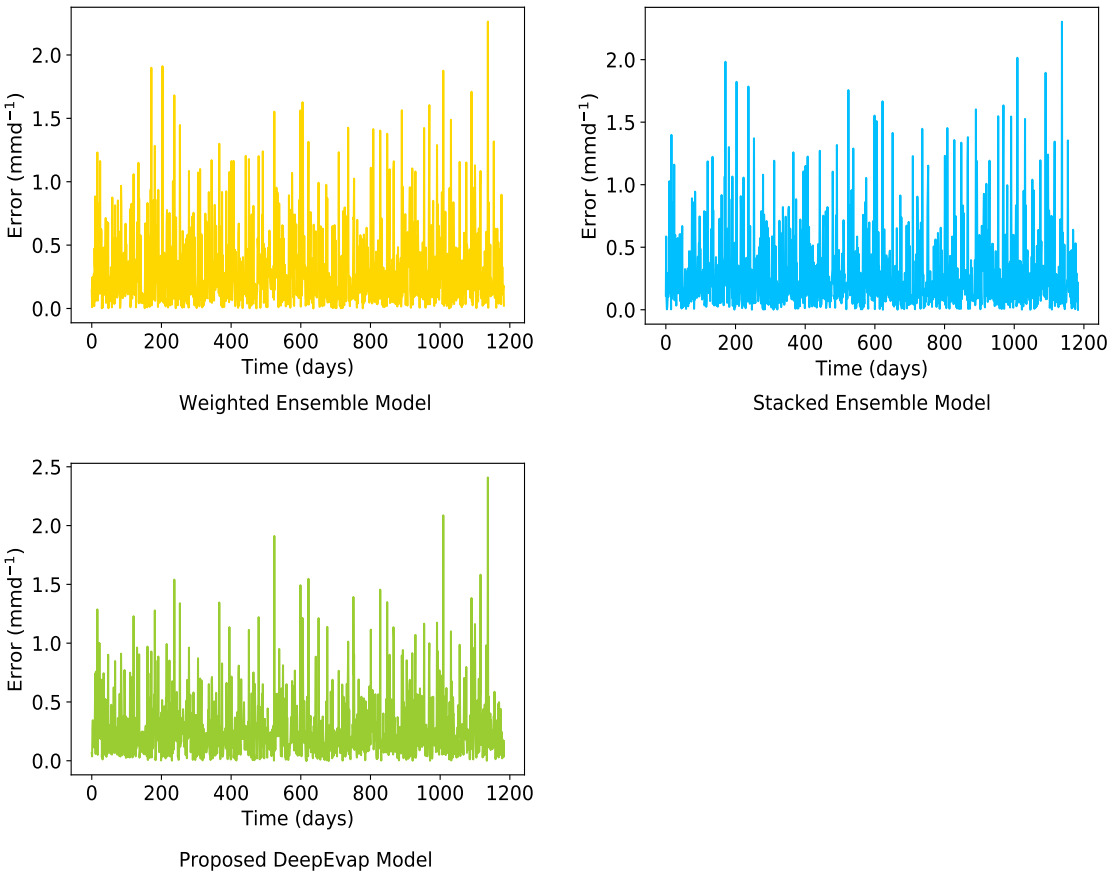

Figure 5.10: Error detected in the estimation of ET_0 of Ludhiana station

It is observed from the heat map that for Ludhiana station, the pairs {CNN-SVR, CNN-XGB} and {SM, WM} have DM values in the range of [-1.96,1.96]. Thus for these pairs, the null hypothesis can not be rejected, i.e., no model is superior to each other. However, the remaining pairs of the models are significant at a 5% significance level. The DM values for pairs {SM, PM} and {WM, PM} are 4.9 and 5.5, respectively, which shows the significant difference in the prediction performance of the proposed DeepEvap approach, stacked and a weighted ensemble model. In Fig-

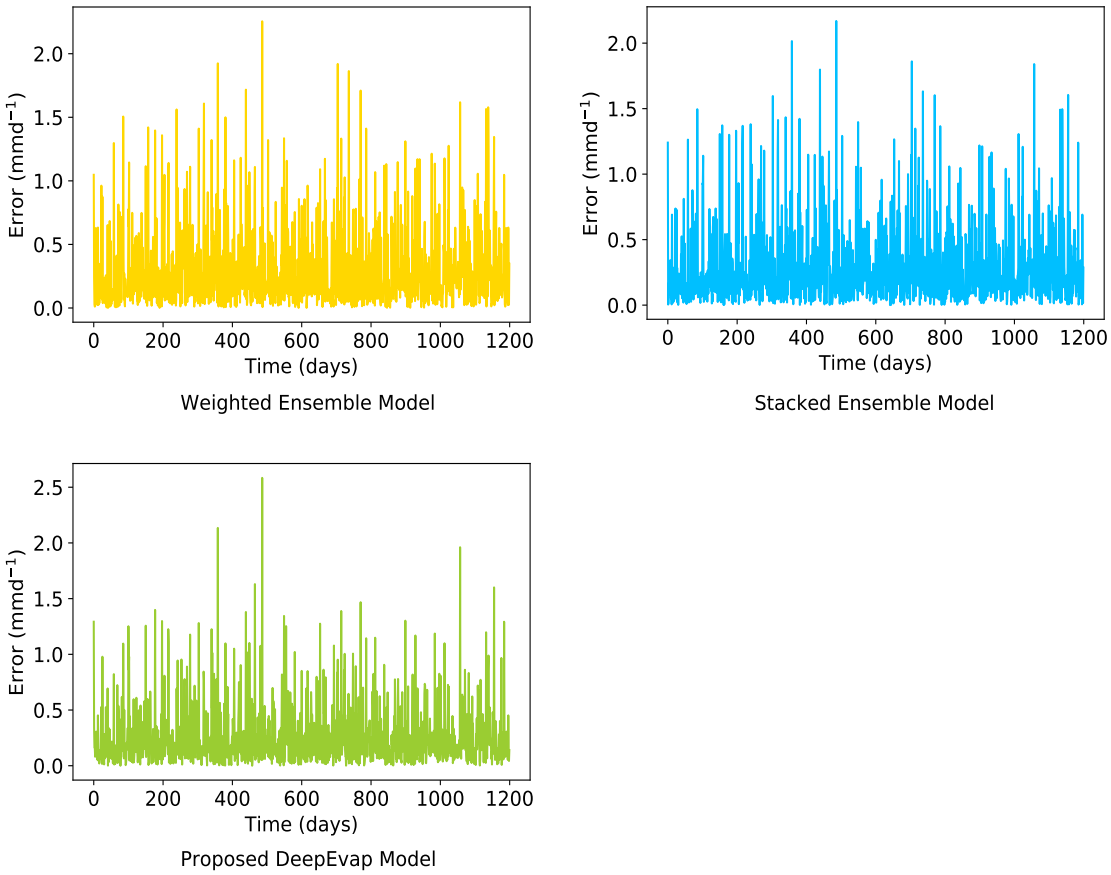

Figure 5.11: Error detected in the estimation of ET_0 of Patiala station

ure 5.12 (b), the heat map of the Patiala station shows that DM values for the pairs {Conv-LSTM, CNN-SVR}, {CNN-SVR, CNN-XGB}, {Conv-LSTM, WM} are in the range of [-1.96,1.96] and thus null hypothesis for these pairs can not be rejected. In other words, these models are not better than each other significantly. However, for all other pairs of models involved in the study, DM values show a significant difference in the prediction of ET_o values. The DM values for the pairs {SM, PM} and {WM, PM} are 5 and 5.3, respectively, and thus null hypothesis is rejected. The overall results of the Diebold-Mariano study demonstrate that prediction results obtained from the proposed ensemble model differ significantly from existing ensemble models and baseline models.

This study examines the proposed DRL based ensemble approach, DeepEvap in respect to how this approach can predict ET_o values using T_{min}, T_{max}, and R_s. Traore *et al.* [53] also used T_{max}, T_{min}, and R_s as input set to predict ET_o using Multi-layer Perceptron (MLP) and achieve MSE value 0.770 mmd^{-1}. However, this study is able to achive MSE value 0.001889 mmd^{-1}. Fan *et al.* [37] explored different input combinations to model ET_o process and with combination T_{max}, T_{min},

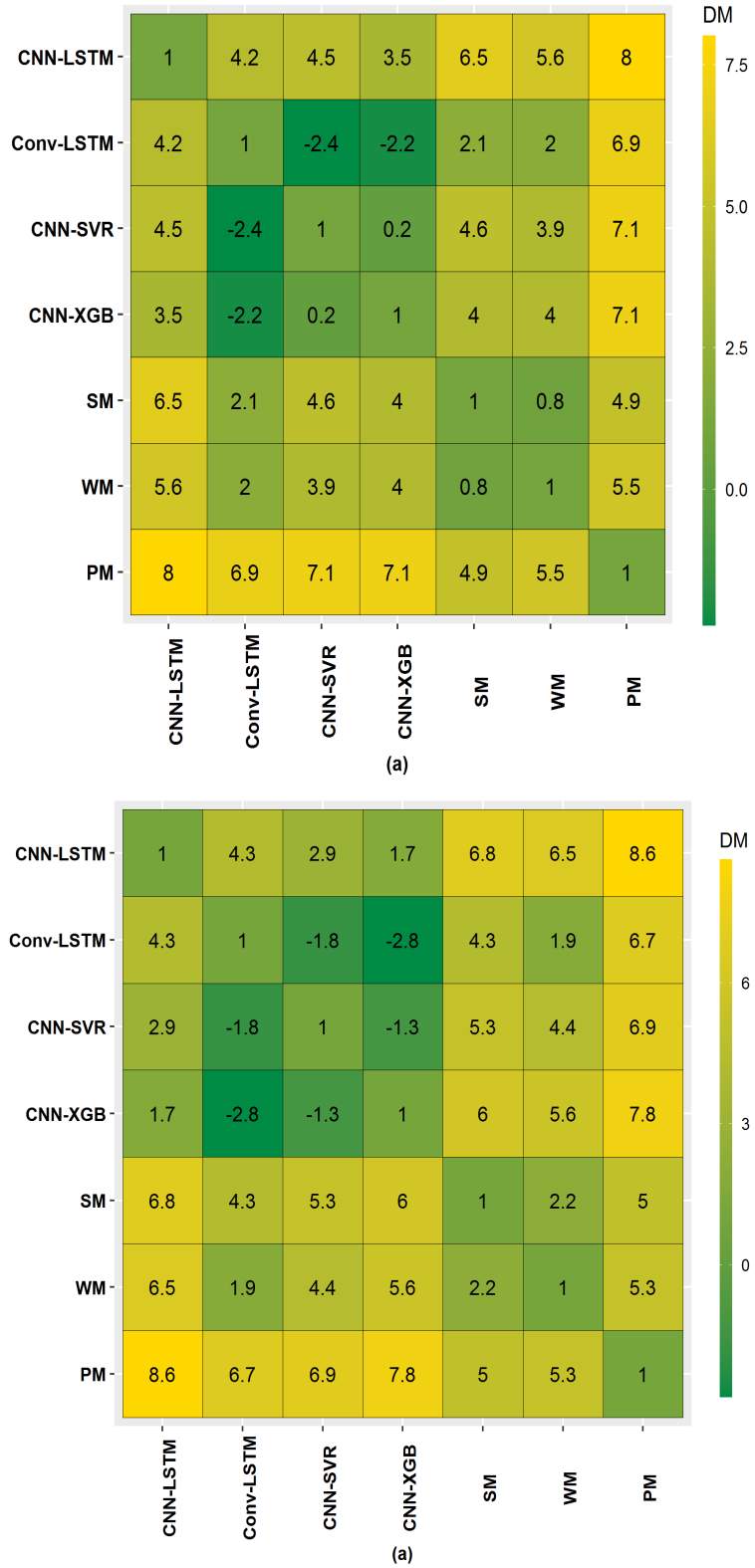

Figure 5.12: DM values for (a) Ludhiana station (b) Patiala station

and R_s as input dataset ,the R^2 =0.91 to 0.95 for different station was achieved. The proposed DeepEvap approach used in the study has obtained R^2=0.96 for a different dataset. This comparison reveals the usefulness of the proposed DeepEvap

approach for modeling the ET_o process.

Chapter 6

Hybrid Models for Estimation of Crop Evapotranspiration

The main objective of this chapter is to predict daily wheat and rice evapotranspiration values. Two hybrid models, i.e., CNN-XGB and CNN-SVR, are proposed to achieve reliable prediction of crop evapotranspiration (ET_c) of both crops using limited input climate data. Further, the projection of the future changes in wheat and rice ET_c is examined using RCP 4.5 and RCP 8.5 emission scenarios. This may help to develop adaptation strategies to increase production potential in climate change scenarios.

6.1 Overview

Crop water requirements are vital for developing effective irrigation management techniques to improve crop water usage efficiency. ET_c is the total water loss from the given crop due to the evaporation and transpiration processes. It is considered an essential process in determining crop water requirements. The direct measurement of ET_c requires specialized instruments such as eddy covariance, Bowen ratio equipment, or lysimeter.

Unfortunately, due to the extreme heterogeneity of soil and the dynamic nature of energy transfer, such systems cannot accurately estimate the spatially resolved ET_c at large scales, and also, these direct methods are costly, time-consuming, and cumbersome [97] [225]. Since direct measurement of ET_c is expensive, inconvenient, and complex, several empirical models for ET_c estimation have been introduced over time.

FAO-56 PM method is the most popular and effective technique generally used to estimate crop water requirements. Although it is possible to achieve a reliable estimation of ET_c by this method, the requirements for large-scale meteorological

data (air temperatures, solar radiation, wind speed, and vapor pressure) at precise spatiotemporal scales are not always available in many underdeveloped nations. Therefore, alternative approaches are needed to estimate ET_c that use less meteorological data and provide reliable results. Also, ET_c computations are complicated and non-linear, relying on several meteorological and crop indices variables and their relationships. Thus, it is challenging to develop an empirical model that takes these complicated processes into account [85] [226].

In recent years, AI methods have been successfully implemented to estimate the ET_c of various crops. However, these studies did not consider limited available meteorological data to model the ET_c process. Thus, it is essential to comprehend the temporal distributions of crop evapotranspiration and its estimated future changes utilizing limited meteorological data.

Climate change is considered to have significant impacts on crop production. So, understanding climate change's regional impacts is of utmost importance for adaptation and mitigation programs to handle such situations in the future. A few research studies have been conducted to understand the impact of climate change on crop water requirements. For example, Saadia *et al.* [227] studied the effect of climate change on crop evapotranspiration of winter wheat and tomato crops using the A1B emission scenario and found that ET_c will decrease by approximately 5%. Ye *et al.* [228] investigated climate change impact on rice cultivation using the A1B emission scenario in Southern China and found an increase in crop water requirements by 8-20%. Worqlul *et al.* [229] also investigated the impact of climate change in Ghana using Representative Concentration Pathways (RCP) 4.5 emission scenario and reported that there would be an increase in evapotranspiration by 6-7%.

Further, Xiao *et al.* [230] used RCP 4.5 and RCP 8.5 future climate emission scenarios and found a decrease in ET_c of winter and spring wheat using Agricultural Production Systems Simulator (APSIM) model. Chen *et al.* [231] analyzed the climate change impact on crop evapotranspiration of sorghum crop using RCP 4.5 and RCP 8.5 scenarios in Northern High Plains of Texas, and results indicate that ET_c decreased by 8–25%.

Deep learning models are efficient in handling complex non-linear relationships with a massive amount of data and also show the ability to handle time-series forecasting problems [232] [233]. Estimating crop evapotranspiration also shows similar characteristics, such as complex non-linear relationships among meteorological parameters and the time-dependence nature of these parameters.

In this chapter, the objective is to assist irrigation engineers and agricultural practitioners in adequately estimating ET_c in light of the limited availability of climatic data for efficient crop water demand estimation. Therefore, two hybrid models, Convolution Neural Network-eXtreme Gradient Boosting (CNN-XGB) and Convolution Neural Network-Support Vector Regression (CNN-SVR), are proposed for the reliable estimation of daily ET_c values of wheat and rice crops.

Further, limited climate data (minimum temperature (T_{min}), maximum temperature (T_{max}), mean temperature (T_{mean}), and solar radiation (R_s)) is used for prediction of ET_c values to handle data-scarce situations. Also, the future climate data obtained using two emission scenarios: RCP 4.5 and RCP 8.5 for the time period 2023-2033, are used to project changes in ET_c. The next section provides the methodology opted to conduct the study.

6.2 Methodology

This section describes the proposed methodology opted to conduct the research study. The subsection 6.2.1 provides a detailed description of the meteorological and crop dataset used in the study. In the subsection 6.2.2, the model development process and flowchart are discussed in detail. Finally, the subsection 6.2.3 provides the model evaluation parameters for the performance assessment of the proposed model.

6.2.1 Dataset Collection and Input selection

The geographical area of the conducted study is Ludhiana station in the Punjab state of India. It is the most developed agricultural district and plays a significant role in shaping agriculture of Punjab. It is among the foremost stations in the country where the Intensive Agriculture Development Program (IADP) was introduced. However, the water table is dropping at an alarming rate in the Ludhiana district due to poor irrigation planning. The water level decline ranges from 0.11 m/year - 1.34 m/year, and the water table in the area lies between 9-26 m below ground level (bgl) according to the report of the Central Ground Water Board [234]. The geographical conditions of this station are discussed in the section of Chapter 3.

The meteorological dataset has been obtained from the India Meteorological Department (IMD), Pune, India, from 2003-2015 of the station. The meteorological parameters used in the study includes T_{min}, T_{max}, T_{mean}, and R_s. The mean values of these parameters from 2003-2015 for the wheat and rice crop growing period are

provided in Table 3.11 of chapter 3.

GCMs (General Circulation Models) are the most powerful tools for forecasting future climate data by modeling the reaction of the global climate system to rising greenhouse gas concentrations. However, GCMs are generally incapable of reliably providing the local-scale forecasts required to analyze climate change's impact on the environment, agriculture, water resources, etc. Thus, downscaling techniques are frequently employed to provide output at the required lower spatial scales. This technique assumes that local climate is influenced by the interaction between large-scale atmospheric variables and local factors.

Two GCMs named IPSLCM5A-LR (Institute Pierre-Simon Laplace Circulation Model 5A - Low Resolution) and HadGEM2 (Hadley Centre Global Environmental Model version 2) is used in this study for future climate projection using emission scenarios RCP 4.5 and RCP 8.5 and downscaled data of daily T_{min}, T_{max}, and R_s over the period of 2023-2033 of Ludhiana station is obtained from MarkSim GCM.

Wheat is sown in Punjab state during sowing windows from late October to December and harvested in April. The optimal temperature range for ideal wheat seed germination is $20° - 25°C$, and the optimal temperature for vegetative growth is $16° - 22°C$ [127]. The rice crop is sown from late June to August and harvested in October. It is a tropical plant that needs a lot of heat and humidity to survive. The temperature should be hot, with a mean monthly temperature of $24°C$. The temperature should be $16° - 30°C$ during the sowing period, $20° - 30°C$ at the time of the growth period, and $16° - 27°C$ when the harvesting period is there [128].

Calculation of ET_c

Daily crop Evapotranspiration is calculated by multiplying the reference evapotranspiration with a single crop coefficient (K_c) that integrates the characteristics of the crop during different phenological stages [131], given in eq. (3.3). The crop phenological stages are generally divided into four stages: initial stage, development stage, mid-stage, and late-stage, with different duration. The crop coefficient value is different for each stage and varies with climatic conditions. The planting and harvesting dates of wheat and rice are also obtained from IMD Pune. The length of each stage is calculated from growing degree days (GDD) which is determined as:

$$GDD = \frac{T_{max} + T_{min}}{2} - T_t \tag{6.1}$$

where T_{max}, T_{min}, and T_t represents maximum, minimum, and base temperature. The base temperature for wheat is $5°C$ and $10°C$ for rice crop [129] [127]. The k_c values of wheat and rice are adopted from the research conducted at the Punjab Agricultural University's School of Climate Change, and Agricultural Meteorology in Ludhiana that aims to calculate k_c values of both the crops [130]. The k_c values for the wheat crop used in the study are k_c init = 0.39, k_c mid = 1.26, and k_c late = 0.36, and for rice crop, k_c init = 1.15, k_c mid = 1.36, and k_c late = 0.86. Table 3.7 and Table 3.8 provide the growth stage duration details of wheat and rice crop, respectively.

6.2.2 Model Development

The detailed architecture of CNN-XGB and CNN-SVR is discussed in chapter 5. These models are implemented using python-3.0 on the Google Colab platform to simulate the wheat and rice crop evapotranspiration process. Meteorological parameters such as T_{min}, T_{max}, R_s, and crop coefficient (k_c) of each growing stage are provided as input to these models. These meteorological parameters of Ludhiana station are retrieved from IMD, Pune, and K_c values of wheat and rice crops are collected from the case study conducted by Punjab Agricultural University, Ludhiana station [130].

The correlation matrix between above mentioned meteorological parameters and ET_c of wheat and rice crops is provided in Table 3.9 and 3.10. The objective is to determine which parameters can afford the best prediction of wheat and rice ET_c. The results indicate the highest correlation between R_s and ET_c. Air temperature

Table 6.1: Input scenarios for hybrid models for predicting ET_c

Model	R_s	T_{mean}	T_{max}	T_{min}
CNN_XGB 1	✓			
CNN_SVR 1	✓			
CNN_XGB 2	✓	✓		
CNN_SVR 2	✓	✓		
CNN_XGB 3	✓	✓	✓	
CNN_SVR 3	✓	✓	✓	
CNN_XGB 4	✓	✓	✓	✓
CNN_SVR 4	✓	✓	✓	✓
CNN_XGB 5		✓	✓	✓
CNN_SVR 5		✓	✓	✓

also shows a positive correlation with ET_c. Thus, it can be inferred that radiation and temperature have the highest impact on ET_c and also show good performance

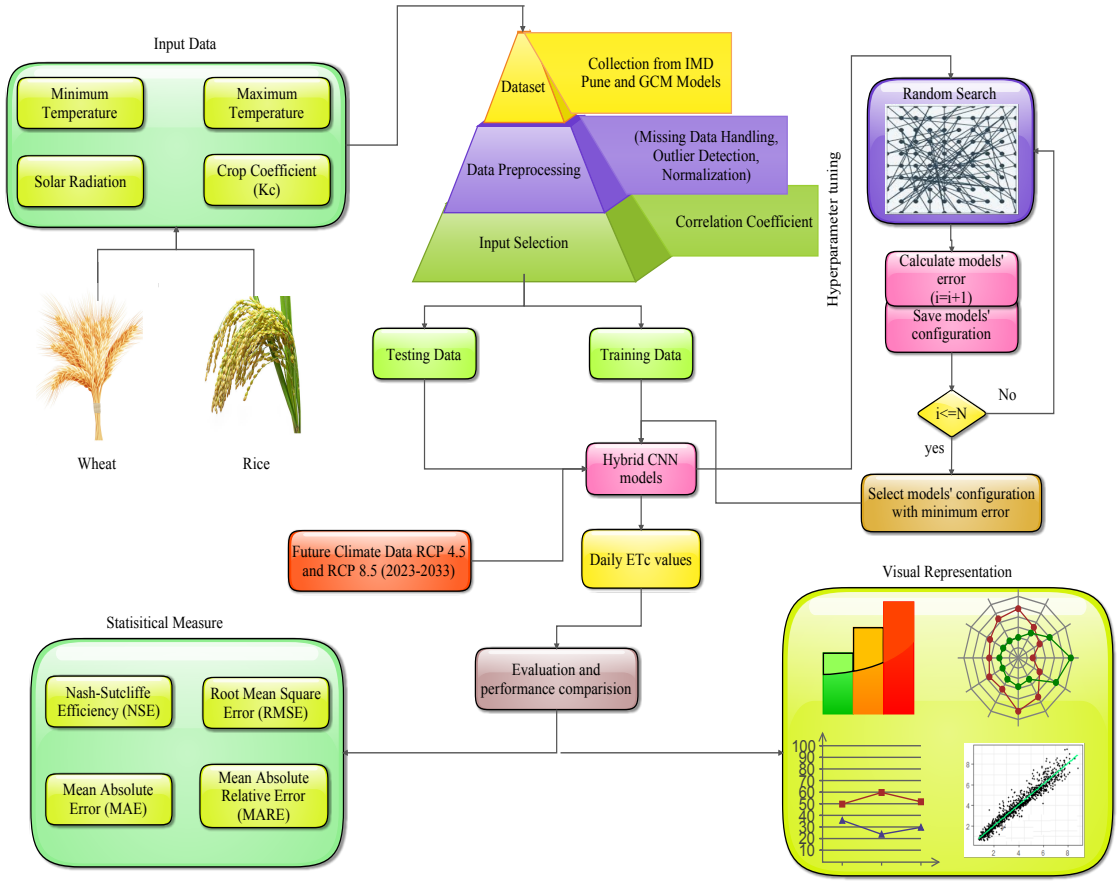

Figure 6.1: Schematic diagram of the proposed work

while estimating ET_c in arid and semi-arid environments [141]. Temperature with solar radiation has been proved as a main driver for predicting evapotranspiration process in past studies [115] and support the choice of using T_{min}, T_{max}, and R_s as limited meteorological parameters for modeling ET_c.

Five different input scenarios are created and analyzed by proposed hybrid models (CNN-XGB and CNN-SVR). Table 6.1 shows the input scenarios that are categorized by placing the subsequent highest correlation with ET_c. The input scenarios considered in the study are: scenario 1 (radiation only), scenario 2 (radiation and mean temperature), scenario 3 (radiation, mean temperature, and max temperature), scenario 4 (radiation, mean temperature, max temperature, and min temperature), and scenario 5 (mean temperature, max temperature, and min temperature) that consider only temperature parameters. Figure 6.1 illustrates the study's schematic consisting of data collection, preprocessing, modeling, and prediction phase. Data preprocessing is important, as raw data can have impurities such as missing or noisy values. The preprocessing of the data is done using missing data treatment, outlier detection, and normalization techniques. The missing data

is handled using the mixgb package of R Language [218] that uses multiple imputations using XGBoost. Outlier detection is performed using z-score method [235] as follows:

$$z = \frac{x_i - \overline{x}}{s} \tag{6.2}$$

where x, $\overline{x}$, and s are data point, mean, and standard deviation, respectively. Data is normalized in range of 0 to 1 using min-max scaler [193] by following equation.

$$x_{norm} = \frac{x_i - x_{max}}{x_{max} - x_{min}} \tag{6.3}$$

where x_{norm}, x_{max}, and x_{min} represents normalized, maximum and minimum values of the collected data respectively. The preprocessed data is split into training and testing data in the ratio of 60:40 and fed to proposed hybrid algorithms CNN-XGB and CNN-SVR. The hyperparameters of these algorithms such as number of filters, activation function, learning rate, number of layers, number of neurons of CNN layer, max_depth, min_child_node, max_leaf_nodes, and gamma values of XGboost algorithms and type of kernel, degree, regularization parameter C, and epsilon value of SVR algorithm is tuned with the help of random search algorithm [194] to get the best model for the given data. The dropout layer is also added to avoid overfitting in the model. The obtained optimal model is tested with test data and evaluated using performance metrics discussed in the next section. These optimal models are further used to predict future ET_c values of wheat and rice crops.

6.2.3 Model Performance Evaluation Criteria

The models used in the study are evaluated for their predictive ability, which is a crucial phase in model development. It involves statistical analysis of the model's predicted values to perceive how accurately the model can approximate the observed or actual values. In this study, ET_c is predicted using CNN-based hybrid models (CNN-XGB, CNN-SVR). The predicted ET_c is compared with observed ET_c values (computed by eq. (3.3)) using the following performance measures: Nash-Sutcliffe Efficiency (NSE) (see eq. 4.22), Root Mean Square Error (RMSE) (see eq. 4.20), Mean Absolute Error (MAE) (see eq. 4.19), and Mean Absolute Relative Error (MARE) is calculated using the following equation:

$$MARE = \frac{\sum_{i=1}^{N} ET_{ob_i} - ET_{p_i}}{\sum_{i=1}^{N} ET_{ob_i}} \tag{6.4}$$

where ET_{ob_i} (mmd^{-1}) is observed value of ET_c, ET_{p_i} is the predicted value of ET_c for the i^{th} value of data point, $\bar{ET}_{ob}$ is average of observed values of ET_c, and N is the number of data points considered in the study. NSE is a popular and potentially reliable metric for evaluating the predictive competency of hydrologic models.

It ranges from 0 to 1 for unbiased models, with 1 representing a perfect model, and for biased models, it may be algebraically negative [197].

RMSE reflects how closely the data points are to the best fit line. The lower the RMSE value, the better the model prediction. MAE is the mean difference between observed and predicted values without taking directions into account and ranges from 0 to 1. The lower the MAE value, the more accurate the model's prediction [195]. MARE value closer to zero shows the best predictive model.

6.3 Results and Discussion

The effectiveness of the proposed hybrid models (CNN-XGB and CNN-SVR) is assessed by comparing predicted and observed crop evapotranspiration values for wheat and rice crops. The model's performance in predicting ET_c is evaluated using a set of statistical metrics (NSE, RMSE, MAE, MARE), and a visual inspection of results are presented using scatter plots, line plots, and radar charts. The obtained results are summarized in the following sections. Section 6.3.1 and 6.3.2 describe the performance of CNN-XGB and CNN-SVR in predicting wheat and rice evapotranspiration. The estimation of future crop evapotranspiration of wheat and rice crop in the time period of 2023-2033 is presented in Subsection 6.3.3. In the last Subsection 6.3.4, the outcome of the proposed study is discussed in detail.

6.3.1 Performance Assessment of Proposed Models for Estimation of ET_c of Wheat

The viability of the proposed hybrid CNN-XGB and CNN-SVR models during the training and testing phase in terms of statistical metrics is shown in Table 6.2.

For scenario 1, the CNN-XGB on account of (NSE = 0.9008, RMSE = 0.4112, MAE = 0.2957, and MARE = 0.1544) is superior to CNN-SVR (NSE = 0.8804, RMSE = 0.4517, MAE = 0.3310, and MARE = 0.1726) in testing data. Besides, Figure 6.2 (a) shows the scatter plot of CNN-XGB and CNN-SVR for scenario 1.

It can be observed that predicted values obtained by CNN-XGB are in greater agreement with observed values as compared to CNN-SVR. Figure 6.3 demonstrates the line graph of CNN-XGB and CNN-SVR in comparison to actual observed values of wheat ET_c. A line graph shows change in values over time and help in determining the relationship between two sets of values. According to Figure 6.3 (a), CNN-XGB model predicted ET_c values are more closer to actual observed values of ET_c than CNN-SVR model.

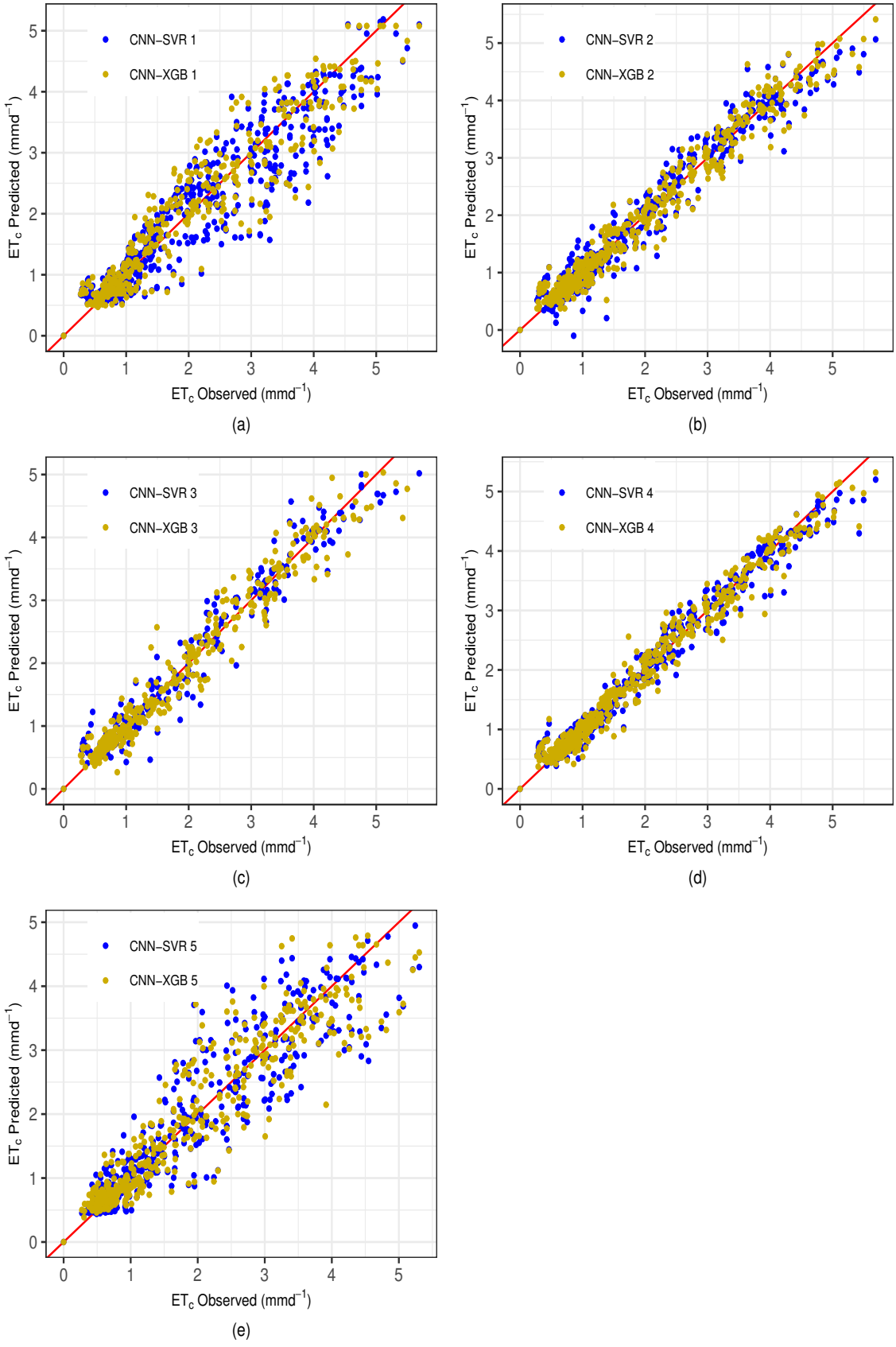

Figure 6.2: Comparison of hybrid models for different input scenarios of wheat crop

The statistical indices for scenario 2 reported in Table 6.2 shows that the CNN-XGB owing to highest (NSE = 0.9667) and lowest diagnostic errors (RMSE = 0.2385, MAE=0.1753, and MARE = 0.0914) provides the best performance for predicting wheat ET_c. Computationally, it can be stated that CNN-XGB shows decrement in the error i.e., RMSE, MAE, and MARE by 11%, 9.6%, and 9.6% respectively as compared to CNN-SVR (NSE = 0.9575, RMSE = 0.2694, MAE=0.1941 and MARE=0.1012).

Table 6.2: Performance Comparison of hybrid models for Wheat ET_c

Model	**Training Data**			
	NSE	**RMSE** (mmd^{-1})	**MAE** (mmd^{-1})	**MARE** (mmd^{-1})
CNN_SVR 1	0.9132	0.4012	0.2818	0.1466
CNN_XGB 1	0.9499	0.3059	0.3382	0.1109
CNN_SVR 2	0.9634	0.2604	0.1733	0.0926
CNN_XGB 2	0.9882	0.1476	0.1818	0.0552
CNN_SVR 3	0.9622	0.2648	0.1813	0.0933
CNN_XGB 3	0.9823	0.1809	0.1335	0.0674
CNN_SVR 4	0.9803	0.1911	0.1300	0.0675
CNN_XGB 4	0.9907	0.1314	0.1385	0.0487
CNN_SVR 5	0.8491	0.5052	0.3560	0.1933
CNN_XGB 5	0.9071	0.3964	0.2793	0.1512
Model	**Testing Data**			
	NSE	**RMSE** (mmd^{-1})	**MAE** (mmd^{-1})	**MARE** (mmd^{-1})
CNN_SVR 1	0.8804	0.4517	0.3310	0.1726
CNN_XGB 1	0.9008	0.4112	0.2957	0.1544
CNN_SVR 2	0.9575	0.2694	0.1941	0.1012
CNN_XGB 2	0.9667	0.2385	0.1753	0.0914
CNN_SVR 3	0.9564	0.2727	0.1949	0.1017
CNN_XGB 3	0.9550	0.2771	0.2040	0.1064
CNN_SVR 4	0.9765	0.2002	0.1407	0.0734
CNN_XGB 4	0.9745	0.2087	0.1482	0.0773
CNN_SVR 5	0.8521	0.4864	0.3394	0.1832
CNN_XGB 5	0.8723	0.4527	0.3103	0.1672

Figure 6.2 (b) depicts that the data points obtained from the CNN-XGB are more concentrated around the identity line. Figure 6.3 (b) illustrates that the prediction of CNN-XGB is closer to the actual observation. However, the CNN-SVR model shows slightly similar results to the CNN-XGB model for this input scenario.

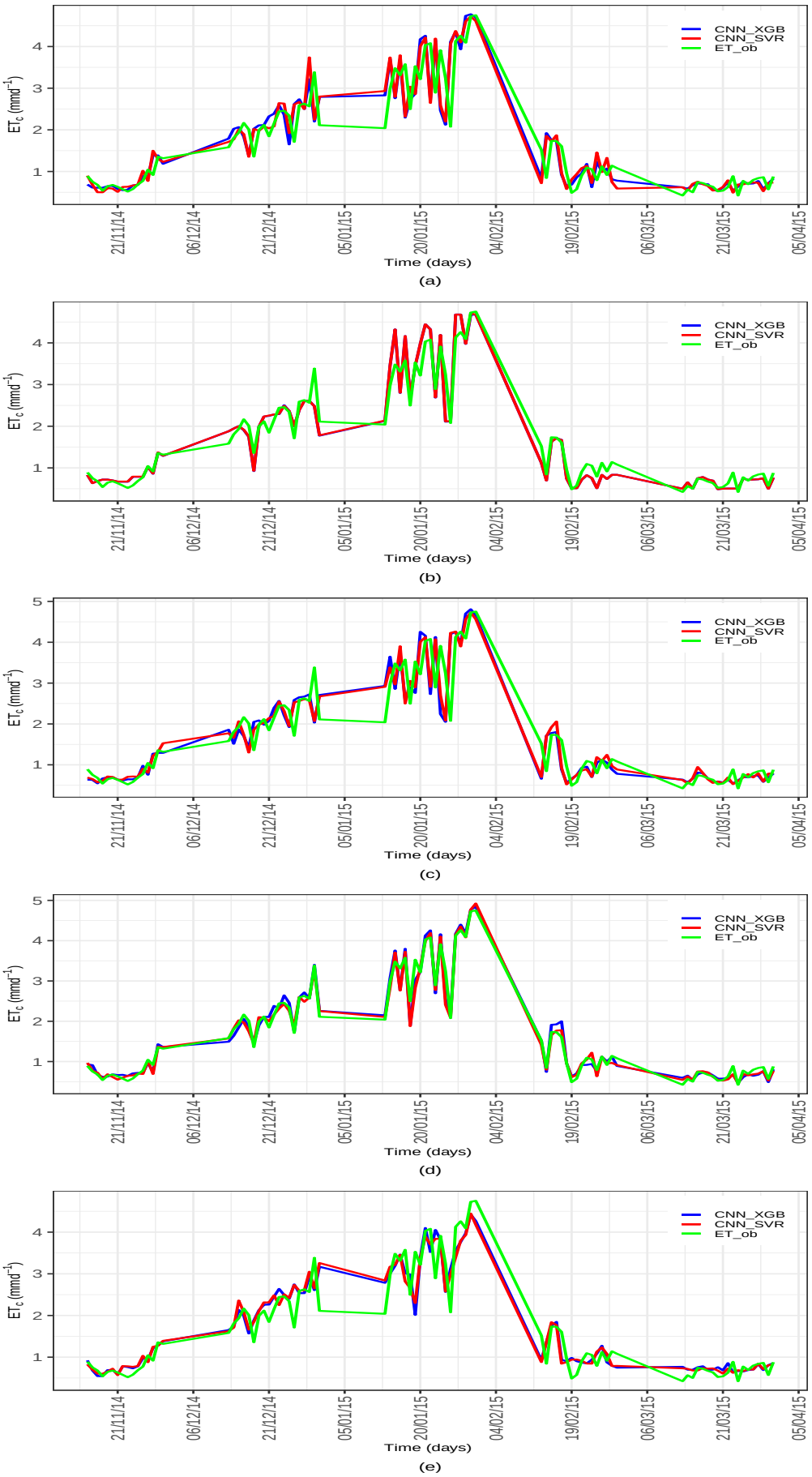

Figure 6.3: Prediction of wheat ET_c by hybrid models for different input scenarios

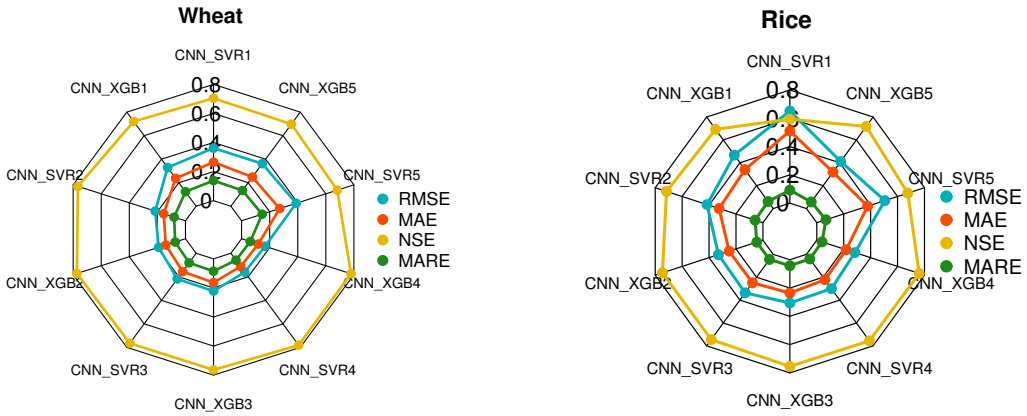

Figure 6.4: Comparison of hybrid models for wheat and rice ET_c

The predictive capability examination of the proposed hybrid models provided to predict the ET_c of wheat crop exhibits the superiority of the CNN-XGB model regarding (NSE = 0.9823, RMSE = 0.1809) as compared to CNN-SVR (NSE = 0.9622 and RMSE = 0.2648) for training data in scenario 3. However, CNN-XGB (NSE = 0.9550) and CNN-SVR (NSE = 0.9564) models have slightly similar performance for testing data. Figure 6.2 (c) confirmed equal agreement with actual and predicted ET_c using both hybrid models. Figure 6.3 (c) illustrates the distribution of predicted values by hybrid models and actual observed values and illustrates that prediction values of CNN-XGB and CNN-SVR show slightly similar results with actual wheat ET_c values. In scenario 4, the evaluation of statistical metrics demonstrates the more efficiency of CNN-XGB with respect to higher (NSE=0.9907) and lower errors (RMSE = 0.1314, MAE = 0.1385 and MARE = 0.0487) than CNN-SVR for training data. However, CNN-SVR exhibits a similar performance for testing with NSE=0.9765 to CNN-XGB (NSE = 0.9745). In input scenario 5, CNN-XGB (NSE = 0.907, RMSE = 0.396, MAE = 0.279, and MARE = 0.151) shows better performance as compared to CNN-SVR (NSE = 0.849, RMSE = 0.505, MAE = 0.356, and MARE = 0.193) for training data as well as testing data with NSE = 0.872 (CNN-XGB) as compared to NSE=0.852 (CNN-SVR). Furthermore, the efficiency of these hybrid models is significantly greater in scenario 4 as compared to other scenarios according to the distribution pattern in Figure 6.2 and 6.3.

The statistical values for hybrid models of all scenarios are displayed in Figure 6.4 to evaluate the performance of the models and analyze their predictive potential for wheat ET_c. It is evident that CNN-XGB shows fewer errors in all five scenarios, which is identified as an efficient model and yielded reliable precision for predicting wheat ET_c. However, CNN-SVR shows similar performance to CNN-XGB for scenarios 2, 3, and 4 for wheat ET_c prediction. The analysis also shows that the

best prediction results have been obtained using these hybrid modes for scenario 4 when T_{min}, T_{max}, T_{mean}, and R_s are provided as input. The year-wise analysis of the

Table 6.3: Comparison of total predicted wheat ET_c by hybrid models with actual ET_c values

Year	**Actual**	**CNN-XGB**	**CNN-XGB**		
	(mm)	**(mm)**	**MAE** (mmd^{-1})	**NSE**	**RMSE** (mmd^{-1})
2003	269.69	280.42	0.181	0.977	0.242
2004	285.28	285.62	0.123	0.987	0.172
2005	246.95	258.77	0.166	0.97	0.225
2006	296.62	294.54	0.129	0.971	0.184
2007	262.46	264.64	0.134	0.968	0.2
2008	287.42	279.08	0.119	0.987	0.158
2009	267.57	268.49	0.119	0.985	0.161
2010	261.55	261.40	0.097	0.991	0.132
2011	267.39	268.01	0.095	0.991	0.131
2012	270.04	270.41	0.096	0.991	0.131
2013	286.49	274.75	0.167	0.977	0.224
2014	283.09	279.32	0.141	0.978	0.208
2015	255.89	253.69	0.120	0.975	0.183
Year	**Actual**	**CNN-SVR**	**CNN-SVR**		
	(mm)	**(mm)**	**MAE** (mmd^{-1})	**NSE**	**RMSE** (mmd^{-1})
2003	269.69	280.98	0.216	0.969	0.279
2004	285.28	284.66	0.145	0.982	0.199
2005	246.95	262.52	0.204	0.96	0.259
2006	296.62	304.42	0.161	0.958	0.22
2007	262.46	262.68	0.182	0.947	0.257
2008	287.42	275.30	0.162	0.975	0.229
2009	267.57	266.23	0.153	0.977	0.197
2010	261.55	259.81	0.123	0.986	0.167
2011	267.39	267.08	0.124	0.985	0.169
2012	270.04	269.79	0.125	0.985	0.169
2013	286.49	264.82	0.26	0.952	0.321
2014	283.09	277.21	0.193	0.967	0.256
2015	255.89	254.08	0.154	0.968	0.209

total actual wheat ET_c and estimated wheat ET_c using CNN-XGB and CNN-SVR is provided in Table 6.3.

Table 6.4: Performance comparison of hybrid models for rice ET_c

Model	Training Data			
	NSE	**RMSE** (mmd^{-1})	**MAE** (mmd^{-1})	**MARE** (mmd^{-1})
CNN_SVR 1	0.730	0.847	0.709	0.123
CNN_XGB 1	0.913	0.484	0.623	0.067
CNN_SVR 2	0.870	0.587	0.606	0.083
CNN_XGB 2	0.966	0.304	0.383	0.041
CNN_SVR 3	0.920	0.460	0.314	0.062
CNN_XGB 3	0.967	0.297	0.318	0.041
CNN_SVR 4	0.939	0.404	0.277	0.051
CNN_XGB 4	0.983	0.216	0.159	0.030
CNN_SVR 5	0.829	0.675	0.499	0.092
CNN_XGB 5	0.883	0.559	0.480	0.078
Model	**Testing Data**			
	NSE	**RMSE** (mmd^{-1})	**MAE** (mmd^{-1})	**MARE** (mmd^{-1})
CNN_SVR 1	0.742	0.814	0.638	0.115
CNN_XGB 1	0.866	0.584	0.425	0.077
CNN_SVR 2	0.895	0.519	0.407	0.073
CNN_XGB 2	0.933	0.413	0.314	0.057
CNN_SVR 3	0.931	0.421	0.311	0.056
CNN_XGB 3	0.945	0.382	0.294	0.053
CNN_SVR 4	0.945	0.375	0.277	0.050
CNN_XGB 4	0.951	0.354	0.273	0.049
CNN_SVR 5	0.845	0.632	0.472	0.085
CNN_XGB 5	0.897	0.514	0.398	0.072

6.3.2 Performance Assessment of Proposed Models for Estimation of ET_c of Rice

Sophisticated metrics and graphical visualization of data are used to examine the ability of the proposed hybrid models to predict rice ET_c. Table 6.4 shows the comparison of CNN-XGB and CNN-SVR for all input scenarios for rice ET_c. According to Table 6.4, the results belong to the scenario 1 proved that the CNN-XGB model by statistical criteria (NSE = 0.866, RMSE = 0.584, MAE = 0.425 and MARE = 0.077) outperformed the CNN-SVR (NSE = 0.742, RMSE=0.814, MAE= 0.638 and MARE=0.115) for testing data. Figure 6.5 depicts the comparison between predicted and observed rice ET_c values in all input scenarios. The superiority of CNN-XGB is evident in Figure 6.5(a) based on distributed pattern around the perfect line (1:1 line) as the CNN-SVR model is far away from observed values. The predicted ET_c and actual observed values in the form of a line graph are presented

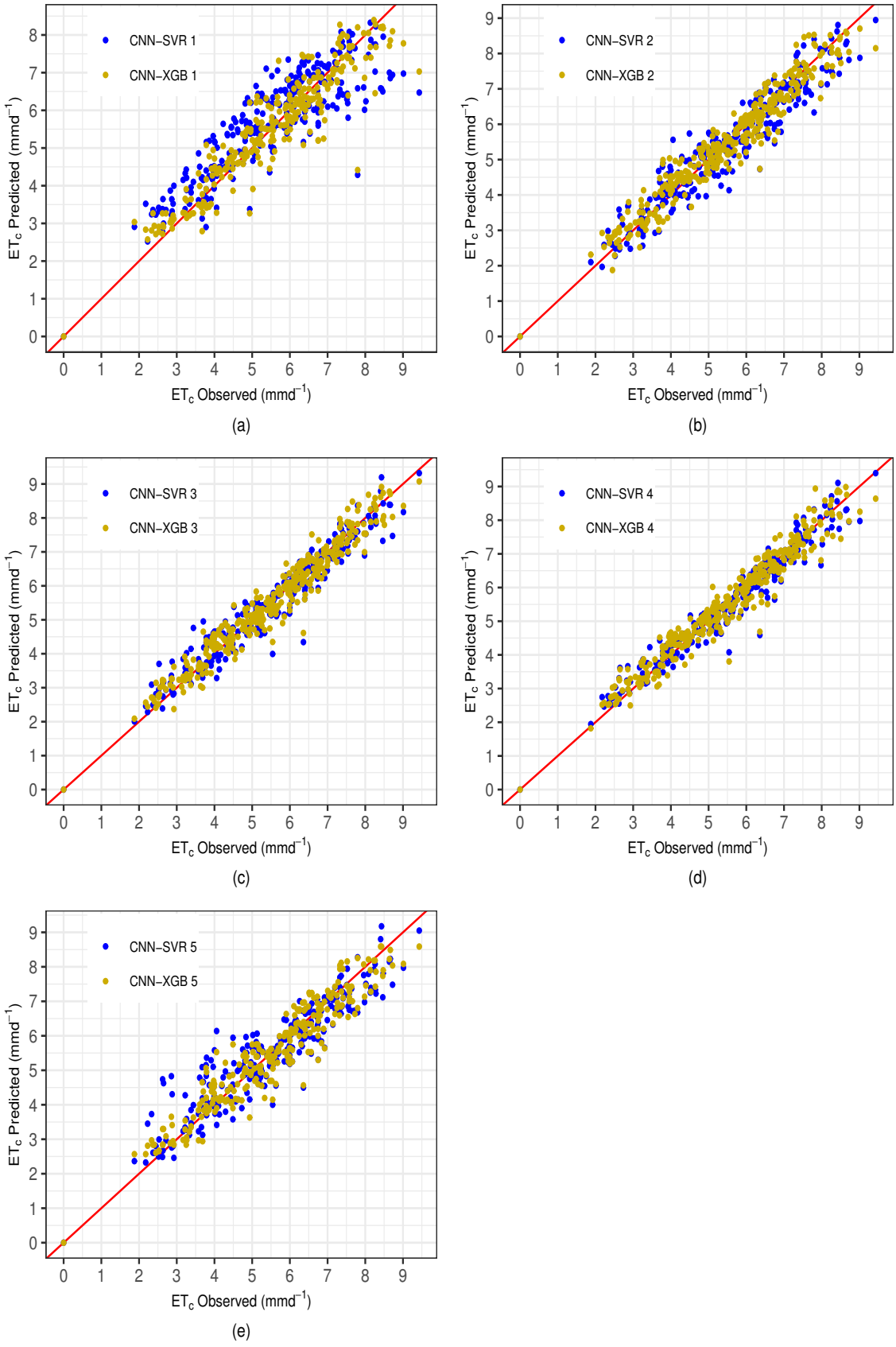

Figure 6.5: Comparison of hybrid models for different input scenarios of rice crop

in Figure 6.6 for a better assessment of the effectiveness of proposed hybrid models. The predicted values obtained by CNN-XGB are closer to the observed ET_c of the rice crop than CNN-SVR in scenario 1, as shown in Figure 6.6 (a).

The robustness of proposed models for input scenario 2 shows that CNN-XGB with NSE value (NSE = 0.933) and lower error values (RMSE = 0.413, MAE=0.314, and MARE = 0.057) provides better prediction than CNN-SVR for testing data. On the other hand, CNN-SVR has a higher error value (RMSE=0.519, MAE = 0.407, and MARE = 0.073) and a lower NSE value (NSE = 0.895), which confirms that CNN-SVR is not able to provide the reliable estimation of rice ET_c values for input scenario 2. Figure 6.5 (b) and Figure 6.6 (b) also proved that CNN-XGB outperforms CNN-SVR. In input scenario 3, the statistical indicators shows that CNN-XGB (NSE=0.967, RMSE=0.297, MAE=0.318, and MARE=0.041) shows better performance as compared to CNN-SVR (NSE=0.920, RMSE=0.460, MAE=0.314, and MARE=0.062) for training data. However, for testing data, CNN-XGB (NSE=0.945) and CNN-SVR (0.931) exhibit similar results as shows in Figure 6.5 (c) and 6.6 (c). The effectiveness of the proposed hybrid models is examined for input scenario 4; the outcome of this scenario also concludes the superiority of the CNN-XGB (NSE=0.983) model to CNN-SVR (NSE=0.939) using training data. However, for testing data, CNN-SVR (NSE=0.951) exhibits a similar performance as CNN-XGB (NSE=0.945) in this situation. Figure 6.5 (d) and 6.6 (d) also confirmed similarity between predicted values of rice ET_c of CNN-XGB and CNN-SVR. Finally, in input scenario 5, CNN-XGB (NSE=0.883, RMSE=0.559, MAE=0.480, and MARE=0.078) shows better performance as compared to CNN-SVR (NSE=0.829, RMSE=0.675, MAE=0.499, and MARE=0.092) for training data as well as testing data with NSE=0.897 (CNN-XGB) as compared to NSE=0.845 (CNN-SVR).

The performance comparison of proposed hybrid models to predict the ET_c of rice crop clearly shows the superiority of the CNN-XGB model compared to CNN-SVR for all scenarios. The radar plot of statistical metrics values of all scenarios is presented in Figure 6.4 of rice crop using both hybrid models. The radar plot demonstrates that for input scenarios 1,2, and 5, the CNN-SVR model can not provide reliable performance. However, for input scenarios 3 and 4, CNN-SVR is able to provide reliable performance and show results somewhat similar to CNN-XGB for testing data. The best result for rice ET_c is obtained for input scenario 4 (T_{min} T_{max}, T_{mean}, K_c) using both hybrid models with NSE $\backsimeq$ 0.95 for testing data. The year-wise analysis of the total actual rice ET_c and estimated rice ET_c using CNN-XGB and CNN-SVR is provided in Table 6.5.

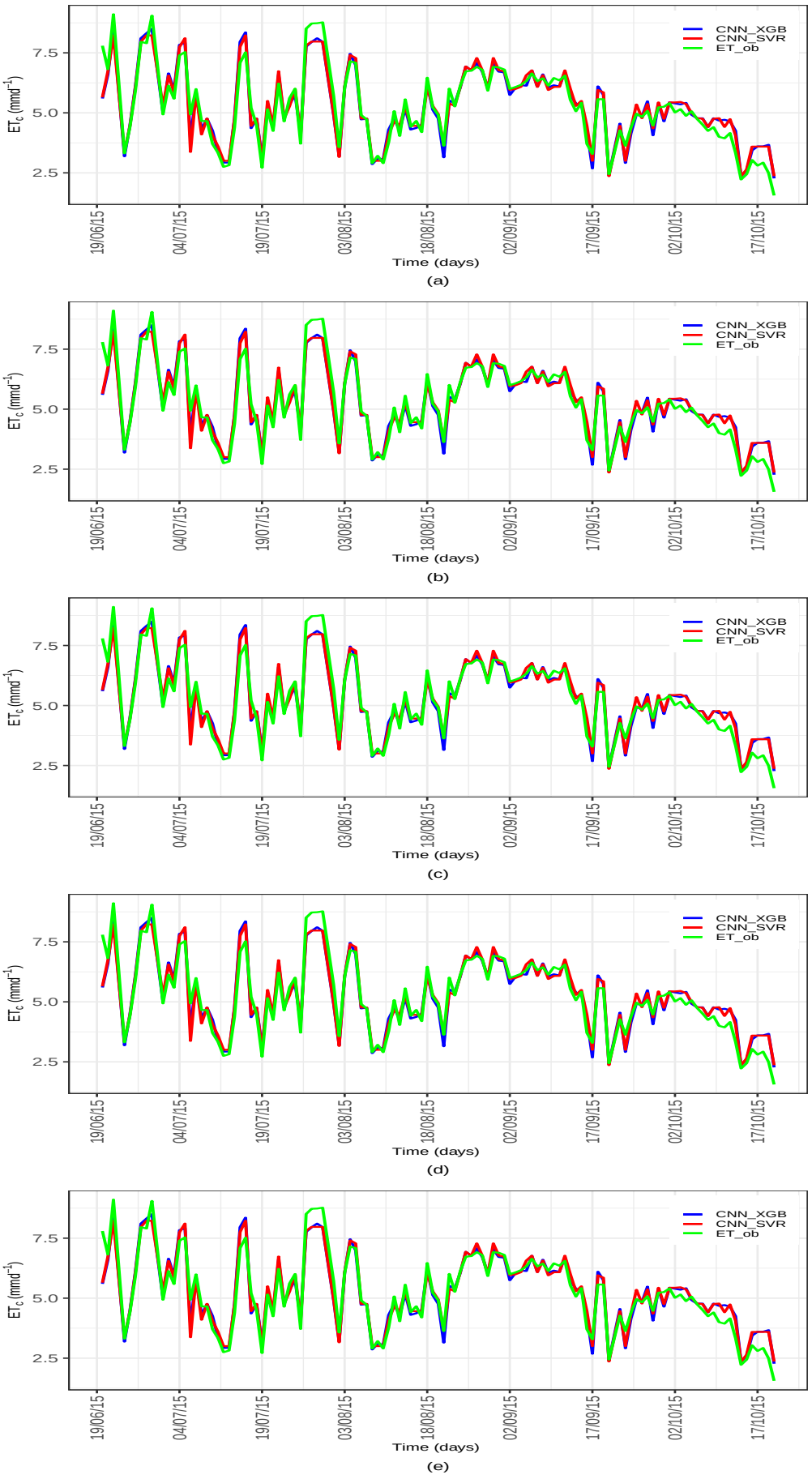

Figure 6.6: Prediction of rice ET_c by hybrid models for different input scenario

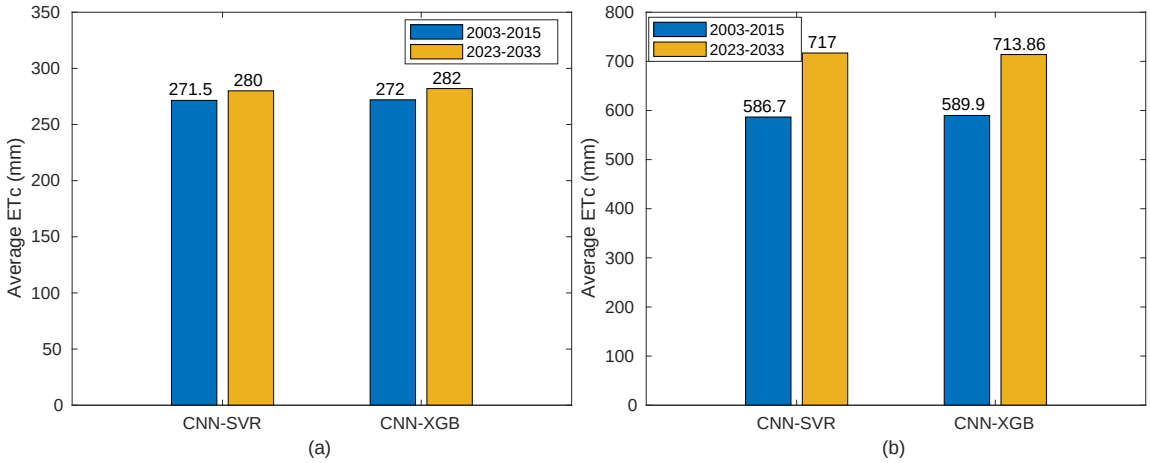

Figure 6.7: Comparison of averages annual ET_c of a) wheat and b) rice crop

The rise in T_{max} is from 29.9°C to 33.03°C and 33.26°C respectively for RCP 4.5 and 8.5. Similarly, corresponding T_{min} also shows increment in their values from 17.5°C to 18.79°C and 18.85°C respectively. The average T_{max} will increase by 11.5 % and 10.5 % for RCP 8.5 and 4.5 and correspondingly T_{min} will increase by 7.37 % and 7.03 %.

6.3.3 Estimation of Rice and Wheat ET_c in 2023-2033

The projected climate variables under two emission scenarios (RCP 4.5 and RCP 8.5) for 2023-2033 show a rise in their values compared to average historic data from 2003-2015. The proposed hybrid models (CNN-XGB and CNN-SVR) are trained and tested on historical data (2003-2015) and then applied to projected climate data for 2023-2033 to predict future values of wheat and rice ET_c. Table 6.6 and 6.7 depict future ET_c values for wheat and rice ET_c of both emission scenarios using CNN-SVR and CNN-XGB. It is evident from Figure 6.7 that the average ET_c value for rice crop is going to increase in the future by 20% to 22% than historical time period (Table 6.5). The average across of two emission scenarios indicates that ET_c of the wheat crop would increase by 3% to 4% than the historical time period (Table 6.3) as predicted by the proposed models. Results demonstrate that the proposed hybrid models effectively reproduce the present ET_c values with limited meteorological data and can be utilized as a robust and trustworthy approach to estimate future ET_c values.

6.3.4 Discussion

The applied predictive models demonstrate the tremendous potential of hybridized AI models in addressing the ET_c modeling process using a limited dataset. The integration of CNN with XGB and SVR is evaluated for the prediction of crop evap-

Table 6.5: Comparison of total predicted rice ET_c by hybrid models with actual ET_c values

Year	Actual (mm)	CNN-XGB (mm)	CNN-XGB MAE (mmd^{-1})	CNN-XGB NSE	CNN-XGB RMSE (mmd^{-1})
2003	566.3	573.8	0.199	0.963	0.254
2004	706.5	687.9	0.284	0.929	0.406
2005	672.0	668.1	0.205	0.977	0.276
2006	566.8	567.2	0.211	0.961	0.305
2007	553.0	553.4	0.234	0.963	0.322
2008	545.0	549.8	0.202	0.954	0.285
2009	571.2	576.0	0.22	0.96	0.282
2010	577.3	581.8	0.214	0.967	0.279
2011	569.0	578.2	0.224	0.967	0.299
2012	552.5	562.9	0.206	0.958	0.264
2013	543.2	557.3	0.229	0.952	0.295
2015	624.2	623.3	0.182	0.975	0.256
Year	**Actual (mm)**	**CNN-SVR (mm)**	**CNN-SVR MAE (mmd^{-1})**	**CNN-SVR NSE**	**CNN-SVR RMSE (mmd^{-1})**
2003	566.3	593.7	0.397	0.761	0.642
2004	706.5	655.3	0.7	0.722	0.802
2005	672.0	645.0	0.599	0.845	0.71
2006	566.8	570.8	0.334	0.916	0.449
2007	553.0	557.2	0.399	0.89	0.559
2008	545.0	556.7	0.347	0.821	0.566
2009	571.2	562.2	0.338	0.916	0.411
2010	577.3	566.0	0.369	0.915	0.45
2011	569.0	567.6	0.326	0.939	0.403
2012	552.5	579.7	0.319	0.894	0.419
2013	543.2	558.0	0.306	0.924	0.37
2015	624.2	628.5	0.32	0.926	0.439

otranspiration of wheat and rice crop using limited meteorological parameters such as T_{max}, T_{min}, T_{mean}, and R_s that are readily available and proved as prime data inputs for the estimation of evapotranspiration in previous studies [236] [237]. The outputs yielded by these two hybrid models are then compared using statistical metrics such as NSE, RMSE, MAE, and MARE and visual representation using scatter plots, line plots, and radar charts.

It is worth noting that the performance of these models varies with different

Table 6.6: Prediction of total wheat ET_c of future data using RCP 4.5 and 8.5

Year	CNN-SVR			CNN-XGB		
	RCP 4.5 ETc(mm)	RCP 8.5 ETc (mm)	Average ETc (mm)	RCP 4.5 ETc(mm)	RCP 8.5 ETc (mm)	Average ETc (mm)
2023	278.3	265.2	271.8	278.1	273.5	275.8
2024	280.5	268.1	274.3	275.1	275.7	275.4
2025	282.8	280.4	281.6	277.2	278.7	277.9
2026	284.1	272.1	278.1	278.7	275.3	277.0
2027	290.2	278.4	284.3	285.0	287.4	286.2
2028	283.2	280.7	281.9	277.7	285.4	281.6
2029	281.7	272.3	277.0	278.9	282.8	280.9
2030	297.9	288.4	293.2	295.4	289.1	292.2
2031	280.9	277.1	279.0	287.7	289.3	288.5
2032	286.5	277.7	282.1	283.3	287.6	285.4

Table 6.7: Prediction of total rice ET_c of future data using RCP 4.5 and 8.5

Year	CNN-SVR			CNN-XGB		
	RCP 4.5 ETc(mm)	RCP 8.5 ETc (mm)	Average ETc (mm)	RCP 4.5 ETc(mm)	RCP 8.5 ETc (mm)	Average ETc (mm)
2023	714.8	713.2	714.0	722.5	713.1	717.8
2024	714.5	713.2	713.9	721.6	714.7	718.2
2025	714.2	712.9	713.5	720.6	714.6	717.6
2026	711.4	713.6	712.5	714.7	712.7	713.7
2027	710.5	714.4	712.5	716.8	715.5	716.1
2028	711.2	715.4	713.3	717.8	715.4	716.6
2029	711.0	713.2	712.1	715.0	714.1	714.5
2030	709.7	714.1	711.9	714.4	715.6	715.0
2031	704.0	722.1	713.0	710.5	723.7	717.1
2032	705.2	718.1	711.6	709.1	720.6	714.9
2033	705.8	747.4	726.6	710.4	725.7	718.1

input scenarios of meteorological parameters. This clearly explains the complexity of modeling the ET_c process as various climate factors affect it. However, proposed hybrid models, especially CNN-XGB, provides superior performance in estimating ET_c of wheat and rice crop. The study is further extended to estimate wheat and rice water requirement in the time period of 2023-2033 using two GCM models for emission scenarios: RCP 4.5 and 8.5. The results reveal that the projected water requirement for rice and wheat crop is expected to increase in the coming years due to climate change.

Table 6.8: Comparison of the proposed approach with existing studies

Author(s)	**Input parameters**	**Crop**	**Study area**	**Model**	**Time Duration**	**CC impact on ET_c**	**Result**
Nikam *et al.* [238]	T_{min}, T_{max}, R_s, RH, SSH, WSP, Days after sowing, Evaporation, k_c	Wheat	Delhi, India	ANN	2001-2007	×	NSE=0.776
Saggi *et al.* [114]	T_{min}, T_{max}, R_s, RH, SSH, WSP, k_c	Wheat	Ludhiana, India	FG, RRF	2012-2014	×	R^2=0.94
Yamaç *et al.* [115]	T_{mean}, R_s, WSP, RH, k_c	Potato	Valenzano, Southern Italy	AdaBoost, ANN, KNN	2009-2010	×	R^2=0.81-0.97
Elbeltagi *et al.* [122]	T_{min}, T_{max}, R_s, k_c	Wheat	Ad Daqahliyah, Al Gharbiyah, Ash Sharqiyah, and Al Ismailiyah, Egypt	DNN	2006-2016	√	R^2=0.94-0.95

Author(s)	Input parameters	Crop	Study area	Model	Time Duration	CC impact on ET_c	Result
Maselli *et al.* [239]	T_{mea}, R_s, Pr k_c	grassland, cropland	Central Italy	modified NDVI	2006-2016	×	$R2$=0.81-0.93
Yamaç *et al.* [119]	T_{min}, T_{max}, R_s, k_c	sugarbeet	Çumra, Konya, Turkey	AdaBoost, RF, kNN, SVM	2012-2013	×	R^2=0.96-0.97
Proposed study	T_{min}, T_{max}, T_{mean} R_s, k_c	Wheat, Rice	Ludhiana, India	CNN-XGB, CNN-SVR	2003-2015	√	R^2=0.97-0.98

Temperature is one of the most critical factors affecting the evapotranspiration process. The simulation of future data (2023-2033) reveals the increase in minimum temperature by 7.03%, 7.37%, and maximum temperature by 10.5%, 11.5% for RCP 4.5 and RCP 8.5, respectively. Thus, as the temperature increases, evapotranspiration also increases. It is because evaporation rises as there is more energy available to transform the water from the liquid state to the vapor state, while transpiration rises as plants open their stomata and emit more water vapor due to an increase in temperature. This might cause an increase in the value of ET_c for wheat and rice crop in the near future (2023-2033).

Nikam *et al.* [238] first attempted to model crop evapotranspiration of wheat crop using an artificial neural network approach and obtained R^2 = 0.776, RMSE = 1.334, and MAE = 0.892. Saggi *et al.* [114] also attempted to estimate wheat crop evapotranspiration using Fuzzy-Genetic (FG) and Random Forest (RRF) models and achieved R^2 = 0.94, RMSE = 0.352, and MAE = 0.218. However, in the present study, the proposed hybrid models have provided better performance as provided as shown in Figure 6.2 and Table 6.2 for wheat crop with R^2 = 0.976, RMSE = 0.20, and MAE = 0.1407. Moreover, the results obtained in the study are consistent with the study conducted by Yamacc *et al.* [115] in Southern Italy for potato ET_c prediction using four different input scenarios of meteorological data and achieved R^2 = 0.81-0.97 by employing ML algorithms.

The results of present study is closer to Elbeltagi *et al.* [122] who estimated monthly ET_c values of the wheat crop for a study area in Egypt using a deep neural network and achieved R^2 = 0.95-0.97 for training and 0.94 - 0.95 for testing data. The present study is able to achieve R^2= 0.98 - 0.99 for training and R^2 = 0.97-0.98 for testing data for wheat crop evapotranspiration. In addition, the results are in agreement with Yammac [119], who applied AI algorithms to estimate sugar beet ET_c values in semi-arid regions for different combination of input data and achieved R^2 from 0.96 to 0.97 for input combinaion T_{max}, T_{min}, and R_s. The proposed models provides adequate results as compared to Maselli *et al.* [239], who proposed improved version of normalized difference vegetation index (NDVI) to model ET_c in Mediterranean regions and achieved R^2 = 0.81-0.93. These comparisons reveal the usefulness of the proposed hybrid models and supports that ET_c can be successfully estimated using only limited input data (T_{max}, T_{min}, T_{mean}, and R_s). The comparison of the proposed approach with previous related studies is also presented in Table 6.8.

Chapter 7

Conclusions and Scope for Future Work

This chapter summarizes the dissertation by providing an overview of the conducted research studies, the key findings, the conclusion reached, and the directions for future work. The proposed research studies in this thesis aim to provide an efficient approach to determine the precise water requirements of crops to achieve water sustainability in agriculture. To achieve this aim, Deep Learning based approaches have been designed and developed to predict the reference evapotranspiration (ET_0) and crop evapotranspiration (ET_c). Moreover, these proposed research studies also take limited climate data into consideration to eliminate the limitation of data scarcity.

7.1 Summary

In Chapter 3, the geographical conditions of the study locations are presented, along with a description of the crop and meteorological datasets that were used in the research. Ludhiana, Amritsar and Patiala stations of Punjab are selected to conduct the study. The statistical and cross-correlation of the meteorological data of these stations are discussed. Further, the crop characterstics of these stations are also described.

In Chapter 4, the two deep learning-based hybrid models (CNN-LSTM and Conv-LSTM) have been introduced to predict the daily ET_0 values of the Ludhiana and Amritsar stations of Punjab, India. The respective models are used to investigate different input combinations of meteorological data to identify the minimum required meteorological parameters. The proposed models are evaluated using different model evaluation parameters. Further, the performance of these models is compared with existing temperature and radiation-based empirical models, i.e., Hargreaves, Makkink, and Ritchie.

In Chapter 5, the deep reinforcement-based ensemble approach, i.e., DeepEvap, is introduced to predict daily ET_0 values of Ludhiana and Patiala stations. DeepEvap ensembles the predicting power of four hybrid baseline models, i.e., CNN-LSTM, Conv-LSTM, CNN-SVR, and CNN-XGB, for the prediction of ET_0. Moreover, the proposed DeepEvap ensemble model also incorporates time-varying input characteristics to remove the static nature of existing ensemble techniques by dynamically selecting baseline models for each specific input to predict ET_0. The performance of DeepEvap is evaluated against existing ensemble approaches (e.g., stacked and weighted) and baseline models using different evaluation parameters. Further, an attempt is made in the direction to extend the findings of the previous study by considering only required minimum meteorological parameters, i.e., T_{min}, T_{max}, and R_s to predict ET_o values.

In Chapter 6, the hybrid models of CNN with two powerful machine learning models (CNN-XGB and CNN-SVR) are proposed for the prediction of daily crop evapotranspiration of wheat and rice crops. Four different input scenarios of meteorological parameters (T_{min}, T_{max}, T_{mean}, and R_s) and k_c are examined for obtaining satisfactory performance. Further, future climate data (2023-2033), using two emission scenarios, is considered to project the changes in wheat and rice water requirement.

7.2 Conclusions

The main conclusions of the conducted study are drawn from the investigations:

- The foremost strength of the conducted study is the reliability of both the hybrid deep learning algorithms: Conv-LSTM and CNN-LSTM, in modeling the ET_0 process under data-scarce situations.
- T_{min}, T_{max}, and R_s are identified as the minimum required meteorological parameters used to predict reliable prediction of ET_0 (NSE=0.9415-0.9483, MAE=0.0383-0.0345, and RMSE=0.053-0.0500) in semi-arid region.
- The combination of T_{min}, T_{max}, and R_s with other available meteorological parameters could provide comparable performance to gold standard FAO-PM model.
- The input combination of T_{min}, T_{max}, R_s, WSP, and RH could be considered as best input combination for both the stations with R2=0.989-0.991.
- The proposed models (CNN-LSTM and Conv-LSTM) show better performance than empirical models (e.g., Hargreaves, Makkink, and Ritchie) using limited

meteorological data.

- Although both the proposed hybrid models provide satisfactory results, the Conv-LSTM model provides more accurate results in almost every possible input combination considered in the study.
- The proposed DRL-based ensemble approach is effective in integrating four baseline hybrid deep learning models (CNN-LSTM, Conv-LSTM, CNN-XGB, and CNN-SVR) and enhances the prediction of ET_o by minimizing the mean square error.
- The present research study deals with the issue of the lack of the majority of meteorological parameters essential to estimate ET_o values in underdeveloped regions. The DeepEvap use T_{min}, T_{max}, and R_s to predict daily ET_o and achieves decent success with $R^2 \simeq 0.96$ and MSE $\simeq 0.0018$ for both stations.
- Although the proposed DRL ensemble approach provides closer performance to other existing ensemble approaches, the major aspect of the proposed ensemble approach is to implement an intelligent and a coherent system that surmounts the state-of-art deep learning models. Also, they should be able to work in an unknown dynamic environment (such as climate change) and provide reasonable accuracy using limited climate data. Thus, unlike other approaches that use only historical data to predict outcomes, the DRL approach can become more intelligent via iterations and work in an unknown dynamic environment of future climate data.
- CNN-XGB and CNN-SVR yield excellent results for estimating ET_c employing a limited meteorological dataset, with NSE = 0.95 for rice and NSE = 0.97-0.98 for the wheat crop.
- The input scenario 4 (T_{min}, T_{max}, T_{mean}, and R_s) yield better performance than other input scenarios.
- Both CNN-SVR and CNN-XGB models are capable of providing a reliable prediction of ET_c using limited meteorological data. However, the CNN-XGB model yielded slightly better results for both crops in all input scenarios.
- According to proposed hybrid models, the wheat ET_c will rise by 3–4% and rice ET_c by 20–22% for future data (2023-2033).
- This applied technique can aid in the development of intelligent systems that can calculate the water requirements of specific crops, which is incredibly useful for agronomists and water resource managers in establishing sustainable water policies.

7.3 Contributions

The main research contributions of this thesis are as follows:

- The research study focuses on developing a model that can handle data-scarce situations by utilizing fewer climate variables and predicting ET_o values with reasonable accuracy. To achieve this, Convolution neural network-Long short term memory (CNN-LSTM), Convolution-Long Short Term Memory (Conv-LSTM) are proposed in this study.

- T_{max} , T_{min} , and R_s are proved to be prime data inputs in the proposed study for ET_o modeling.

- An attempt is also made to incorporate time-varying characteristics of inputs by dynamically selecting models and to remove the static nature of ensemble techniques. In the proposed DeepEvap approach, the Deep Q Network (DQN) agent of DRL is trained to dynamically select the baseline model to predict the ET_o value for each specific input.

- Two hybrid models, CNN-XGB and CNN-SVR are proposed to predict daily crop evapotranspiration of wheat and rice crops. This study also deals with the limited availability of climate data to model the ET_c process.

- The study also investigates the climate change impact on the crop water requirement of wheat and rice crops using Representative Concentration Pathway (RCP) 4.5 and 8.5 emission scenarios of Ludhiana station of Punjab.

7.4 Scope for Future Work

The journey of research never ends. This dissertation introduced the notion that deep learning based approaches can be applied successfully to determine the crop water requirement. The primary objectives have been achieved successfully, and the following are future directions for further study.

- Geographical information systems (GIS) and remote sensing technologies have been widely employed in modeling hydrological processes. Remote sensing technology has provided non-invasive, time and cost-effective approaches for detecting the plant water status, soil moisture, and meteorological parameters for ET prediction over a wider variety of temporal scales than any manual method. Further research should be directed toward the integration of remote sensing-based data and AI to better interpret remote sensing data for irrigation scheduling.

- The biggest challenge for modeling ET_o using AI is to develop a procedure/model that can be applied to all climate regions. Most of the research in this field has focused only on a single climate region to model ET_o, which makes it unacceptable for different climate regions. There is great demand for the development of a generalized AI model for the ET_o process using less meteorological data.

- Climate change is considered as a major concern since historical trends may no longer be valid in the future. Therefore, future research studies should focus on developing AI-based ET_o models that consider climate change for the realistic ET_o projection. Data and sampling for training and testing should be done with care to ensure data uniformity and minimum climate change influence. Furthermore, models should be kept as up-to-date as feasible. Dynamic modeling, such as reinforcement learning, may be used to meet this demand by updating the training data and providing results on real-time data. Therefore, more studies are required using the dynamic modeling concept to predict the behavior of water requirements in the future.

List of Publications

Journal Publications

1. **Gitika Sharma**, Ashima Singh and Sushma Jain,A hybrid deep neural network approach to estimate reference evapotranspiration using limited climate data, **Neural Computing and Applications**, https://doi.org/10.1007/s00521-021-06661-9,34, 4013–4032 , 2021. [SCIE Indexed, Impact Factor 5.102].

2. **Gitika Sharma**, Ashima Singh and Sushma Jain, DeepEvap: Deep reinforcement learning based ensemble approach for estimating reference evapotranspiration, **Applied Soft Computing**, https://doi.org/10.1016/j.asoc.2022.109113, 125, 109113, 2022 [SCIE Indexed, Impact Factor 8.263].

3. **Gitika Sharma**, Ashima Singh and Sushma Jain, Hybrid Deep Learning Techniques for Estimation of Daily Crop Evapotranspiration using Limited Climate Data, **Computers and Electronics in Agriculture**, https://doi.org/10.1016/j.compag.2022.107338, 202, 107338, 2022 [SCIE Indexed, Impact Factor 6.757]

   Communicated

4. **Gitika Sharma**, Ashima Singh and Sushma Jain, Artificial Intelligence for Irrigation Scheduling: A Systematic Review. [Under review].

References

[1] Smart Farming powered by Analytics. [Online]. Available: https://www.wipro.com/analytics/smart-farming-powered-by-analytics/

[2] V. Dhawan, "Water and agriculture in india," in *Background paper for the South Asia expert panel during the Global Forum for Food and Agriculture*, vol. 28, 2017, pp. 80–85.

[3] ——, "Water and agriculture in India," in *Background paper for the South Asia expert panel during the Global Forum for Food and Agriculture*, vol. 28, 2017.

[4] O. Kisi, "The potential of different ANN techniques in evapotranspiration modelling," *Hydrological Processes: An International Journal*, vol. 22, no. 14, pp. 2449–2460, 2008.

[5] Water scarcity. Accessed:2022-05-30. [Online]. Available: https://www.fao.org/land-water/water/water-scarcity/en/

[6] U. Desa, "World population prospects 2019: Highlights," *New York (US): United Nations Department for Economic and Social Affairs*, vol. 11, no. 1, p. 125, 2019.

[7] World bank open data. Accessed:2022-05-30. [Online]. Available: https://data.worldbank.org

[8] Z. Gu, Z. Qi, R. Burghate, S. Yuan, X. Jiao, and J. Xu, "Irrigation scheduling approaches and applications: A review," *Journal of Irrigation and Drainage Engineering*, vol. 146, no. 6, p. 04020007, 2020.

[9] W. R. Walker *et al.*, *Guidelines for designing and evaluating surface irrigation systems*. FAO, 1989.

[10] I. Haddeland *et al.*, "Global water resources affected by human interventions and climate change," *Proceedings of the National Academy of Sciences*, vol. 111, no. 9, pp. 3251–3256, 2014.

[11] P. H. Krishnashetty, J. Balasangameshwara, S. Sreeman, S. Desai, and A. B. Kantharaju, "Cognitive computing models for estimation of reference evapotranspiration: A review," *Cognitive Systems Research*, vol. 70, pp. 109–116, 2021.

[12] S. Kang, X. Hao, T. Du, L. Tong, X. Su, H. Lu, X. Li, Z. Huo, S. Li, and R. Ding, "Improving agricultural water productivity to ensure food security in China under changing environment: From research to practice," *Agricultural Water Management*, vol. 179, pp. 5–17, 2017.

[13] Y. Osroosh, R. T. Peters, C. S. Campbell, and Q. Zhang, "Comparison of irrigation automation algorithms for drip-irrigated apple trees," *Computers and Electronics in Agriculture*, vol. 128, pp. 87–99, 2016.

[14] M. Cruz-Blanco, I. Lorite, and C. Santos, "An innovative remote sensing based reference evapotranspiration method to support irrigation water management under semi-arid conditions," *Agricultural water management*, vol. 131, pp. 135–145, 2014.

[15] L. S. Pereira, R. G. Allen, M. Smith, and D. Raes, "Crop evapotranspiration estimation with FAO56: Past and future," *Agricultural Water Management*, vol. 147, pp. 4–20, 2015.

[16] M. A. Yassin, A. Alazba, and M. A. Mattar, "Artificial neural networks versus gene expression programming for estimating reference evapotranspiration in arid climate," *Agricultural Water Management*, vol. 163, pp. 110–124, 2016.

[17] B. K. Pandey and D. Khare, "Identification of trend in long term precipitation and reference evapotranspiration over Narmada river basin (India)," *Global and planetary change*, vol. 161, pp. 172–182, 2018.

[18] M. Gocic and S. Trajkovic, "Service-oriented approach for modeling and estimating reference evapotranspiration," *Computers and Electronics in Agriculture*, vol. 79, no. 2, pp. 153–158, 2011.

[19] A. Pour-Ali Baba, J. Shiri, O. Kisi, A. F. Fard, S. Kim, and R. Amini, "Estimating daily reference evapotranspiration using available and estimated climatic data by adaptive neuro-fuzzy inference system (ANFIS) and artificial neural network (ANN)," *Hydrology Research*, vol. 44, no. 1, pp. 131–146, 2013.

[20] O. Kisi and M. Zounemat-Kermani, "Comparison of two different adaptive neuro-fuzzy inference systems in modelling daily reference evapotranspiration," *Water resources management*, vol. 28, no. 9, pp. 2655–2675, 2014.

[21] D. Petković, M. Gocic, S. Trajkovic, S. Shamshirband, S. Motamedi, R. Hashim, and H. Bonakdari, "Determination of the most influential weather parameters on reference evapotranspiration by adaptive neuro-fuzzy methodology," *Computers and Electronics in Agriculture*, vol. 114, pp. 277–284, 2015.

[22] B. Keshtegar, O. Kisi, H. Ghohani Arab, and M. Zounemat-Kermani, "Subset modeling basis ANFIS for prediction of the reference evapotranspiration," *Water resources management*, vol. 32, no. 3, pp. 1101–1116, 2018.

[23] M. Zakhrouf, H. Bouchelkia, and M. Stamboul, "Neuro-fuzzy systems to estimate reference evapotranspiration," *Water SA*, vol. 45, no. 2, pp. 232–238, 2019.

[24] W. Jing, Z. M. Yaseen, S. Shahid, M. K. Saggi, H. Tao, O. Kisi, S. Q. Salih, N. Al-Ansari, and K.-W. Chau, "Implementation of evolutionary computing models for reference evapotranspiration modeling: short review, assessment and possible future research directions," *Engineering applications of computational fluid mechanics*, vol. 13, no. 1, pp. 811–823, 2019.

[25] S. Traore, Y. Luo, and G. Fipps, "Gene-expression programming for short-term forecasting of daily reference evapotranspiration using public weather forecast information," *Water resources management*, vol. 31, no. 15, pp. 4891–4908, 2017.

[26] J. Shiri, "Evaluation of FAO56-PM, empirical, semi-empirical and gene expression programming approaches for estimating daily reference evapotranspiration in hyper-arid regions of Iran," *Agricultural water management*, vol. 188, pp. 101–114, 2017.

[27] M. A. Mattar, "Using gene expression programming in monthly reference evapotranspiration modeling: a case study in Egypt," *Agricultural Water Management*, vol. 198, pp. 28–38, 2018.

[28] M. A. Mattar and A. Alazba, "Gep and mlr approaches for the prediction of reference evapotranspiration," *Neural Computing and Applications*, vol. 31, no. 10, pp. 5843–5855, 2019.

[29] M. Valipour, M. A. Gholami Sefidkouhi, M. Raeini-Sarjaz, and S. M. Guzman, "A hybrid data-driven machine learning technique for evapotranspiration modeling in various climates," *Atmosphere*, vol. 10, no. 6, p. 311, 2019.

[30] M. H. Kazemi, J. Shiri, P. Marti, and A. Majnooni-Heris, "Assessing temporal data partitioning scenarios for estimating reference evapotranspiration with machine learning techniques in arid regions," *Journal of Hydrology*, vol. 590, p. 125252, 2020.

[31] M. Khoshravesh, M. A. G. Sefidkouhi, and M. Valipour, "Estimation of reference evapotranspiration using multivariate fractional polynomial, bayesian regression, and robust regression models in three arid environments," *Applied Water Science*, vol. 7, no. 4, pp. 1911–1922, 2017.

[32] M. M. Reis, A. J. da Silva, J. Z. Junior, L. D. T. Santos, A. M. Azevedo, and É. M. G. Lopes, "Empirical and learning machine approaches to estimating reference evapotranspiration based on temperature data," *Computers and electronics in agriculture*, vol. 165, p. 104937, 2019.

[33] O. Kisi, "Modeling reference evapotranspiration using three different heuristic regression approaches," *Agricultural Water Management*, vol. 169, pp. 162–172, 2016.

[34] Y. Feng, N. Cui, D. Gong, Q. Zhang, and L. Zhao, "Evaluation of random forests and generalized regression neural networks for daily reference evapotranspiration modelling," *Agricultural Water Management*, vol. 193, pp. 163–173, 2017.

[35] A. Rashid Niaghi, O. Hassanijalilian, and J. Shiri, "Estimation of reference evapotranspiration using spatial and temporal machine learning approaches," *Hydrology*, vol. 8, no. 1, p. 25, 2021.

[36] A. S. Ponraj and T. Vigneswaran, "Daily evapotranspiration prediction using gradient boost regression model for irrigation planning," *The Journal of Supercomputing*, vol. 76, no. 8, pp. 5732–5744, 2020.

[37] J. Fan, W. Yue, L. Wu, F. Zhang, H. Cai, X. Wang, X. Lu, and Y. Xiang, "Evaluation of SVM, ELM and four tree-based ensemble models for predicting daily reference evapotranspiration using limited meteorological data in different climates of China," *Agricultural and forest meteorology*, vol. 263, pp. 225–241, 2018.

[38] J. Fan, X. Ma, L. Wu, F. Zhang, X. Yu, and W. Zeng, "Light gradient boosting machine: An efficient soft computing model for estimating daily reference evapotranspiration with local and external meteorological data," *Agricultural Water Management*, vol. 225, p. 105758, 2019.

[39] G. Huang, L. Wu, X. Ma, W. Zhang, J. Fan, X. Yu, W. Zeng, and H. Zhou, "Evaluation of CatBoost method for prediction of reference evapotranspiration in humid regions," *Journal of Hydrology*, vol. 574, pp. 1029–1041, 2019.

[40] F. Granata, "Evapotranspiration evaluation models based on machine learning algorithms—a comparative study," *Agricultural Water Management*, vol. 217, pp. 303–315, 2019.

[41] O. Kisi, B. Keshtegar, M. Zounemat-Kermani, S. Heddam, and N.-T. Trung, "Modeling reference evapotranspiration using a novel regression-based method: radial basis M5 model tree," *Theoretical and Applied Climatology*, vol. 145, no. 1, pp. 639–659, 2021.

[42] S. Mehdizadeh, J. Behmanesh, and K. Khalili, "Using MARS, SVM, GEP and empirical equations for estimation of monthly mean reference evapotranspiration," *Computers and electronics in agriculture*, vol. 139, pp. 103–114, 2017.

[43] O. Mohammadrezapour, J. Piri, and O. Kisi, "Comparison of SVM, ANFIS and GEP in modeling monthly potential evapotranspiration in an arid region (Case study: Sistan and Baluchestan Province, Iran)," *Water Supply*, vol. 19, no. 2, pp. 392–403, 2019.

[44] M. Y. Chia, Y. F. Huang, and C. H. Koo, "Support vector machine enhanced empirical reference evapotranspiration estimation with limited meteorological parameters," *Computers and Electronics in Agriculture*, vol. 175, p. 105577, 2020.

[45] A. Seifi and H. Riahi, "Estimating daily reference evapotranspiration using hybrid gamma test-least square support vector machine, gamma test-ANN, and gamma test-ANFIS models in an arid area of Iran," *Journal of Water and Climate Change*, vol. 11, no. 1, pp. 217–240, 2020.

[46] N. Manikumari, A. Murugappan, and G. Vinodhini, "Time series forecasting of daily reference evapotranspiration by neural network ensemble learning for irrigation system," in *IOP Conference Series: Earth and Environmental Science*, vol. 80, no. 1. IOP Publishing, 2017, p. 012069.

[47] R. Salam and A. R. M. T. Islam, "Potential of RT, Bagging and RS ensemble learning algorithms for reference evapotranspiration prediction using climatic data-limited humid region in Bangladesh," *Journal of Hydrology*, vol. 590, p. 125241, 2020.

[48] V. Nourani, G. Elkiran, and J. Abdullahi, "Multi-step ahead modeling of reference evapotranspiration using a multi-model approach," *Journal of Hydrology*, vol. 581, p. 124434, 2020.

[49] J. Martín, J. A. Sáez, and E. Corchado, "On the suitability of stacking-based ensembles in smart agriculture for evapotranspiration prediction," *Applied Soft Computing*, vol. 108, p. 107509, 2021.

[50] A. Laaboudi, B. Mouhouche, and B. Draoui, "Neural network approach to reference evapotranspiration modeling from limited climatic data in arid regions," *International journal of biometeorology*, vol. 56, no. 5, pp. 831–841, 2012.

[51] S. Kim, V. P. Singh, Y. Seo, and H. S. Kim, "Modeling nonlinear monthly evapotranspiration using soft computing and data reconstruction techniques," *Water resources management*, vol. 28, no. 1, pp. 185–206, 2014.

[52] O. Kisi and Y. Kilic, "An investigation on generalization ability of artificial neural networks and M5 model tree in modeling reference evapotranspiration," *Theoretical and applied climatology*, vol. 126, no. 3, pp. 413–425, 2016.

[53] S. Traore, Y. Luo, and G. Fipps, "Deployment of artificial neural network for short-term forecasting of evapotranspiration using public weather forecast restricted messages," *Agricultural Water Management*, vol. 163, pp. 363–379, 2016.

[54] M. K. Nema, D. Khare, and S. K. Chandniha, "Application of artificial intelligence to estimate the reference evapotranspiration in sub-humid doon valley," *Applied Water Science*, vol. 7, no. 7, pp. 3903–3910, 2017.

[55] V. Z. Antonopoulos and A. V. Antonopoulos, "Daily reference evapotranspiration estimates by artificial neural networks technique and empirical equations using limited input climate variables," *Computers and Electronics in Agriculture*, vol. 132, pp. 86–96, 2017.

[56] S. Gavili, H. Sanikhani, O. Kisi, and M. H. Mahmoudi, "Evaluation of several soft computing methods in monthly evapotranspiration modelling," *Meteorological Applications*, vol. 25, no. 1, pp. 128–138, 2018.

[57] Y. Z. Kaya, M. Zelenakova, F. Üneş, M. Demirci, H. Hlavata, and P. Mesaros, "Estimation of daily evapotranspiration in Košice City (Slovakia) using several soft computing techniques," *Theoretical and Applied Climatology*, vol. 144, no. 1, pp. 287–298, 2021.

[58] S. S. Abdullah, M. A. Malek, N. S. Abdullah, O. Kisi, and K. S. Yap, "Extreme learning machines: a new approach for prediction of reference evapotranspiration," *Journal of Hydrology*, vol. 527, pp. 184–195, 2015.

[59] Y. Feng, N. Cui, L. Zhao, X. Hu, and D. Gong, "Comparison of ELM, GANN, WNN and empirical models for estimating reference evapotranspiration in humid region of Southwest China," *Journal of Hydrology*, vol. 536, pp. 376–383, 2016.

[60] M. Gocic, D. Petković, S. Shamshirband, and A. Kamsin, "Comparative analysis of reference evapotranspiration equations modelling by extreme learning machine," *Computers and Electronics in Agriculture*, vol. 127, pp. 56–63, 2016.

[61] A. P. Patil and P. C. Deka, "An extreme learning machine approach for modeling evapotranspiration using extrinsic inputs," *Computers and electronics in agriculture*, vol. 121, pp. 385–392, 2016.

[62] D. Kumar, J. Adamowski, R. Suresh, and B. Ozga-Zielinski, "Estimating evapotranspiration using an extreme learning machine model: case study in north Bihar, India," *Journal of Irrigation and Drainage Engineering*, vol. 142, no. 9, p. 04016032, 2016.

[63] Y. Feng, Y. Peng, N. Cui, D. Gong, and K. Zhang, "Modeling reference evapotranspiration using extreme learning machine and generalized regression neural network only with temperature data," *Computers and Electronics in Agriculture*, vol. 136, pp. 71–78, 2017.

[64] P. Banda, B. Cemek, and E. Küçüktopcu, "Estimation of daily reference evapotranspiration by neuro computing techniques using limited data in a semi-arid environment," *Archives of Agronomy and Soil Science*, vol. 64, no. 7, pp. 916–929, 2018.

[65] H. Sanikhani, O. Kisi, E. Maroufpoor, and Z. M. Yaseen, "Temperature-based modeling of reference evapotranspiration using several artificial intelligence models: application of different modeling scenarios," *Theoretical and applied climatology*, vol. 135, no. 1, pp. 449–462, 2019.

[66] J. A. Bellido-Jiménez, J. Estévez, and A. P. García-Marín, "New machine learning approaches to improve reference evapotranspiration estimates using intra-daily temperature-based variables in a semi-arid region of Spain," *Agricultural Water Management*, vol. 245, p. 106558, 2021.

[67] S. Adamala, N. Raghuwanshi, A. Mishra, and R. Singh, "Generalized wavelet neural networks for evapotranspiration modeling in india," *ISH Journal of Hydraulic Engineering*, vol. 25, no. 2, pp. 119–131, 2019.

[68] M. K. Saggi and S. Jain, "Reference evapotranspiration estimation and modeling of the Punjab Northern India using deep learning," *Computers and Electronics in Agriculture*, vol. 156, pp. 387–398, 2019.

[69] Z. Chen, Z. Zhu, H. Jiang, and S. Sun, "Estimating daily reference evapotranspiration based on limited meteorological data using deep learning and classical machine learning methods," *Journal of Hydrology*, vol. 591, p. 125286, 2020.

[70] J. Yin, Z. Deng, A. V. Ines, J. Wu, and E. Rasu, "Forecast of short-term daily reference evapotranspiration under limited meteorological variables using a hybrid bi-directional long short-term memory model (Bi-LSTM)," *Agricultural Water Management*, vol. 242, p. 106386, 2020.

[71] L. B. Ferreira and F. F. da Cunha, "Multi-step ahead forecasting of daily reference evapotranspiration using deep learning," *Computers and Electronics in Agriculture*, vol. 178, p. 105728, 2020.

[72] P. d. O. e Lucas, M. A. Alves, P. C. d. L. e Silva, and F. G. Guimarães, "Reference evapotranspiration time series forecasting with ensemble of convolutional neural networks," *Computers and Electronics in Agriculture*, vol. 177, p. 105700, 2020.

[73] M. Nagappan, V. Gopalakrishnan, and M. Alagappan, "Prediction of reference evapotranspiration for irrigation scheduling using machine learning," *Hydrological Sciences Journal*, vol. 65, no. 16, pp. 2669–2677, 2020.

[74] F. Granata and F. Di Nunno, "Forecasting evapotranspiration in different climates using ensembles of recurrent neural networks," *Agricultural Water Management*, vol. 255, p. 107040, 2021.

[75] D. K. Roy, "Long short-term memory networks to predict one-step ahead reference evapotranspiration in a subtropical climatic zone," *Environmental Processes*, vol. 8, no. 2, pp. 911–941, 2021.

[76] L. B. Ferreira and F. F. da Cunha, "New approach to estimate daily reference evapotranspiration based on hourly temperature and relative humidity using machine learning and deep learning," *Agricultural Water Management*, vol. 234, p. 106113, 2020.

[77] M. Gocić, S. Motamedi, S. Shamshirband, D. Petković, S. Ch, R. Hashim, and M. Arif, "Soft computing approaches for forecasting reference evapotranspiration," *Computers and Electronics in Agriculture*, vol. 113, pp. 164–173, 2015.

[78] A. P. Patil and P. C. Deka, "Performance evaluation of hybrid Wavelet-ANN and Wavelet-ANFIS models for estimating evapotranspiration in arid regions of India," *Neural Computing and Applications*, vol. 28, no. 2, pp. 275–285, 2017.

[79] O. Kisi and M. Alizamir, "Modelling reference evapotranspiration using a new wavelet conjunction heuristic method: wavelet extreme learning machine vs wavelet neural networks," *Agricultural and Forest Meteorology*, vol. 263, pp. 41–48, 2018.

[80] Y. Tikhamarine, A. Malik, A. Kumar, D. Souag-Gamane, and O. Kisi, "Estimation of monthly reference evapotranspiration using novel hybrid machine learning approaches," *Hydrological sciences journal*, vol. 64, no. 15, pp. 1824–1842, 2019.

[81] S. Maroufpoor, O. Bozorg-Haddad, and E. Maroufpoor, "Reference evapotranspiration estimating based on optimal input combination and hybrid artificial intelligent model: Hybridization of artificial neural network with grey wolf optimizer algorithm," *Journal of Hydrology*, vol. 588, p. 125060, 2020.

[82] J. Dong, X. Liu, G. Huang, J. Fan, L. Wu, and J. Wu, "Comparison of four bio-inspired algorithms to optimize KNEA for predicting monthly reference evapotranspiration in different climate zones of China," *Computers and Electronics in Agriculture*, vol. 186, p. 106211, 2021.

[83] H. Tao, L. Diop, A. Bodian, K. Djaman, P. M. Ndiaye, and Z. M. Yaseen, "Reference evapotranspiration prediction using hybridized fuzzy model with firefly algorithm: Regional case study in Burkina Faso," *Agricultural water management*, vol. 208, pp. 140–151, 2018.

[84] D. K. Roy, R. Barzegar, J. Quilty, and J. Adamowski, "Using ensembles of adaptive neuro-fuzzy inference system and optimization algorithms to predict reference evapotranspiration in subtropical climatic zones," *Journal of Hydrology*, vol. 591, p. 125509, 2020.

[85] L. Wu, H. Zhou, X. Ma, J. Fan, and F. Zhang, "Daily reference evapotranspiration prediction based on hybridized extreme learning machine model with bio-inspired optimization algorithms: Application in contrasting climates of China," *Journal of Hydrology*, vol. 577, p. 123960, 2019.

[86] B. Mohammadi and S. Mehdizadeh, "Modeling daily reference evapotranspiration via a novel approach based on support vector regression coupled with whale optimization algorithm," *Agricultural Water Management*, vol. 237, p. 106145, 2020.

[87] S. Yan, L. Wu, J. Fan, F. Zhang, Y. Zou, and Y. Wu, "A novel hybrid WOA-XGB model for estimating daily reference evapotranspiration using local and external meteorological data: Applications in arid and humid regions of China," *Agricultural Water Management*, vol. 244, p. 106594, 2021.

[88] L. Gao, D. Gong, N. Cui, M. Lv, and Y. Feng, "Evaluation of bio-inspired optimization algorithms hybrid with artificial neural network for reference crop evapotranspiration estimation," *Computers and Electronics in Agriculture*, vol. 190, p. 106466, 2021.

[89] L. Wu, Y. Peng, J. Fan, Y. Wang, and G. Huang, "A novel kernel extreme learning machine model coupled with K-means clustering and firefly algorithm for estimating monthly reference evapotranspiration in parallel computation," *Agricultural Water Management*, vol. 245, p. 106624, 2021.

[90] B. Zhu, Y. Feng, D. Gong, S. Jiang, L. Zhao, and N. Cui, "Hybrid particle swarm optimization with extreme learning machine for daily reference evapotranspiration prediction from limited climatic data," *Computers and Electronics in Agriculture*, vol. 173, p. 105430, 2020.

[91] D. Gong, W. Hao, L. Gao, Y. Feng, and N. Cui, "Extreme learning machine for reference crop evapotranspiration estimation: Model optimization and spatiotemporal assessment across different climates in China," *Computers and Electronics in Agriculture*, vol. 187, p. 106294, 2021.

[92] A. K. Verma, M. K. Jha, and R. K. Mahana, "Evaluation of HEC-HMS and WEPP for simulating watershed runoff using remote sensing and geographical information system," *Paddy and Water Environment*, vol. 8, no. 2, pp. 131–144, 2010.

[93] Z. Chen, R. Shi, and S. Zhang, "An artificial neural network approach to estimate evapotranspiration from remote sensing and ameriflux data," *Frontiers of earth Science*, vol. 7, no. 1, pp. 103–111, 2013.

[94] V. Douna, V. Barraza, F. Grings, A. Huete, N. Restrepo-Coupe, and J. Beringer, "Towards a remote sensing data based evapotranspiration estimation in Northern Australia using a simple random forest approach," *Journal of Arid Environments*, vol. 191, p. 104513, 2021.

[95] C. Carter and S. Liang, "Evaluation of ten machine learning methods for estimating terrestrial evapotranspiration from remote sensing," *International Journal of Applied Earth Observation and Geoinformation*, vol. 78, pp. 86–92, 2019.

[96] Y. Liu, S. Zhang, J. Zhang, L. Tang, and Y. Bai, "Assessment and comparison of six machine learning models in estimating evapotranspiration over croplands using remote sensing and meteorological factors," *Remote Sensing*, vol. 13, no. 19, p. 3838, 2021.

[97] R. Bachour, W. R. Walker, A. M. Ticlavilca, M. McKee, and I. Maslova, "Estimation of spatially distributed evapotranspiration using remote sensing and a relevance vector machine," *Journal of Irrigation and Drainage Engineering*, vol. 140, no. 8, p. 04014029, 2014.

[98] A. Rahimikhoob, "Comparison of M5 model tree and artificial neural network's methodologies in modelling daily reference evapotranspiration from NOAA satellite images," *Water Resources Management*, vol. 30, no. 9, pp. 3063–3075, 2016.

[99] Z. Zhang, Y. Gong, and Z. Wang, "Accessible remote sensing data based reference evapotranspiration estimation modelling," *Agricultural Water Management*, vol. 210, pp. 59–69, 2018.

[100] N. Kim, K. Kim, S. Lee, J. Cho, and Y. Lee, "Retrieval of daily reference evapotranspiration for croplands in South Korea using machine learning with satellite images and numerical weather prediction data," *Remote Sensing*, vol. 12, no. 21, p. 3642, 2020.

[101] J. Mosre and F. Suárez, "Actual evapotranspiration estimates in arid cold regions using machine learning algorithms with in situ and remote sensing data," *Water*, vol. 13, no. 6, p. 870, 2021.

[102] P. S. Käfer, N. S. da Rocha, L. R. Diaz, E. A. Kaiser, D. C. Santos, G. P. Veeck, D. R. Robérti, S. B. Rolim, and G. G. de Oliveira, "Artificial neural networks model based on remote sensing to retrieve evapotranspiration over the Brazilian Pampa," *Journal of Applied Remote Sensing*, vol. 14, no. 3, p. 038504, 2020.

[103] L. Neissi, M. Golabi, M. Albaji, and A. A. Naseri, "Evaluating evapotranspiration using data mining instead of physical-based model in remote sensing," *Theoretical and Applied Climatology*, vol. 147, no. 1, pp. 701–716, 2022.

[104] A. Barzkar, S. Shahabi, S. Niazmradi, and M. R. Madadi, "A comparative study of remote sensing and gene expression programming for estimation of evapotranspiration in four distinctive climates," *Stochastic Environmental Research and Risk Assessment*, vol. 35, no. 7, pp. 1437–1452, 2021.

[105] S. H. B. Dias, R. Filgueiras, E. I. Fernandes Filho, G. S. Arcanjo, G. H. d. Silva, E. C. Mantovani, and F. F. d. Cunha, "Reference evapotranspiration of Brazil modeled with machine learning techniques and remote sensing," *Plos one*, vol. 16, no. 2, p. e0245834, 2021.

[106] Y. Liu, S. Zhang, J. Zhang, L. Tang, and Y. Bai, "Using artificial neural network algorithm and remote sensing vegetation index improves the accuracy of the penman-monteith equation to estimate cropland evapotranspiration," *Applied Sciences*, vol. 11, no. 18, p. 8649, 2021.

[107] H. Z. Abyaneh, A. M. Nia, M. B. Varkeshi, S. Marofi, and O. Kisi, "Performance evaluation of ANN and ANFIS models for estimating garlic crop evapotranspiration," *Journal of irrigation and drainage engineering*, vol. 137, no. 5, pp. 280–286, 2011.

[108] M.-B. Aghajanloo, A.-A. Sabziparvar, and P. Hosseinzadeh Talaee, "Artificial neural network–genetic algorithm for estimation of crop evapotranspiration in a semi-arid region of Iran," *Neural Computing and Applications*, vol. 23, no. 5, pp. 1387–1393, 2013.

[109] H. Tabari, C. Martinez, A. Ezani, and P. Hosseinzadeh Talaee, "Applicability of support vector machines and adaptive neurofuzzy inference system for modeling potato crop evapotranspiration," *Irrigation science*, vol. 31, no. 4, pp. 575–588, 2013.

[110] N. Shrestha and S. Shukla, "Support vector machine based modeling of evapotranspiration using hydro-climatic variables in a sub-tropical environment," *Agricultural and Forest Meteorology*, vol. 200, pp. 172–184, 2015.

[111] Y. Feng, D. Gong, X. Mei, and N. Cui, "Estimation of maize evapotranspiration using extreme learning machine and generalized regression neural network on the China Loess Plateau," *Hydrology Research*, vol. 48, no. 4, pp. 1156–1168, 2017.

[112] D. Tang, Y. Feng, D. Gong, W. Hao, and N. Cui, "Evaluation of artificial intelligence models for actual crop evapotranspiration modeling in mulched and non-mulched maize croplands," *Computers and electronics in agriculture*, vol. 152, pp. 375–384, 2018.

[113] N. Abrishami, A. R. Sepaskhah, and M. H. Shahrokhnia, "Estimating wheat and maize daily evapotranspiration using artificial neural network," *Theoretical and Applied Climatology*, vol. 135, no. 3, pp. 945–958, 2019.

[114] M. K. Saggi and S. Jain, "Application of fuzzy-genetic and regularization random forest (FG-RRF): estimation of crop evapotranspiration (ETc) for maize and wheat crops," *Agricultural Water Management*, vol. 229, p. 105907, 2020.

[115] S. S. Yamaç and M. Todorovic, "Estimation of daily potato crop evapotranspiration using three different machine learning algorithms and four scenarios of available meteorological data," *Agricultural Water Management*, vol. 228, p. 105875, 2020.

[116] Z. Chen, S. Sun, Y. Wang, Q. Wang, and X. Zhang, "Temporal convolution-network-based models for modeling maize evapotranspiration under mulched drip irrigation," *Computers and electronics in agriculture*, vol. 169, p. 105206, 2020.

[117] M. Hashemi and A. R. Sepaskhah, "Evaluation of artificial neural network and penman–monteith equation for the prediction of barley standard evapotranspiration in a semi-arid region," *Theoretical and Applied Climatology*, vol. 139, no. 1, pp. 275–285, 2020.

[118] J. Fan, J. Zheng, L. Wu, and F. Zhang, "Estimation of daily maize transpiration using support vector machines, extreme gradient boosting, artificial and deep neural networks models," *Agricultural Water Management*, vol. 245, p. 106547, 2021.

[119] S. S. Yamaç, "Artificial intelligence methods reliably predict crop evapotranspiration with different combinations of meteorological data for sugar beet in a semiarid area," *Agricultural Water Management*, vol. 254, p. 106968, 2021.

[120] N. Ohana-Levi, A. Ben-Gal, S. Munitz, and Y. Netzer, "Grapevine crop evapotranspiration and crop coefficient forecasting using linear and non-linear multiple regression models," *Agricultural Water Management*, vol. 262, p. 107317, 2022.

[121] X. Shan, N. Cui, H. Cai, X. Hu, and L. Zhao, "Estimation of summer maize evapotranspiration using MARS model in the semi-arid region of northwest China," *Computers and Electronics in Agriculture*, vol. 174, p. 105495, 2020.

[122] A. Elbeltagi, J. Deng, K. Wang, A. Malik, and S. Maroufpoor, "Modeling long-term dynamics of crop evapotranspiration using deep learning in a semi-arid environment," *Agricultural Water Management*, vol. 241, p. 106334, 2020.

[123] R. Mann *et al.*, "Cropping pattern in Punjab (1966-67 to 2014-15)," *Economic and Political Weekly*, vol. 52, no. 3, pp. 30–33, 2017.

[124] ICAR, *State-Specific Technological Interventions for Higher Agricultural Growth*. Indian Council of Agricultural Research New Delhi, 2007.

[125] Indian Council of Agricultural Research: *Punjab*. Accessed: July 31, 2022. [Online]. Available: https://icar.org.in/files/state-specific/chapter/99.htm

[126] G. W. Y. BOOK and N. Delhi, "Central Ground Water Board," *Ground Water*, vol. 2019, p. 20, 2020.

[127] S. H. Prabhjyot-Kaur, V. Rao, S. Hundal, S. Sandhu, S. Nayyar, B. Rao, and A. Kaur, "Agrometeorology of wheat in Punjab state of India," 2015.

[128] Apni Kheti. [Online]. Available: https://www.apnikheti.com/en/pn/agriculture/crops/cereals/rice

[129] S. Sandhu, P. Kaur, and K. Gill, "Weather based agro indices and grain yield of rice cultivars transplanted on different dates in Punjab," *International Journal of Agriculture Food Science & Technology*, vol. 10, no. 4, pp. 1019–1026, 2013.

[130] J. Kaur, K. Gill, S. Kaur, and R. Aggarwal, "Estimation of crop coefficient for rice and wheat crops at Ludhiana," *Journal of Agrometeorology*, vol. 19, no. 2, pp. 170–171, 2017.

[131] M. E. Jensen, "Water consumption by agricultural plants (chapter 1)," 1968.

[132] N. J. Rosenberg, B. L. Blad, and S. B. Verma, *Microclimate: the biological environment*. John Wiley & Sons, 1983.

[133] R. G. Allen, L. S. Pereira, D. Raes, M. Smith *et al.*, "Crop evapotranspiration-Guidelines for computing crop water requirements-FAO Irrigation and drainage paper 56," *Fao, Rome*, vol. 300, no. 9, p. D05109, 1998.

[134] J. Doorenbos, "Guidelines for predicting crop water requirements," *Food and Agriculture organization. Rome, Irrig. Drainage pap.*, vol. 24, pp. 169–178, 1975.

[135] J. Doorenbos and W. Pruitt, "Crop water requirements. FAO irrigation and drainage paper 24," *Land and Water Development Division, FAO, Rome*, vol. 144, no. 1, 1977.

[136] M. Jensen, R. Burman, and R. Allen, "Evapotranspiration and irrigation water requirements: ASCE manual no. 70," *New York, NY*, 1990.

[137] M. Smith, A. Segeren, L. Santos Pereira, A. Perrier, and R. Allen, "Report on the expert consultation on procedures for revision of FAO guidelines for prediction of crop water requirements. Rome, Italy, 28-31 May 1990," 1991.

[138] C. W. Thornthwaite, "An approach toward a rational classification of climate," *Geographical review*, vol. 38, no. 1, pp. 55–94, 1948.

[139] S. C. S. US Department of Agriculture, "Irrigation water requirements, technical release no. 21," 1970.

[140] J. Doorenbos and W. Pruitt, "Crop water requirements. FAO irrigation and drainage paper 24," *Land and Water Development Division, FAO, Rome*, vol. 144, no. 1, 1977.

[141] G. H. Hargreaves and Z. A. Samani, "Reference crop evapotranspiration from temperature," *Applied engineering in agriculture*, vol. 1, no. 2, pp. 96–99, 1985.

[142] L. Turc, "Evaluation des besoins en eau d'irrigation, évapotranspiration potentielle," *Annales Agronomiques*, vol. 12, pp. 13–49, 1961.

[143] M. E. Jensen and H. R. Haise, "Estimating evapotranspiration from solar radiation," *Journal of the Irrigation and Drainage Division*, vol. 89, no. 4, pp. 15–41, 1963.

[144] M. E. Jensen, D. C. Robb, and C. E. Franzoy, "Scheduling irrigations using climate-crop-soil data," *Journal of the Irrigation and Drainage Division*, vol. 96, no. 1, pp. 25–38, 1970.

[145] C. H. B. Priestley and R. J. Taylor, "On the assessment of surface heat flux and evaporation using large-scale parameters," *Monthly weather review*, vol. 100, no. 2, pp. 81–92, 1972.

[146] J. Doorenbos, "Guidelines for predicting crop water requirements," *FAO irrigation and drainage paper*, vol. 24, pp. 1–179, 1977.

[147] G. F. Makkink, "Testing the penman formula by means of lysimeters," *Journal of the Institution of Water Engineerrs*, vol. 11, pp. 277–288, 1957.

[148] J. Jones and J. Ritchie, "Crop growth models," *Management of farm irrigation systems. ASAE Monograph*, no. 9, pp. 80–86, 1990.

[149] J. E. Christiansen, "Pan evaporation and evapotranspiration from climatic data," *Journal of the Irrigation and Drainage Division*, vol. 94, no. 2, pp. 243–266, 1968.

[150] J. Christiansen and G. Hargreaves, "Irrigation requirements from evaporation," *Transaction of the Internatinal Commission on Irrigation and Drainage*, vol. 23, pp. 569–596, 1969.

[151] H. L. Penman, "Natural evaporation from open water, bare soil and grass," *Proceedings of the Royal Society of London. Series A. Mathematical and Physical Sciences*, vol. 193, no. 1032, pp. 120–145, 1948.

[152] P. HL, "Vegetation and hydrology (technical communication 53, Commonwealth Bureau of Soils)," *Harpenden, England*, vol. 124, 1963.

[153] J. Businger, "Some remarks on Penman's equations for the evapotranspiration." *Netherlands Journal of Agricultural Science*, vol. 4, no. 1, pp. 77–80, 1956.

[154] C. Van Bavel, "Potential evaporation: the combination concept and its experimental verification," *Water Resources Research*, vol. 2, no. 3, pp. 455–467, 1966.

[155] J. L. Monteith, "Evaporation and environment," in *Symposia of the society for experimental biology*, vol. 19. Cambridge University Press (CUP) Cambridge, 1965, pp. 205–234.

[156] J. L. Wright and M. E. Jensen, "Peak water requirements of crops in southern Idaho," *Journal of the Irrigation and Drainage Division*, vol. 98, no. 2, pp. 193–201, 1972.

[157] J. Doorenbos, "Guidelines for predicting crop water requirements," *Food and Agriculture organization. Rome, Irrigation Drainage paper*, vol. 24, pp. 169–178, 1975.

[158] M. Frere and G. Popov, *Agrometeorological crop monitoring and forecasting.* FAO, 1979.

[159] J. L. Wright, "New evapotranspiration crop coefficients," *Journal of the Irrigation and Drainage Division*, vol. 108, no. 1, pp. 57–74, 1982.

[160] R. Snyder and W. Pruitt, "Eto: User's guide and program documentation," *University of California, Davis, USA*, 1992.

[161] R. G. Allen, L. S. Pereira, D. Raes, M. Smith *et al.*, "Crop evapotranspiration-guidelines for computing crop water requirements-FAO irrigation and drainage paper 56," *FAO, Rome*, vol. 300, no. 9, p. D05109, 1998.

[162] I. A. Walter, R. G. Allen, R. Elliott, M. Jensen, D. Itenfisu, B. Mecham, T. Howell, R. Snyder, P. Brown, S. Echings *et al.*, "ASCE's standardized reference evapotranspiration equation," in *Watershed management and operations management*, 2000, pp. 1–11.

[163] R. G. Allen, A. J. Clemmens, C. M. Burt, K. Solomon, and T. O'Halloran, "Prediction accuracy for projectwide evapotranspiration using crop coefficients and reference evapotranspiration," *Journal of irrigation and drainage engineering*, vol. 131, no. 1, p. 24, 2005.

[164] J. Xu, S. Peng, J. Ding, Q. Wei, and Y. Yu, "Evaluation and calibration of simple methods for daily reference evapotranspiration estimation in humid East China," *Archives of Agronomy and Soil Science*, vol. 59, no. 6, pp. 845–858, 2013.

[165] V. Gonzalez-Dugo, P. J. Zarco-Tejada, and E. Fereres, "Applicability and limitations of using the crop water stress index as an indicator of water deficits in citrus orchards," *Agricultural and forest meteorology*, vol. 198, pp. 94–104, 2014.

[166] R. D. Jackson, S. Idso, R. Reginato, and P. Pinter Jr, "Canopy temperature as a crop water stress indicator," *Water resources research*, vol. 17, no. 4, pp. 1133–1138, 1981.

[167] S. Idso, R. Jackson, P. Pinter Jr, R. Reginato, and J. Hatfield, "Normalizing the stress-degree-day parameter for environmental variability," *Agricultural meteorology*, vol. 24, pp. 45–55, 1981.

[168] S. O. Ihuoma and C. A. Madramootoo, "Recent advances in crop water stress detection," *Computers and Electronics in Agriculture*, vol. 141, pp. 267–275, 2017.

[169] B. A. King and K. C. Shellie, "Wine grape cultivar influence on the performance of models that predict the lower threshold canopy temperature of a water stress index," *Computers and Electronics in Agriculture*, vol. 145, pp. 122–129, 2018.

[170] A. Pou, M. P. Diago, H. Medrano, J. Baluja, and J. Tardaguila, "Validation of thermal indices for water status identification in grapevine," *Agricultural water management*, vol. 134, pp. 60–72, 2014.

[171] M. Möller, V. Alchanatis, Y. Cohen, M. Meron, J. Tsipris, A. Naor, V. Ostrovsky, M. Sprintsin, and S. Cohen, "Use of thermal and visible imagery for estimating crop water status of irrigated grapevine," *Journal of experimental botany*, vol. 58, no. 4, pp. 827–838, 2007.

[172] H. G. Jones, "Use of infrared thermometry for estimation of stomatal conductance as a possible aid to irrigation scheduling," *Agricultural and forest meteorology*, vol. 95, no. 3, pp. 139–149, 1999.

[173] R. G. Allen, L. S. Pereira, T. A. Howell, and M. E. Jensen, "Evapotranspiration information reporting: I. factors governing measurement accuracy," *Agricultural Water Management*, vol. 98, no. 6, pp. 899–920, 2011.

[174] J. Šimůnek, M. T. Van Genuchten, and M. Šejna, "Recent developments and applications of the hydrus computer software packages," *Vadose Zone Journal*, vol. 15, no. 7, 2016.

[175] S. Neitsch, J. Arnold, J. Kiniry, and J. Williams, "Soil and water assessment tool (SWAT), theoretical documentation. Blackland Research Center, Grassland," *Soil and Water Research Laboratory, Agricultural Research Service, Temple, TX*, 2005.

[176] A. Armstrong, J. Legros, and M. Voltz, "ACCESS-II: a detailed model for crop growth and water conditions," *International agrophysics*, vol. 10, no. 3, pp. 171––184.

[177] J. Fernández, C. Slawinski, F. Moreno, R. Walczak, and M. Vanclooster, "Simulating the fate of water in a soil–crop system of a semi-arid Mediterranean area with the WAVE 2.1 and the EURO-ACCESS-II models," *Agricultural Water Management*, vol. 56, no. 2, pp. 113–129, 2002.

[178] K. C. Perera, A. W. Western, B. Nawarathna, and B. George, "Forecasting daily reference evapotranspiration for Australia using numerical weather prediction outputs," *Agricultural and forest meteorology*, vol. 194, pp. 50–63, 2014.

[179] R. Ding, S. Kang, F. Li, Y. Zhang, L. Tong, and Q. Sun, "Evaluating eddy covariance method by large-scale weighing lysimeter in a maize field of northwest China," *Agricultural Water Management*, vol. 98, no. 1, pp. 87–95, 2010.

[180] R. G. Allen, I. A. Walter, R. Elliott, T. A. Howell, D. Itenfisu, and M. E. Jensen, "The ASCE standardized reference evapotranspiration equation," 2005.

[181] H. Tabari, M. E. Grismer, and S. Trajkovic, "Comparative analysis of 31 reference evapotranspiration methods under humid conditions," *Irrigation Science*, vol. 31, no. 2, pp. 107–117, 2013.

[182] L. Ruan, Y. Bai, S. Li, S. He, and L. Xiao, "Workload time series prediction in storage systems: a deep learning based approach," *Cluster Computing*, pp. 1–11, 2021.

[183] H. Afzaal, A. A. Farooque, F. Abbas, B. Acharya, and T. Esau, "Computation of evapotranspiration with artificial intelligence for precision water resource management," *Applied Sciences*, vol. 10, no. 5, p. 1621, 2020.

[184] T. N. Sainath, O. Vinyals, A. Senior, and H. Sak, "Convolutional, long short-term memory, fully connected deep neural networks," in *2015 IEEE international conference on acoustics, speech and signal processing (ICASSP)*. IEEE, 2015, pp. 4580–4584.

[185] X. Shi, Z. Chen, H. Wang, D.-Y. Yeung, W.-K. Wong, and W.-c. Woo, "Convolutional LSTM network: A machine learning approach for precipitation nowcasting," *Advances in neural information processing systems*, vol. 28, 2015.

[186] R. Pascanu, C. Gulcehre, K. Cho, and Y. Bengio, "How to construct deep recurrent neural networks," *arXiv preprint arXiv:1312.6026*, 2013.

[187] A. Koca, H. F. Oztop, Y. Varol, and G. O. Koca, "Estimation of solar radiation using artificial neural networks with different input parameters for Mediterranean region of Anatolia in Turkey," *Expert Systems with Applications*, vol. 38, no. 7, pp. 8756–8762, 2011.

[188] K. Sanjar, O. Bekhzod, J. Kim, A. Paul, and J. Kim, "Missing data imputation for geolocation-based price prediction using KNN–mcf method," *ISPRS International Journal of Geo-Information*, vol. 9, no. 4, p. 227, 2020.

[189] A. W.-C. Liew, N.-F. Law, and H. Yan, "Missing value imputation for gene expression data: computational techniques to recover missing data from available information," *Briefings in bioinformatics*, vol. 12, no. 5, pp. 498–513, 2011.

[190] B. Holt and R. A. Benfer Jr, "Estimating missing data: an iterative regression approach," *Journal of Human Evolution*, vol. 39, no. 3, pp. 289–296, 2000.

[191] G. Tutz and S. Ramzan, "Improved methods for the imputation of missing data by nearest neighbor methods," *Computational Statistics & Data Analysis*, vol. 90, pp. 84–99, 2015.

[192] L. Beretta and A. Santaniello, "Nearest neighbor imputation algorithms: a critical evaluation," *BMC medical informatics and decision making*, vol. 16, no. 3, pp. 197–208, 2016.

[193] L. Al Shalabi and Z. Shaaban, "Normalization as a preprocessing engine for data mining and the approach of preference matrix," in *2006 International conference on dependability of computer systems*. IEEE, 2006, pp. 207–214.

[194] J. Bergstra and Y. Bengio, "Random search for hyper-parameter optimization." *Journal of machine learning research*, vol. 13, no. 2, 2012.

[195] C. J. Willmott and K. Matsuura, "Advantages of the mean absolute error (MAE) over the root mean square error (RMSE) in assessing average model performance," *Climate research*, vol. 30, no. 1, pp. 79–82, 2005.

[196] C. J. Willmott, "On the validation of models," *Physical geography*, vol. 2, no. 2, pp. 184–194, 1981.

[197] R. H. McCuen, Z. Knight, and A. G. Cutter, "Evaluation of the nash–sutcliffe efficiency index," *Journal of hydrologic engineering*, vol. 11, no. 6, pp. 597–602, 2006.

[198] Y. Osroosh, R. T. Peters, C. S. Campbell, and Q. Zhang, "Automatic irrigation scheduling of apple trees using theoretical crop water stress index with an innovative dynamic threshold," *Computers and Electronics in Agriculture*, vol. 118, pp. 193–203, 2015.

[199] Y. Tikhamarine, A. Malik, D. Souag-Gamane, and O. Kisi, "Artificial intelligence models versus empirical equations for modeling monthly reference evapotranspiration," *Environmental Science and Pollution Research*, vol. 27, no. 24, pp. 30 001–30 019, 2020.

[200] J. Shiri, "Modeling reference evapotranspiration in island environments: assessing the practical implications," *Journal of Hydrology*, vol. 570, pp. 265–280, 2019.

[201] O. Kisi and K. S. Parmar, "Application of least square support vector machine and multivariate adaptive regression spline models in long term prediction of river water pollution," *Journal of Hydrology*, vol. 534, pp. 104–112, 2016.

[202] R. C. Deo, P. Samui, and D. Kim, "Estimation of monthly evaporative loss using relevance vector machine, extreme learning machine and multivariate adaptive regression spline models," *Stochastic Environmental Research and Risk Assessment*, vol. 30, no. 6, pp. 1769–1784, 2016.

[203] K. Khosravi, P. Daggupati, M. T. Alami, S. M. Awadh, M. I. Ghareb, M. Panahi, B. T. Pham, F. Rezaie, C. Qi, and Z. M. Yaseen, "Meteorological data mining and hybrid data-intelligence models for reference evaporation simulation: A case study in iraq," *Computers and Electronics in Agriculture*, vol. 167, p. 105041, 2019.

[204] V. Nourani, G. Elkiran, and J. Abdullahi, "Multi-station artificial intelligence based ensemble modeling of reference evapotranspiration using pan evaporation measurements," *Journal of Hydrology*, vol. 577, p. 123958, 2019.

[205] B. A. Tama and K.-H. Rhee, "Tree-based classifier ensembles for early detection method of diabetes: an exploratory study," *Artificial Intelligence Review*, vol. 51, no. 3, pp. 355–370, 2019.

[206] Z. Qu, K. Zhang, W. Mao, J. Wang, C. Liu, and W. Zhang, "Research and application of ensemble forecasting based on a novel multi-objective optimization algorithm for wind-speed forecasting," *Energy Conversion and Management*, vol. 154, pp. 440–454, 2017.

[207] Z. Yang and J. Wang, "A combination forecasting approach applied in multistep wind speed forecasting based on a data processing strategy and an optimized artificial intelligence algorithm," *Applied Energy*, vol. 230, pp. 1108–1125, 2018.

[208] A. Masih, "Application of ensemble learning techniques to model the atmospheric concentration of SO2," *Global Journal of Environmental Science and Management*, vol. 5, no. 3, pp. 309–318, 2019.

[209] Y. Wang, A. Wang, Q. Ai, and H. Sun, "Ensemble based fuzzy weighted extreme learning machine for gene expression classification," *Applied Intelligence*, vol. 49, no. 3, pp. 1161–1171, 2019.

[210] C. Chen and H. Liu, "Dynamic ensemble wind speed prediction model based on hybrid deep reinforcement learning," *Advanced Engineering Informatics*, vol. 48, p. 101290, 2021.

[211] S. Cui, Y. Yin, D. Wang, Z. Li, and Y. Wang, "A stacking-based ensemble learning method for earthquake casualty prediction," *Applied Soft Computing*, vol. 101, p. 107038, 2021.

[212] C. Guo, M. Liu, and M. Lu, "A dynamic ensemble learning algorithm based on K-means for ICU mortality prediction," *Applied Soft Computing*, vol. 103, p. 107166, 2021.

[213] R. S. Sutton, A. G. Barto *et al.*, *Introduction to reinforcement learning*. MIT press Cambridge, 1998, vol. 135.

[214] Y. Shi, W. Li, L. Zhu, K. Guo, and E. Cambria, "Stock trading rule discovery with double deep Q-network," *Applied Soft Computing*, vol. 107, p. 107320, 2021.

[215] V. Mnih, K. Kavukcuoglu, D. Silver, A. A. Rusu, J. Veness, M. G. Bellemare, A. Graves, M. Riedmiller, A. K. Fidjeland, G. Ostrovski *et al.*, "Human-level control through deep reinforcement learning," *nature*, vol. 518, no. 7540, pp. 529–533, 2015.

[216] H. Van Hasselt, A. Guez, and D. Silver, "Deep reinforcement learning with double q-learning," in *Proceedings of the AAAI conference on artificial intelligence*, vol. 30, no. 1, 2016.

[217] L.-J. Lin, "Self-improving reactive agents based on reinforcement learning, planning and teaching," *Machine learning*, vol. 8, no. 3-4, pp. 293–321, 1992.

[218] Y. Deng and T. Lumley, "Multiple Imputation Through XGBoost," *arXiv preprint arXiv:2106.01574*, 2021.

[219] H. Naeem and A. A. Bin-Salem, "A CNN-LSTM network with multi-level feature extraction-based approach for automated detection of coronavirus from CT scan and X-ray images," *Applied Soft Computing*, vol. 113, p. 107918, 2021.

[220] S. Xingjian, Z. Chen, H. Wang, D.-Y. Yeung, W.-K. Wong, and W.-c. Woo, "Convolutional LSTM network: A machine learning approach for precipitation nowcasting," in *Advances in neural information processing systems*, 2015, pp. 802–810.

[221] L. Torlay, M. Perrone-Bertolotti, E. Thomas, and M. Baciu, "Machine learning–XGBoost analysis of language networks to classify patients with epilepsy," *Brain informatics*, vol. 4, no. 3, pp. 159–169, 2017.

[222] A. Ogunleye and Q.-G. Wang, "XGBoost model for chronic kidney disease diagnosis," *IEEE/ACM transactions on computational biology and bioinformatics*, vol. 17, no. 6, pp. 2131–2140, 2019.

[223] G. Rosenthal and J. A. Rosenthal, *Statistics and data interpretation for social work*. Springer publishing company, 2011.

[224] H. Chen, Q. Wan, and Y. Wang, "Refined diebold-mariano test methods for the evaluation of wind power forecasting models," *Energies*, vol. 7, no. 7, pp. 4185–4198, 2014.

[225] X. Jiang, S. Kang, L. Tong, and F. Li, "Modification of evapotranspiration model based on effective resistance to estimate evapotranspiration of maize for seed production in an arid region of northwest China," *Journal of Hydrology*, vol. 538, pp. 194–207, 2016.

[226] J. Fan, L. Wu, F. Zhang, H. Cai, W. Zeng, X. Wang, and H. Zou, "Empirical and machine learning models for predicting daily global solar radiation from sunshine duration: A review and case study in China," *Renewable and Sustainable Energy Reviews*, vol. 100, pp. 186–212, 2019.

[227] S. Saadi, M. Todorovic, L. Tanasijevic, L. S. Pereira, C. Pizzigalli, and P. Lionello, "Climate change and mediterranean agriculture: Impacts on winter wheat and tomato crop evapotranspiration, irrigation requirements and yield," *Agricultural water management*, vol. 147, pp. 103–115, 2015.

[228] Q. Ye, X. Yang, S. Dai, G. Chen, Y. Li, and C. Zhang, "Effects of climate change on suitable rice cropping areas, cropping systems and crop water requirements in southern China," *Agricultural Water Management*, vol. 159, pp. 35–44, 2015.

[229] A. W. Worqlul, Y. T. Dile, J. Jeong, Z. Adimassu, N. Lefore, T. Gerik, R. Srinivasan, and N. Clarke, "Effect of climate change on land suitability for surface irrigation and irrigation potential of the shallow groundwater in Ghana," *Computers and electronics in agriculture*, vol. 157, pp. 110–125, 2019.

[230] D. Xiao, H. Bai, and D. L. Liu, "Impact of future climate change on wheat production: a simulated case for China's wheat system," *Sustainability*, vol. 10, no. 4, p. 1277, 2018.

[231] Y. Chen, G. W. Marek, T. H. Marek, J. E. Moorhead, K. R. Heflin, D. K. Brauer, P. H. Gowda, and R. Srinivasan, "Simulating the impacts of climate change on hydrology and crop production in the Northern High Plains of Texas using an improved SWAT model," *Agricultural Water Management*, vol. 221, pp. 13–24, 2019.

[232] T. Fischer and C. Krauss, "Deep learning with long short-term memory networks for financial market predictions," *European Journal of Operational Research*, vol. 270, no. 2, pp. 654–669, 2018.

[233] A. Ignatov, "Real-time human activity recognition from accelerometer data using Convolutional Neural Networks," *Applied Soft Computing*, vol. 62, pp. 915–922, 2018.

[234] (2017) AQUIFER MAPPING AND MANAGEMENT PLAN, Ludhiana District, Punjab. Central Ground Water Board, Ministry of Water Resources, River Development and Ganga Rejuvenation, Government of India. Accessed: 2022-09-01. [Online]. Available: http://cgwb.gov.in/AQM/NAQUIM_REPORT/Punjab/Ludhiayana.pdf

[235] K. S. Kannan, K. Manoj, and S. Arumugam, "Labeling methods for identifying outliers," *International Journal of Statistics and Systems*, vol. 10, no. 2, pp. 231–238, 2015.

[236] A. Elbeltagi, L. Zhang, J. Deng, A. Juma, and K. Wang, "Modeling monthly crop coefficients of maize based on limited meteorological data: A case study in Nile Delta, Egypt," *Computers and Electronics in Agriculture*, vol. 173, p. 105368, 2020.

[237] R. Awal, H. Habibi, A. Fares, and S. Deb, "Estimating reference crop evapotranspiration under limited climate data in West Texas," *Journal of Hydrology: Regional Studies*, vol. 28, p. 100677, 2020.

[238] S. S. Nikam, A. Mishra, A. Sarangi, P. B. Shirsath, D. Singh, and V. Ramasubramanian, "Artificial neural network models to predict wheat crop evapotranspiration," *Journal of Agricultural Engineering*, vol. 47, no. 2, pp. 20–25, 2010.

[239] F. Maselli, M. Chiesi, L. Angeli, L. Fibbi, B. Rapi, M. Romani, F. Sabatini, and P. Battista, "An improved NDVI-based method to predict actual evapotranspiration of irrigated grasses and crops," *Agricultural Water Management*, vol. 233, p. 106077, 2020.